NORTHWESTERN UNIVERSITY

Computational Modeling of Polymerization and Degradation of Complex Polymer Systems

A DISSERTATION

SUBMITTED TO THE GRADUATE SCHOOL

IN PARTIAL FULFILLMENT OF THE REQUIREMENTS

for the degree

DOCTOR OF PHILOSOPHY

Field of Chemical and Biological Engineering

By

Rebecca E. Harmon

EVANSTON, ILLINOIS

June 2022

Abstract

Computational Modeling of Polymerization and Degradation of Complex Polymer Systems

Rebecca E. Harmon

Oil paintings are complex works of art, even on the molecular level. Drying oils cure into a solid film through autoxidation and polymerization reactions and then degrade, leading to changes in material properties and film stability. This chemistry can be captured in a computational model and used by researchers in the coatings industry and art conservation to study polymer films through non-invasive means. However, there are numerous challenges in simulating how the complex polymers like those in painted works cure and degrade, mainly regarding the balance of tractability and accuracy of different computational models.

In this dissertation, the context and chemistry of oil paint curing is described first. The next portion is a broader application of polymer modeling to polyolefin pyrolysis, which underscores the importance of selecting the right computational methods for the information and properties that are desired. A comparison of global and kinetic models is given, highlighting the level of detail acquired by explicitly considering reaction types rather than global fitting, which empirically matches experimental data but misses the effects attributed to tacticity and the chemical bonds in polypropylene and polyethylene pyrolysis. Following the utility of kinetic models, a broad lumping approach is applied to reaction types to fit a monomer-based kinetic model of ethyl linoleate, a representative molecule of larger drying oils found in paint, to experimental FTIR measurements. Advantages of this method are in automatically generating particular monomeric fragments as ethyl linoleate oligomerizes. The sensitivity of the model to kinetic rate parameters

also highlights the overall influence of reaction types and the importance of subdividing reaction families based on local reactivity. This body of work culminates in a framework that is applied to ethyl linoleate autoxidation with stochastic simulation to capture both the formation of polymers and track the evolution of experimental measures of interest. Concluding remarks and a perspective on the future of computational modeling of complex polymer systems close the dissertation.

Acknowledgments

First and foremost, I wish to thank my outstanding advisors, Prof. Linda Broadbelt and Prof. *dr*. Piet Iedema. I am deeply grateful for their mentorship, guidance, and support throughout my PhD career. Linda, you are a role model to me in many ways, and I appreciate having you in my corner. I am thankful for the latitude you provided me to pursue unique opportunities and valuable advice in navigating them with intention. Piet, thank you for the incredible opportunity to join your group at the University of Amsterdam. I will always cherish my time in the Netherlands working on such an interesting project. It has been an honor to work with you both.

Thank you to my committee members, Dr. Francesca Casadio and Prof. Wesley Burghardt, for their thoughtful questions and perspectives throughout my PhD candidacy and reviews. In addition to their technical expertise, I admire their dedication to innovative teaching and outreach, as it has informed my perspective on higher education, communication, and service.

Financial support from the National Science Foundation (NSF) Partnerships for International Research and Education (PIRE) program under Grant No. 1743748 is gratefully acknowledged. I also gratefully acknowledge financial support through the Northwestern Institute on Complex Systems Data Science Fellowship and Terminal Year Fellowship at Northwestern University. This research was supported in part through the computational resources and staff contributions provided for the Quest high performance computing facility at Northwestern University which is jointly supported by the Office of the Provost, the Office for Research, and Northwestern University Information Technology. Thank you to the Chemical and Biological Engineering (ChBE) and van ‘t Hoff Institute for Molecular Sciences (HIMS) staff and program assistants and evaluators with the PIRE program for administrative support.

I thank the many professors, graduate students, and friends who have made this educational endeavor enjoyable and meaningful. Special thanks to Prof. Randy Snurr for his mentorship in the Teaching Apprentice Program; Alex Prybutok for her shared love of engineering education and the countless hours on Zoom as we prepared for the job search and PhD defenses; Dr. Sribala Gorugantu as a coauthor and for sharing walks to Lake Michigan to watch the sunrise; and Victoria Cooley for being an inspiring researcher and friend I could always rely on in the highs and lows of graduate school. Thank you also to Elsa Koninckx, Blaise Kimmel, Ren Lopez, Gwen dePolo, and Grant Marsden for the smiles and memories.

To Broadbelt Group members past and present, thank you for always being there to help out, hang out, or work out (at group fitness classes). A special thank you to Dr. Lindsay Oakley for laying the foundation of this research during her PhD and kindly answering my many questions as I picked up the project.

To CompChem Group members past and present, thank you for welcoming me during my stays in Amsterdam. Your friendship and conversations over coffee and treats will always be a highlight I cherish. A special thank you, as well, to Dr. Yuliia Orlova for being an excellent colleague and collaborator in our shared research topic.

In getting to where I am today, I sincerely thank my phenomenal mentors from Iowa State University: Prof. Jen Heinen, Prof. JP Tessonnier, Prof. Monica Lamm, and Dr. Joel Johnson, among many others who shaped my adventure.

A huge thank you to my family, especially my parents Roger and Wendy, for encouraging me to continue my academic career and always being my biggest cheerleaders. Your encouragement from the beginning to follow my interests and serve others set the scaffolding for

how I want to continue my career and give back. Thank you to the Hagenows for their love and support with many tasty leftovers, rolls of quarters, and treats to bring back to Evanston.

Last but certainly not least, I sincerely thank my husband, Jonathan Hagenow, whose encouragement and love was always felt, even when we were states, countries, and time zones apart. I am grateful for the sacrifices you made for me to pursue my education and career.

This has been an incredible five years of research, travel, friendship, and personal growth. I will remember fondly my time in Evanston and Amsterdam and the extraordinary people with whom I had the fortune of crossing paths.

This work is dedicated to Dr. Tom Thurow, whose legacy continues through the seeds sown during his life and work.

Table of Contents

List of Figures

List of Tables

Chapter 1 Introduction

1.1 Overview

The field of conservation science works to conserve objects through the study of material properties and degradation intervention. In doing so, these objects can be maintained to answer questions of composition, methods, and context.[1] Painted works of art, in particular, pose a challenge to conservation efforts. A painting is a heterogeneous mixture of organic and inorganic components in layered thin films on a substrate, like canvas or wood panel. This complex composite undergoes chemical and physical changes over time that can be accelerated due to environmental conditions like light, temperature, and relative humidity, which may result in metal soap formation, color fading, and cracking.[2–7]

Conservation scientists aim to uncover the maximum amount of information about a painting's composition and degree of degradation with the least amount of intervention to the artwork. Analytical research from millimeter-sized paint cross-sections is invaluable, but non-destructive imaging methods are increasingly preferred such as x-ray fluorescence, hyperspectral imaging, and optical coherence tomography.[4,8–10] To utilize the data from these types of methods, the National Science Foundation is presently funding CuBISM, Computationally-Based Imaging of Structure in Materials, a research and educational program based at Northwestern University. This collaborative program aims to develop refined, non-invasive tools for the conservation field using computational imaging to correlate material properties to an object's appearance and materials modeling to study curing and degradation mechanisms. Stemming from the latter approach, the underlying composition of an artwork and the chemistry by which it dried can inform

mechanical properties and stability, details that are important to art conservators as they work to maintain and protect priceless pieces of cultural heritage.

Currently, accelerated aging is the main method to predict physical properties and paint stability, especially in the coatings industry, a $145 billion enterprise as of 2017.[11,12] Days of accelerated aging under ultraviolet or intense visible light, elevated temperatures, and relative humidity correlate with brittleness after years of natural aging in paint samples. However, this method is imperfect in matching paint film composition between elevated and ambient conditions. For example, Douny *et al.* found accelerated aging at 60 °C underestimates primary oxidation products such as hydroperoxides and overestimates secondary oxidation products such as aldehydes.[13] Aging at relatively high temperatures also accelerates the rate of evaporation of free fatty acids (FFA) formed by hydrolysis of triglycerides, like that shown in Figure 1.1. In naturally aged films, hydrolysis is a dominant process that both embrittles the film and builds up FFA concentrations that temper brittleness through plasticization. However, at 80 °C, the rate of evaporation of certain plasticizers, like palmitic and stearic acids, is greater than or equivalent to the rate of ester hydrolysis.[11] As a result, the relative loss of these plasticizers contributes more to the mechanism of embrittlement than hydrolysis. The chemical differences between naturally and artificially aged films prevent direct translation of intervention methods such as cleaning solvents.

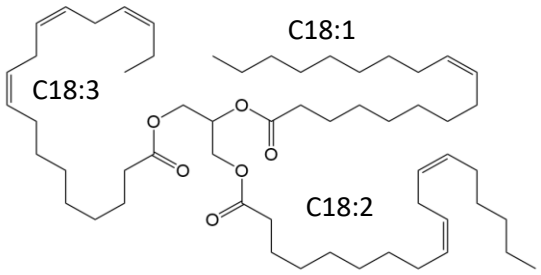

Figure 1.1. A typical representation of a linseed oil triglyceride with linolenic (C18:3), linoleic (C18:2), and oleic (C18:1) fatty acid tails.

Instead of relying solely on physical samples, a robust computational model could capture both accelerated and "natural" chemistry during an oil paint's lifetime. Chemical reaction modeling will benefit art conservation and the coatings industry as a non-invasive technique to study paint. For an effective solution, considerations must be made on the type of model developed, specified, outputs, and the level of detail necessary for comparable observations between an *in silico* sample and one studied physically.

Additionally, the broader polymer science field is advancing by developing new ways to capture complex mixtures of polymers as the polymerize or depolymerize as part of continuous recycling or re-use efforts. The work put forth in this dissertation falls within the broad efforts of modeling polymers in useful and innovative ways as material and chemical space continue to grow in complexity. Broadly, this dissertation covers the relevance of computational modeling to polymers, as well as demonstrates a new framework applied to multifunctional polymer systems motivated by art conservation science challenges but designed to be translated to other complex polymer systems.

1.2 Outline of Research

Chapter 2 is a review published in Progress in Organic Coatings on the autoxidation chemistry of linseed oil, a common oil paint binder.[14] This work was written jointly with Dr. Yuliia Orlova of the University of Amsterdam. The chapter summarizes the literature surrounding the polymerization chemistry of drying oils, reaction kinetics, and methods of studying such systems. Relevant experiments such as size-exclusion chromatography, Fourier-transform infrared spectroscopy (FTIR), and thermogravimetric analysis are reviewed. Computational experiments and methods are also summarized—particularly the existing kinetic models of autoxidation. The

chapter touches on future directions, though a more thorough discussion on future perspectives is shared in Chapter 6.

Chapter 3 is a peer-reviewed article published in ACS Energy & Fuels on the Insight into Polyethylene and Polypropylene Pyrolysis: Global and Mechanistic Models.[15] This chapter falls within the scope of the broader polymer science field that is advancing by developing new ways to capture complex mixtures of polymers as they polymerize or depolymerize as part of continuous recycling or re-use efforts. Here, historical literature data on polyolefin pyrolysis are considered. Empirical models correctly capture the sigmoidal behavior of the rate of pyrolysis in both polyethylene (PE) and polypropylene (PP) pyrolysis. A mechanistic model of PE pyrolysis also effectively captures the experimental trends by using relevant reaction families and kinetic parameters. However, a mechanistic model of PP pyrolysis fails to capture the sigmoidal behavior, even with the same kinetic parameters. It instead has a trend consistent with atactic PP pyrolysis. The differences between PE and PP are embedded in the heats of reaction and the inclusion of a pendant methyl group along the PP backbone. Thus, this work suggests that mechanistic models complement global model studies to understand effects beyond overall or lumped measures, particularly for polyolefin systems.

After demonstrating the benefits of a detailed deterministic kinetic model, Chapter 4 applies a kinetic model of ethyl linoleate (EL) autoxidation to untangling electrospray ionization-mass spectrometry (ESI-MS) spectrum data. The model was generated using automated reaction network generation on monomer fragments, and the concentrations of monomer types was solved using a system of ordinary differential equations. Kinetic rate parameters were optimized manually to FTIR data for un-catalyzed autoxidation of EL. A sensitivity analysis of the complex, non-linear

model is performed and demonstrates the importance of key reaction types on the production of crosslinks and other oxidative products. A quantitative analysis of monomers and dimers identified from ESI-MS using the model is given, along with a reaction pathway analysis to demonstrate the utility of the model to elucidate potential paths or lack thereof to species of interest.

Chapter 5 puts forth a framework, based on stochastic modeling, that overcomes computational barriers reached in previous kinetic modeling efforts of drying oil curing. This method combines three key aspects: on-the-fly chemical species generation to prevent the need for *a priori* polymer distribution; monomer approach by Orlova et al.[16,17] paired with coarse-grain polymer graphs that maintain the monomer identities and crosslink information to form full polymeric species rather to surpass the limits of explicit species by their atom counts and without needing a random graph approach to determine the composition of oligomers or polymers formed; and stochastic simulation of reaction families to prevent the combinatorial explosion of ordinary differential equations in a stiff system and for implicit model reduction rather than solving for the concentration of insignificant species. This chapter outlines the methodology and its application to a case study of ethyl linoleate autoxidation. The model goes beyond the oligomers generated by Oakley et al.[18,19]

Finally, the thesis concludes with a summary of the technical outcomes and themes presented. Several perspectives are given in how polymer modeling can continue to improve by being applied to more complex systems. These future endeavors are attainable and set the stage for continued collaboration at the intersection of art and chemical engineering

Chapter 2 Review of the Kinetics and Simulations of Linseed Oil Autoxidation

This review summarizes computational modeling literature concerning linseed oil autoxidation in the context of oil paint. After discussing the chemical structure and composition of linseed oil, an overview is given of polymer properties of the material and the experimental techniques used to infer these properties. The review proceeds with the survey of existing computational modeling techniques used to investigate the drying process of linseed oil.

This chapter is adapted from the following peer-reviewed article: Orlova, Y.[1]; Harmon, R. E.[1]; Broadbelt, L. J.; Iedema, P. D. Review of the Kinetics and Simulations of Linseed Oil Autoxidation. *Prog. Org. Coatings* **2021**, *151*. https://doi.org/10.1016/j.porgcoat.2020.106041

[1] Equal contribution

2.1 Introduction

This literature review is motivated by the need for a resource that gathers relevant chemical kinetics for the autoxidation of linseed oil and the opportunities that computer simulation can offer this century-old field. Linseed oil is a prominent drying oil, particularly known for its use as a varnish and oil paint binder since the 15th century.[20] At the advent of the paint tube, oil paint production expanded beyond the mortar and pestle where chemists were working to perfect the revolutionizing products. Dried (polymerized) linseed oil is an insoluble binder with stability and structure to last hundreds of years. Its properties depend on composition and crosslinks, each affected by environmental conditions[21] and additives such as driers[22] and elevated temperatures.[23]

Up to this point, several key reviews consolidated literature and resources related to the autoxidation pathways that cure linseed oil and the inevitable degradation pathways that wear it down. However, this review is written from the perspective of collaborative research that leverages a century of experiments to understand linseed oil on the molecular level using computer modeling tools as technological advances in the 21st century. It is also centered around the drying oil's application and long-time behavior in art and art conservation science efforts[24] in contrast to prominent efforts in food science research[25] with related oils.

Linseed oil and its model systems have been investigated as a binding medium of oil paint in numerous experimental research works preceding computational modeling.[2,26,27] Thorough studies were done regarding the influence of drier on the autoxidation of ethyl linoleate and linseed oil reporting the behavior of key functional groups and of small volatile compounds.[28–36] Reviews by Honzíček,[37] Soucek et al.,[38] Juita et al.[39] and van Gorkum et al.[30] provide detailed descriptions

of the autoxidation reaction mechanism. These research works provide valuable information about the chemistry of linseed oil and serve as a reference for computational modeling.

The term “model” is used in two contexts in this review: (1) a model compound that represents a simplified chemical species and (2) a computational model for simulating a complex, physical system. A chemical model compound shares some essential chemical properties with the real compound, but it can be tested under better defined conditions. For example, ethyl linoleate (EL) is commonly used as a model system for linseed oil, as EL represents the linoleic ester of linseed oil. Also, EL is available as a purified substance, whereas linseed oil is only available as a natural mix of triglycerides with different ratios of fatty esters. Yet, the EL model offers the advantage of a detailed quantitative and theoretical interrogation of the physical system.

This review yields access to key research related to the drying and degradation of linseed oil of relevant kinetic detail, pathways, and methods and thus forms a starting point for work in this interdisciplinary field. Section 2.2 characterizes the structure and variations in composition of the linseed oil. Proceeding with the polymerizing nature of linseed oil, Section 2.3 explains the formation of the linseed oil films in terms of a free radical polymerization process. Section 2.4 provides an overview of the reaction pathways characterizing linseed oil during its autoxidation including recent findings in β-scission and epoxidation mechanisms. Section 2.5 proceeds with the description of several experimental techniques that are relevant for validation of various models. Computational methods elaborated on in Section 2.6 of this review are quantum chemical calculations and kinetic modeling. Kinetic modeling is most comparable to physical experiments, as concentrations of some initial, intermediate and final compounds can be quantified in a relatively straightforward manner. The sensitivity of systems can also be readily investigated using

kinetic modeling. Following the findings in computational modeling, the review finally discusses the future directions in modeling for linseed oil research.

2.2 Drying Oils

Drying oils are natural, bio-based oils that harden or “dry” into a solid film when exposed daylight and ambient oxygen. The oil is a mixture of triglycerides, where each molecule consists of three fatty acids attached to glycerol by ester bonds. Fatty acids are carboxylic acids with a hydrocarbon chain that is saturated fully with hydrogen atoms or unsaturated with one to four double bonds along the chain. Double bonds may be arranged to form either conjugated or non-conjugated double bonds, the latter causing stronger drier activity.

Properties of drying oils strongly depend on the relative amount of different types of fatty esters. Unsaturated fatty esters undergo a complex autoxidation mechanism eventually forming crosslinks, which lead to the formation of a polymer network. Meanwhile, saturated fatty esters remain virtually unchanged. Depending on the content of various fatty esters, oils are classified as drying, semi-drying and non-drying oils. The ability of an oil to undergo autoxidative drying depends directly on the amount of doubly allylic methylene units (or bis-allylic C–H bonds), which are found in linoleic and linolenic acids. Bis-allylic groups are responsible for the formation of crosslinks, as the bis-allylic H-atom is easily abstracted to form a radical, which forms the onset of reaction pathways ultimately ending up in crosslinks. One bis-allylic group (as in linoleic) may result in up to three crosslinks. This observation leads to the empirical relationship quantifying the oil's ability to dry: Drying index = (% linoleic acid) + 2(% linolenic acid).[38] Oils with a drying index above 70 are classified as drying oils.

The fatty ester content in several oils is summarized in Table 2.1. Although the table provides the most common fatty ester composition, oils have a different degree of unsaturation depending on agricultural temperature zone, [35,40] and oil processing methods.[41] Saturated fats and oleic acid do not contribute to the drying process, implying that olive and coconut oils never dry, while linseed, soybean, walnut and poppy seed oils are prone to drying via crosslinking. Linolenic acid is a major fatty ester in linseed oil, while linoleic acid is a major fatty ester in soybean, poppy seed and walnut oil.[30] Due to their properties, these four oils became widely used as binding media by artists, who were empirically finding the balance in the amounts of linoleic and linolenic acids for their paints.[42] Work by Stenberg et al.[43] compares the drying process of linseed oils with a high content of linoleic fatty esters versus a high content of linolenic fatty esters The authors conclude that a high content of linoleic fatty esters ensures homogeneous drying of the oil film, while linseed oil with a high linolenic fatty ester content dries fast on the surface, leaving unreacted fatty esters below. Drying of linseed oil occurs by chemical crosslinking between monomers, thus increasing viscosity and leading to an insoluble polymer fraction. The viscosity increase is just slow enough to permit artistic changes while creating a painting. Some of the autoxidative drying processes leading to the desired solid polymer network continue afterwards and lead to degradation of the binding medium in the longer term. Therefore, understanding drying and degradation processes of drying oils and their impact on the structure of the binding medium polymer is an important issue in the field of restoration and conservation of art.

Because of the variability of fatty esters in linseed oil mixtures, model systems are often used to isolate certain properties or reactivities to study in a controlled fashion. For example, common model species are unsaturated methyl and ethyl esters of oleic, linoleic, linolenic, and

ricinoleic acid,[29,31,34,44] as well as dienes: 4,7-heptadiene,[45] 3,6-nonadiene,[46] and 2,5-undecadiene.[47] While exploring various aspects of the drying process such as speed of drying and emission of volatile compounds, researchers developed a better understanding of elementary reaction steps leading to the final product.

Table 2.1. Various ratio of fatty esters in oils (in wt%).

Oil	**Saturated**	**Oleic**	**Linoleic**	**Linolenic**
Linseed oil[38]	10	22	16	52
Soybean oil[38]	15	25	51	9
Poppy seed oil [48]	15	20	65	
Walnut oil [49]	9	20–26	50–55	14–15
Olive oil [50]	13–20	62–80	5–15	<1
Coconut oil[38]	91	7	2	

2.3 Polymerization

The extensive usage of linseed oil in works of art is explained by the oil's suitable optical and mechanical properties as a polymer. While drying, linseed oil actively reacts with oxygen and forms a thin continuous film via a polymerization process. Favorable drying properties of linseed oil are achieved due to a high concentrations of linoleic and linolenic acid tails, which are the main polymerizing agents is linseed oil responsible for drying (Figure 2.1).

Drying and hardening of linseed oil is considered as a polymerization of triglycerides via autoxidation, a process involving free radicals. Individual molecules of liquid linseed oil act as initially disconnected monomers. In the presence of oxygen, the triglyceride monomers form covalent crosslinks, which leads to the formation of oligomers and eventually to infinite-size polymers. Free-radical polymerization reactions consist of three main categories: initiation, propagation and termination.[51] Polymerization competes with degradation processes such as scission reactions, decomposition of unstable crosslinks and hydrolysis.

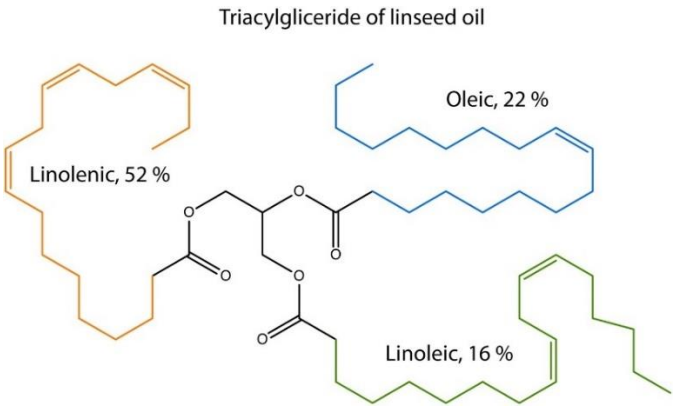

Figure 2.1. An example triglyceride that would be found in linseed oil.

Due to the presence of natural antioxidants in linseed oil,[38,52] initiation occurs after an induction time and leads to the formation of a reactive bis-allylic radical. Due to the presence of these radicals, linseed oil can react with oxygen forming highly reactive peroxyl radicals. This oxygen uptake leads to significant mass increase. During the formation of hydroperoxide groups, the non-conjugated double bonds in the fatty esters become conjugated double bonds. Only unsaturated acids can undergo initiation and are subject to polymerization reactions, while saturated fatty esters remain unreacted along the hydrocarbon chain and act as plasticizers.[53] Initiation is followed by propagation reactions, by which radicals are propagating from one molecule to another. Termination occurs when two radicals meet and form either a covalent crosslink via recombination or two terminal groups, one saturated and one unsaturated, via disproportionation. Crosslinks may also be formed by addition reactions occurring between hydroperoxide radicals and conjugated double bonds. Termination and addition reactions first lead to the formation of oligomers. As polymerization proceeds, few oligomers become very large and eventually form a polymer network of infinite size. The polymer network molecule forms a gel, which is an insoluble species. The weight fraction of gel continues growing at the expense of the

smaller molecules.[53] While the insoluble fraction is forming, low molecular weight molecules are also formed via oxidative scission of alkyl chains (β-scission), decomposition of unstable crosslinks or hydrolysis of ester bonds. Some of these low-molecular compounds are volatile and are released, causing the typical smell of drying paint. The linseed oil polymer does not fully converge into a gel regime, as non-volatile low molecular weight soluble fractions remain in the system even after long drying time.[34] Decomposition reactions are characteristic for the late stage of drying of linseed oil, and they are responsible for the degradation of binding medium. Degradation of the polymer network is enhanced by ambient conditions. Both thermal and photo degradation occur, but the latter is found to be more harmful to the polymer network.[30]

The drying process of linseed oil, as a binding medium of paint, may be influenced by introducing additives, such as driers, extenders and pigments.[27,30,31] The addition of driers influences the amount of crosslinks formed in the linseed oil film. There are different types of driers: primary driers (surface driers), secondary driers (through-driers) and auxiliary driers. Primary driers influence the hydroperoxide decomposition reaction, while through-driers enhance the amount of crosslinks. Auxiliary driers may influence the action of a primary drier and are added mainly to improve the aesthetics of the paint layer.[30] Primary driers are usually combined with secondary driers, as an excess of primary drier may result in wrinkling of the paint film.[54] In contrast, an excess of secondary drier may result in increased brittleness of the dried oil.[55] The behavior of soluble fractions in the presence of cobalt drier was studied by Muizebelt et al.[56] Oligomeric species up to pentamers were detected after one day of drying, while only dimers and compounds with low molecular weights remained in the system after 60 days of drying.

To quantify the extent of drying, the elasticity modulus of the film can be measured. Mecklenburg and Tumosa[57] performed a long-term aging study with titanium white pigment in cold-pressed linseed oil and compared these to other commercial white paints. Using tensile testing, they measured the stress-strain behavior of the samples, which led them to conclude that paint continues to become more brittle, even after 10 years. Various factors are known that may further influence the tensile properties of a film. These include degradation processes and cleaning treatments that leach out low molecular weight molecules that had previously plasticized or maintained the flexibility of the film, thus embrittling the film.[58–60] Van den Berg et al.[61] also found that the presence of polyvalent metal ions has an impact on the stability of a polymer film. In a pure linseed oil film without pigments, hydrolysis of the ester bonds between glycerol and fatty esters causes the network to degrade. Polyvalent metal ions stabilize the network by forming ionomers. Hence, when studying polymer models with respect to reactivity and mechanical properties, one has to include the effect of pigments, as well.

Numerous research works mentioned above intended to improve paint properties regarding durability. Meanwhile, ongoing work in conservation science is performed to better understand the drying and degradation of existing art objects, based on oil paint. A detailed understanding of the oil autoxidation mechanism is necessary to improve conservation and restoration treatments of precious works of art by enhancing efficiency and reducing the need for invasive analysis. It should be realized that specific detrimental chemical phenomena are closely linked to linseed oil chemistry. For instance, the formation of metal soaps is strongly related to the presence of carboxylic acid groups resulting from autoxidation in the oil film.[3] Therefore, it is desirable to

investigate the reaction pathways involving carboxylic acid groups in relation to cleaning, restoration, storage and transport of the art objects.

A remarkable feature of the polymer network formed by linseed oil lies in the diversity of its monomer constituents. The monomers are not identical repeating units as in many industrial polymers (e.g. polyethylene or polystyrene). Linseed oil monomers can undergo many chemical transformations until they reach stable states and become incorporated in the polymer network. Therefore, one may identify two main challenges in understanding the polymerization chemistry of linseed oil: (1) numerous competitive radical reactions involving fatty esters of triglycerides lead to a variety of intermediate molecular species; (2) liquid linseed oil polymerizes to a solid, so reactions conditions change dramatically causing radical reactions to proceed more slowly as their mobility decreases – these reactions will become diffusion-controlled.

In this literature review we report on various aspects of the detailed reaction mechanism of linseed oil polymerization.

2.4 Chemistry and Kinetics

The reaction mechanism of triglycerides is an autoxidation process that proceeds under the influence of oxygen and light. It predominantly consists of the following reactions: oxidation, crosslinking and scission.[62] The autoxidation process consists of a very complex scheme of radical reactions occurring repeatedly to the functional groups of the organic linseed oil molecule. Multiple reactions may occur rapidly and essentially simultaneously, leading to products that are not easily isolated in experiments.[63] The autoxidation of linseed oil is characterized by two competing mechanisms: formation of the polymer network and breakdown of the molecules due

to β-scission, unstable crosslink decomposition and hydrolysis. The schematic representation of the autoxidation process is shown in Figure 2.2.

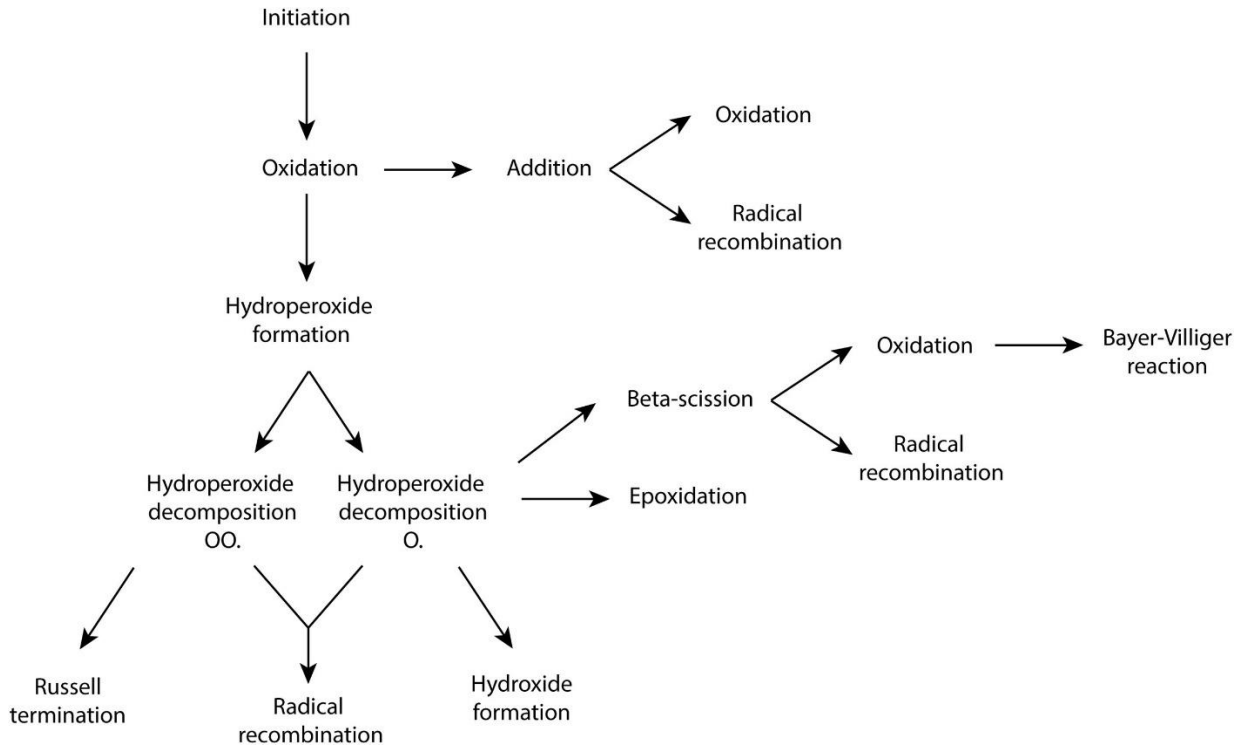

Figure 2.2. A general schematic representation of the reactions occurring during autoxidation of linseed oil.

Consistent with Figure 2.2, the four main stages of free-radical polymerization will now be discussed: (1) initiation; (2) propagation; (3) termination; (4) degradation. In the case of drying oils, these reaction steps lead to a variety of intermediate and end products. We provide many reported reactions for each fatty ester at various stages of drying. Moreover, where possible, the reactions will be reported together with kinetic rate parameters, which influence the speed of reactions as a function of temperature. It must be noted that kinetic parameters cited in the review possess uncertainty, as there is both experimental and computational error in the values.

2.4.1 Initiation

Autoxidation begins with an initiation step involving a tiny amount of radicals that may be created in several ways. During the subsequent propagation step a comparatively higher concentration level of radicals prevails in the system. In linseed oil, the initiation of a radical can be delayed by the presence of natural antioxidants, causing an induction period before propagation starts.[38,52] Differences in induction period are observed in the temperature ranges above 130 °C, 84–130 °C and below 84 °C. The induction period is short above 130 °C, while in the range of 84–130 °C the length of induction increases slowly as the temperature is lowered; below 84 °C the induction period is long and independent of temperature.[63] Initiation happens in two steps: primary initiation and secondary initiation. Primary initiation creates a tiny amount of peroxyl radicals that subsequently take part in the secondary initiation.

During secondary initiation the radical created by primary initiation abstracts a hydrogen atom from a bis-allylic carbon of a linoleic or linolenic fatty ester tail, forming a delocalized pentadienyl or heptadienyl radical, respectively. The alkyl radical rapidly reacts with molecular oxygen and forms a peroxyl radical. Allylic hydrogen abstraction happens predominantly at elevated temperatures.[64] For the resonant structures after allylic and bis-allylic hydrogen abstraction, see Figure 2.3. Initiation can occur spontaneously,[65] or with the aid of UV light,[66] singlet oxygen[46] or active metal catalysts.[33] Spontaneous initiation is rationalized by the fact that linseed oil will cure in air without using a catalyst, although slowly.[65] It has been shown that UV irradiation lowers the activation energy of curing of alkyd resins.[66] Singlet oxygen is much more reactive than triplet oxygen and is capable of attaching to the bis-allylic as well as to allylic carbon and forming a hydroperoxide via a concerted cyclic addition mechanism.[46] Singlet oxygen is

formed from molecular oxygen in the presence of photosensitizers causing the excited state of oxygen by an uptake of at least 22.4 kcal/mol.[46]

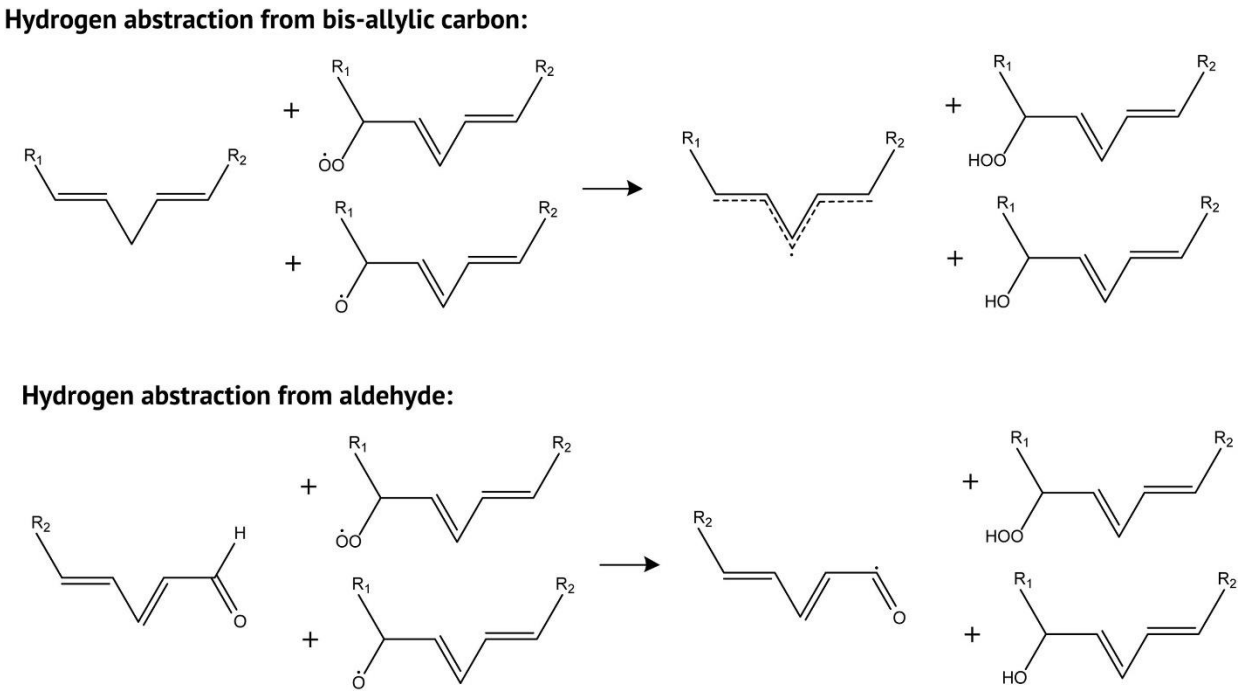

Figure 2.3. Propagation of radicals via hydrogen abstraction from bis-allylic carbon (top) and from an aldehyde (bottom) by alkoxyl and peroxyl radicals.

Metal driers are added to oils to speed up the decomposition of hydroperoxides and initiate autoxidation. A common transition metal catalyst is cobalt(II) 2-ethylhexanoate that undergoes primary initiation by reacting with molecular oxygen forming a peroxyl radical with a rate coefficient in the order of 10^{-1} L/mol*s,[19,31] while Co^{II} becomes Co^{III}. The peroxyl radicals follow secondary initiation and abstract hydrogen to form bis-allylic or allylic radicals. Cobalt hydroperoxide then changes back to Co^{II} and splits off a hydroperoxyl group and then may continue its catalytic activity.

2.4.1.1 Hydrogen abstraction

The abstraction of bis-allylic hydrogen (Figure 2.4) occurs at a rate coefficient on the order of 10^{-1} L/mol*s, while allylic hydrogen is 10^5 times less reactive.[18] The energy barrier for hydrogen abstraction in the case of oleate is even higher, 80 kcal/mol.[63] During the autoxidation mechanism, alkoxyl, peroxyl and alkyl radicals are produced, which also take part in hydrogen abstraction. Peroxyl radicals play a major role in hydrogen abstraction as they exhibit a rather long half-life (up to 7 s) in comparison with alkoxyl (10^{-6} s) and hydroxyl (10^{-9} s) radicals.[39] The rate coefficient of hydrogen abstraction by peroxyl radical is estimated to be 6.6 L/mol*s.[18] The speed of initiation can be measured experimentally by tracking the decrease of bis-allylic carbon concentration as, after oxygen addition, they disappear while the non-conjugated configuration of the double bonds changes into a conjugated configuration.[53]

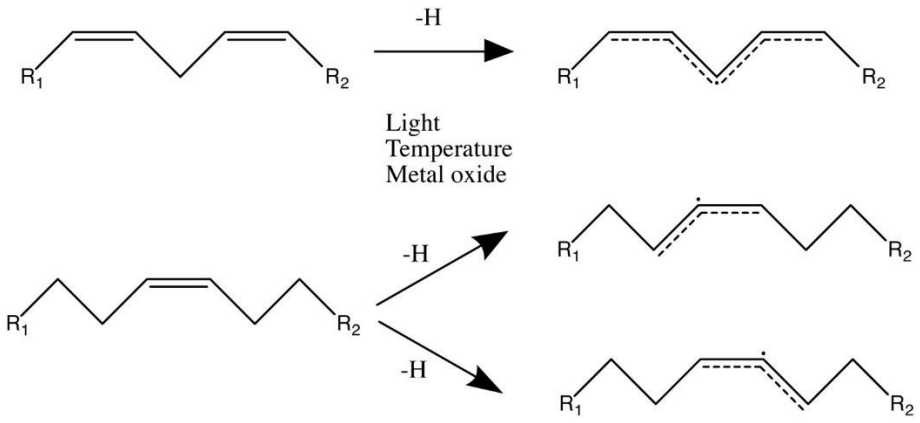

Figure 2.4. Possible initiation of allylic and bis-allylic carbons.

2.4.2 Propagation

The repeated hydrogen abstraction by peroxyl radicals and subsequent reaction with oxygen is responsible for a continuous production of radicals, which in polymer reaction engineering is therefore called the propagation step.

2.4.2.1 Oxidation

Alkyl radicals formed via hydrogen abstraction add oxygen, forming peroxyl radicals. The oxidation mechanism is shown in Figure 2.5. The reaction of oxygen and alkyl radicals happens very rapidly, with a rate constant on the order of 10^8 L/mol*s and an activation energy of 0 kcal/mol. The rate of oxidation varies depending on conditions, such as temperature, the presence of pro-oxidants (oxidizing agents), antioxidants and dissolved oxygen,[67] and the rate also depends on the degree of unsaturation. As mentioned in the work by Wexler,[63] the oxidation rates of triolein, trilinolein and trilinolenin are increasing in order of degree of unsaturation: 1:20:330. When adding to the resonant structure of the backbone, as in linoleic esters, oxygen prefers the position on the 9th or 13th carbon atom, and the resulting functional group is called an outer peroxide. Inner peroxides (C-10 and C-12) appear in minor amounts, possibly resulting from the formation of cyclic peroxides (endoperoxides).[39,68,69] In the case of linolenic acid, hydroperoxides are found at the external as well as at internal positions.[53]

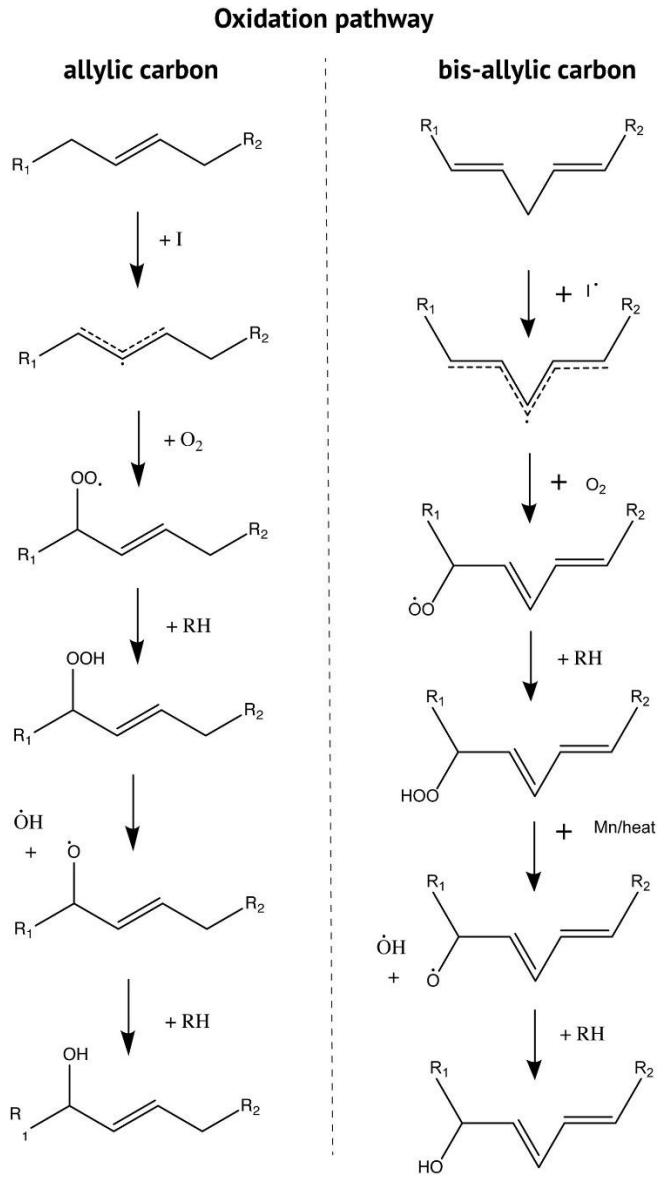

Figure 2.5. Oxidation pathways of fatty esters containing allylic (left) and bis-allylic (right) carbons that are found in fatty esters of linseed oil.

2.4.2.2 Hydroperoxide, Hydroxide Formation

Hydroperoxides are formed from peroxyl radicals after they perform hydrogen abstraction. Being stable intermediates, hydroperoxides mark the initial stage of the autoxidation process. Decomposition of hydroperoxides is a slow unimolecular reaction with a rate constant on the order

of 10^{-13} s^{-1} and an activation energy of 24.6 kcal/mol.[70] A hydroperoxide decomposes into alkoxyl and hydroxyl radicals, and the reaction is accelerated under the influence of light and drying agents containing transition metals like cobalt. The chemistry of hydroperoxide decomposition with cobalt is described in detail in Spier et al.[33]

After hydroperoxide decomposition, the alkoxyl radicals may proceed along several reaction pathways including secondary scission of alkyl chains, recombination with another radical or hydrogen abstraction. In the case of the latter, an alkoxyl radical becomes a hydroxide, which is one of the stable end products of the autoxidation process. The concentration of hydroxides in a linseed oil film reaches a constant value between 200 and 300 h of drying time.[53]

2.4.2.3 Addition

Unsaturated fatty esters participate extensively in hydrogen abstraction, and the addition of oxygen to the alkyl radical is facile, while the previously unsaturated double bonds are rearranged into a conjugated state. The conjugated double bonds are also reactive and are consumed via addition of a peroxyl radical forming a dimer. Thereby, the radical is transferred from the peroxide on one fatty ester to the carbon on the other fatty ester (see Figure 2.6). The previously conjugated structure turns into a resonating double bond between two carbon atoms until the radical reacts with oxygen or undergoes termination. The activation energy of peroxyl radical addition to a conjugated double bond is 6.7 kcal/mol, where the rate parameter is on the order of 10 L/mol*s.

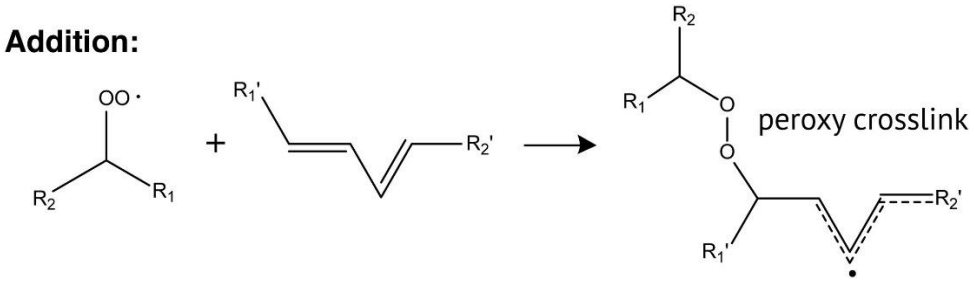

Figure 2.6. Addition of a peroxyl radical to a conjugated double bond resulting in a peroxy crosslink and a resonant double bond.

2.4.2.4. General Behavior of Double Bonds

As described above, a significant rearrangement of the double bonds occurs during the initial autoxidation steps. In the case of oleic fatty esters, there is a *trans*–C=C (double bond), while the polyunsaturated lipids start with *cis*–C=C, which is further consumed via initiation and is turned into a conjugated double bond. Following the addition reaction, one of the conjugated double bonds is broken and the remaining double bond adopts a *trans* configuration. Thus, the *cis*–C=C initially present is consumed fast and completely.[63] Thereafter, the concentration of the remaining *trans*–C=C reaches a constant level.[53]

2.4.2.5 Epoxidation

Epoxides are the simplest cyclic species possible with one oxygen and two carbon atoms. The formation and slow decomposition of epoxides during drying of ethyl linoleate was observed by Muizebelt et al.[34,44] Using quantum chemical calculations, Oakley et al. elucidated the epoxidation of lipid radical species[36] and found that allylic radicals on beta positions to peroxides undergo epoxidation at ambient conditions. The epoxidation proceeds by two pathways representative for the autoxidation of unsaturated fatty esters (shown in Figure 2.8a) having energies of activation of 17.7 kcal/mol and 19.3 kcal/mol, respectively.[36] Both reactions are

unimolecular with rate parameters on the order of 10^{-1}–10^{2} s^{-1}. At elevated temperatures epoxides readily decompose due to the ring-strain.[69] while at ambient conditions Muizebelt captured the subsequent epoxide-ring consumption with the decreased concentration of epoxide groups over 500 days.[34] There is little consensus of the ring-opening mechanism; thus, the review does not provide a detailed account of this reaction.

2.4.3 Termination

The final step of the free-radical polymerization process is radical termination. In this step, two radicals react and either form a single, non-radical product (recombination) or two distinct non-radical products (disproportionation).

2.4.3.1 Recombination

In the linseed oil system, the three main radical types are alkyl, alkoxyl, and peroxyl. When they recombine, they form crosslinks. This is one of two ways crosslinks are formed in the linseed oil polymer network, the other being radical addition as described above. All radical recombination permutations are shown in Figure 2.7a. The distribution of crosslinks in the resulting polymer system depends on oxygen concentration. Under conditions of facile oxygen transport, peroxy and ether crosslinks are formed in equivalent amounts, whereas alkyl crosslinks are formed in a minor amount.[53] Radical recombination is mostly diffusion-controlled; as the polymer becomes more crosslinked, the increased viscosity restricts further radical collisions and thus recombination events.[71,72] In exothermic reactions, the phenomenon of decreasing rates of termination due to viscosity increase is known as autoacceleration or the Trommsdorff-Norrish effect and can lead to dangerous runaway reactions during polymerization of certain synthetic polymers.[73,74] The rate of radical recombination varies based on the polymer system. For example, the rate coefficient for

radical termination in an acrylate system is on the order of 10^9 L/mol*s, whereas rate coefficients for recombination in the linseed oil system ranges from 10^7 to 10^8 L/mol*s.[18,70,75,76] The existence of dimers that cannot be split by hydrogen iodide is a marker for the presence of carbon–carbon, or alkyl crosslinks, the amount of which is shown to be minor.[53,63] Ether links are formed via recombination of alkyl and alkoxyl radicals, the latter being formed after hydroperoxide or polyperoxide (polymer with peroxy crosslinks) decomposition. Muizebelt et al. used the POMMIE NMR (Phase Oscillations to Maximize Editing in Nuclear Magnetic Resonance Spectroscopy) for an EL system and determined from spectra the relative concentrations of ether and peroxy crosslinks.[44] They found that peroxy crosslinks remain constant for over a year, but a net generation of ether crosslinks is detected, mainly originating from the slow decrease of double bonds. Muizebelt et al. also quantified the concentration of alkyl (C–C) crosslinked species from dimers, finding 1% of alkyl crosslinks in pure unreacted EL, and 5% of alkyl crosslinks in EL in the presence of cobalt after five days of drying.[44] Dimers with all three types of crosslinks are shown in Figure 2.7a.

2.4.3.2 Disproportionation

Disproportionation is a second termination reaction, a redox reaction in which the oxidation state of the reactants changes into two different oxidation states of the products. For radical disproportionation, this is commonly in the form of a terminal alkane and a terminal alkene group. In the case of oxygen-rich species, oxygen-centered radicals may collide and form oxidation products such as alcohols and ketones via Russell termination. However, Russell termination is not undisputed for linseed oil polymerization[37,77] as it has too high energy barrier for the recombination of secondary alkylperoxyl radicals.

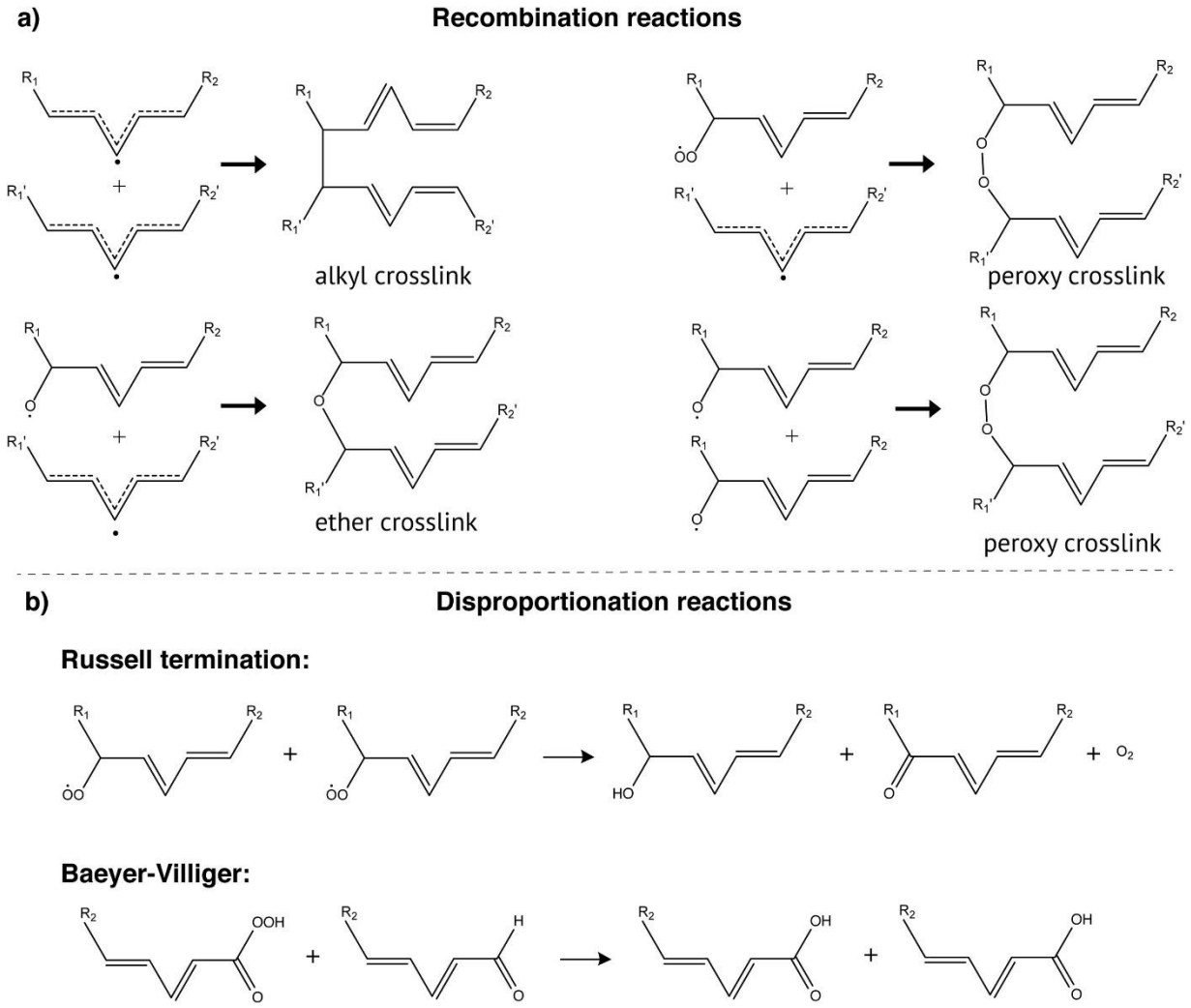

Figure 2.7. Radical recombination reactions lead to three different types of crosslinks: alkyl, ether and peroxy (a). Disproportionation reactions lead to two distinct stable products (b).

Further kinetic studies are required to elucidate and validate the mechanism that leads to oxidation products. Another type of disproportionation is the Baeyer-Villiger reaction, where a peroxy acid reacts with an aldehyde, producing two carboxylic acids. Baeyer-Villiger and Russell termination reactions are shown in Figure 2.7b. The rate coefficient of disproportionation is in the order of 10^6 L/mol*s.[18,70]

2.4.4 Degradation Processes

2.4.4.1 Hydrolysis

In the longer term, after the actual drying process, hydrolysis of ester bonds may disconnect fatty esters from the triglyceride glycerol backbone. Figure 2.8b schematically illustrates hydrolysis, which may occur at each fatty ester leading to glycerol with two remaining fatty esters (diglyceride – DAG), glycerol with one fatty ester (monoglyceride – MAG) or a fully hydrolyzed triglyceride with all fatty esters detached. Hydrolysis is one of the main degradation routes of fatty ester polymer systems. In the presence of water, an ester bond in a triglyceride is broken via hydrolysis and a carboxylic acid is formed on the side of the free fatty ester and alcohol on the side of glycerol. Baij et al.[78] studied the origins of carboxylic acids in oil paints with zinc oxide at various relative humidities (RHs). Erhardt and Mecklenberg[2,11] also studied hydrolysis of oils in detail. They measured the rate of hydrolysis over a decade under varying conditions concerning metal pigments, RH, and temperature and examined the resulting mechanical properties.

2.4.4.2 β-*scission*

Breaking the β-bond to an alkoxyl radical, β-scission propagates the free radical and forms an olefinic species. β-scission is common in thermal cracking, but at ambient conditions it is of limited importance. Products from scission reactions in drying oil systems vary significantly in carbon chain length, as the location of β-bonds next to alkoxyl radicals may vary in oleic, linoleic and linolenic acids. Products of β-scission in linseed oil degradation include volatile n-aldehydes such as ethanal, propanal, butanal, pentanal, hexanal, heptanal and octanal.[79] Oakley et al.[80] validated the mechanism concerning pentanal and proposed a new mechanism to hexanal in the polymerization of EL, as ones previously proposed in literature were too energetically unfavorable

or did not yield the observed product distribution when implemented in a kinetic model. Through quantum chemical calculations, Oakley et al. found that β-scission was more likely to happen according to the scheme shown in Figure 2.8c.

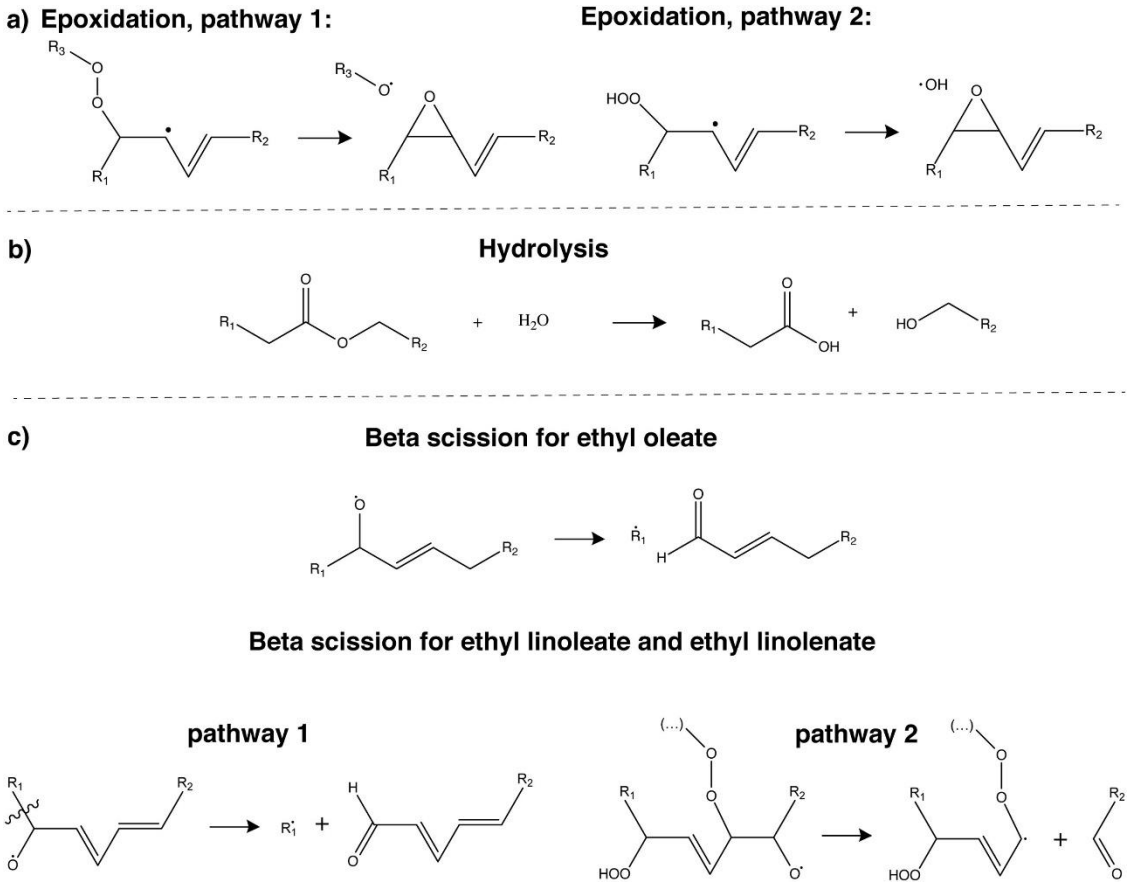

Figure 2.8. Epoxidation from a species with peroxy crosslink (1) and from a species with hydroperoxide (a). Hydrolysis of an ester bond between glycerol and fatty acid (b). β-scission pathways for oleic fatty ester (top) and for linoleic and linolenic fatty esters.

2.4.4.3 Peroxy Crosslink Decomposition

Studies by Muizebelt et al.[34,44] reveal a gradual decrease in peroxy crosslink concentration over one year. This is attributed to slow peroxy crosslink decomposition. In contrast to hydroperoxide decomposition this peroxy crosslink decomposition is apparently not catalyzed by transition metal driers and occurs with an activation energy of 40 kcal/mol.[76]

2.4.4.4 Photodegradation

The continuous exposure of a painting to photons, especially in the proper frequencies of light, will degrade a paint film. This is mainly due to light interactions with the binding medium and pigment particles. Azelaic acid was found to be a marker of photodegradation for linseed oil as a binding medium.[81] Regarding linseed oil in the presence of pigment, titanium white paint, containing anatase titanium dioxide, is photocatalytically active in UV-light.[82] This results in mass loss from the surface of the film and a chalking phenomenon on the surface.

2.5 Experiments

Limitations to experimental investigation of linseed oil polymerization mainly arise due to the large sizes of the polymer molecule accompanied by rapid formation of an insoluble fraction, as well as the great variety of the molecular species. Experimental information is only available for a few aspects of an oil's chemistry. Paragraphs below describe several experimental techniques which generate data relevant for the validation of the outcomes of computational models. While experimental data are used to validate models, vice versa, modeling can also greatly help the interpretation of complex experimental results.

2.5.1 Size Exclusion Chromatography

Separating molecules by their sizes, size exclusion chromatography (SEC) provides the molecular weight distribution of the soluble components of a polymer. Oyman et al.[29] used SEC to explore oligomerization of ethyl linoleate in the presence of driers. The authors show that the difference in measured samples predominately becomes apparent in the peak corresponding to hydroperoxides. This peak gradually appears in the presence of cobalt(II) 2-ethylhexanoate, becoming detectable after 8 h and remaining visible even after 48 h in the presence of

manganese(III) acetylacetonate ($Mn(acac)_3$). The hydroxide peak intensity is always seen to be lower in the presence of $Mn(acac)_3$ with 2,2′-bipyridine. In the work by Lazzari et al.,[53] soluble fractions of linseed oil are analyzed with SEC during drying at the temperature of 80 °C. After 16 h of drying, the chromatogram shows the original molecules of linseed oil and their dimers, while for an aged sample the chromatogram mainly shows low molecular weight compounds as well as higher order oligomers. SEC data on molecular size distribution may be compared to the computed distributions of connected components in the sol as has been obtained by the application of random graph theory.[83,84]

2.5.2 Mass Spectrometry

Exact masses of molecules are measured using mass spectrometry (MS). The intensity of peaks corresponds to a relative amount of molecules with these masses in a measured sample. By attributing the peaks to molecular structures, one may track the variations in peaks' intensities by measuring the samples at different stages of reaction process. The main drawback of such an analytical technique is unwanted fragmentation that occurs to the molecules in the instrument. Moreover, the interpretation of peaks becomes challenging for such systems as linseed oil and its model systems due to a wide variety of peaks indicative of numerous reactions occurring simultaneously. In the pioneering work by Muizebelt et al.,[44] formation of dimers and higher order oligomers during the polymerization of ethyl linoleate was studied using several MS techniques: secondary ion mass spectrometry (SIMS), fast atom bombardment mass spectrometry (FAB-MS) and direct chemical ionization with ammonia mass spectrometry (DCI-MS). SIMS revealed the size of oligomers in terms of monomer units; however, the resolution of the method was not sufficient to track the formation of the species in more detail. Hence, using FAB-MS the range of

monomer and dimer masses was recovered, while with the use of DCI-MS masses of higher order oligomers were revealed in great detail.

Electrospray ionization mass spectrometry (ESI-MS) was used to detect various degradation products, such as free fatty acids, products of hydrolysis and diacids in linseed oil samples.[82,85] This analytical technique provides detailed information about the masses and does not lead to considerable fragmentation of soluble fractions.[86,87]

In relation to modeling, MS data have a resolution that is comparable to the outcome of automated reaction network generation algorithms,[88–91] which reconstruct exact molecular structures from pre-defined reaction rules. Connection between the ESI-MS technique and such an algorithm has been shown for triolein,[92] and it results in computer-aided interpretation of numerous peaks measured by MS.

2.5.3 Fourier-transform Infrared Spectroscopy

While previously described methods are applicable to characterize soluble fractions of oil samples, Fourier-transform infrared spectroscopy (FTIR) allows characterization of the whole sample (sol and gel). This analytical technique performs the identification of functional groups in materials by measuring the absorption of IR radiation in a sample. FTIR analysis is reported in numerous research works on drying oils.[27–29,32,53,85] Table 2.2 in the work by Lazzari et al.[53] summarizes important IR vibrational assignments of linseed oil. The results of FTIR measurements are used to reconstruct the time evolution of relative amounts of functional groups or molecular substructures, such as, for example, *cis* or *trans* double bonds, evolution of hydroxides and carbonyl groups. The limitations appear due to overlap of vibrational bands corresponding to more than one functional group, as shown in the work by Baij et al.,[78] where the contribution of

carboxylic acid is hindered by aldehydes and esters. Profiles from IR spectra can be integrated to obtain relative concentrations of functional groups, which may be used for validation of kinetic models, predicting such concentrations over time. Examples of such modeling for ethyl linoleate are found in works by Oakley et al.[18,19]

2.5.4 Oxygen Uptake

Significant amounts of oxygen are incorporated in the polymer network during autoxidative drying of oils. This quantity can be measured and further used for kinetic model validation. Works by Oyman et al. demonstrate oxygen uptake by ethyl linoleate (EL) for 100 h,[29] and oxygen uptake by linseed and tung oil in the presence of Co(II) 2-ethylhexanoate for 85 h.[93] The measured oxygen uptake forms an absolute measure of concentrations predicted from kinetic modeling, as in the work by Oakley et al.[18]

2.5.5 Peroxide Value

While exploring driers' activity in oils, one needs to monitor the formation and decomposition of peroxides, as these functional groups are targeted by primary driers. Peroxide content in EL, and linseed and tung oils is reported in several works[27,29,32,93] using a standard method of reacting peroxides with iodine.[94] Peroxide value is measured as a concentration profile and may be directly compared with the concentration profiles obtained from the solution of a kinetic model.[18,19]

2.5.6 Thermogravimetric Analysis

While drying, an oil film absorbs oxygen and releases free fatty acids and volatile compounds due to hydrolysis and β-scission. Such chemical processes are characterized by change of mass of the sample. Thermogravimetric analysis (TG) is used to monitor continuous change of

mass of the sample in different temperature regimes. Linseed oil samples aged at 80 °C are investigated with TG in the work by Lazzari et al.,[53] which shows exothermic oxidation processes of unsaturated fatty acids between 150 and 250 °C, oxidative decomposition between 250 and 400 °C and a complete volatilization after 400 °C. In the work by Bonaduce et al.[95] authors monitored the behavior of paint samples made of differently processed linseed oil in the presence of lead white and vine black pigments. The thermogram of the lead white paint is characterized by multiple steps and indicated the presence of carboxylates and free fatty acids, although it is not clear to which extent triglycerides were hydrolyzed. The thermogram of the vine black paint reveals partially hydrolyzed triglycerides, and high molecular weight compounds formed by crosslinking and oxidation.

2.5.7 Nuclear Magnetic Resonance

To analyze the structure of organic molecules, such as those found in drying oils, nuclear magnetic resonance (NMR) is a prevalent method. When placed in a strong magnetic field, isotopic nuclei (commonly ^{1}H and ^{13}C) are perturbed and resonate, giving off a spectra of electromagnetic peaks that can be compared to known frequencies and identified. Several seminal works[34,44,93,96] used ^{1}H NMR, quantitative ^{13}C NMR and ^{13}C NMR with POMMIE to characterize oligomers and crosslinks during ethyl linoleate autoxidation. As a result, quantitative profiles of functional groups during curing were elucidated and have been used to compare to kinetic models.[80] Additionally, NMR has found many applications in the broader field of cultural heritage research, especially following the development of portable NMR sensors.[97–99]

2.6 Computational Modeling

Although performing experiments of the real system are critical in studying the properties of linseed oil-based systems, computational modeling aids in the learning about the kinetics and dynamics of the complex system. One can interrogate a representative model system at different length and time scales ranging from the atomic scale (10^{-15} s and 10^{-10} m) with quantum mechanics to the continuum scale (10^{1} s and 10^{1} m) with equations describing macroscopic objects. Although explicitly modeling triglycerides like linseed oil is relatively new, there is a wealth of fundamental knowledge about related chemistry that can supplement and offer tools in understanding how linseed oil dries and ages.

One way that computational modeling can improve understanding is calculating or approximating kinetic rate constants, especially for short-lived or low-concentration intermediates that are difficult to study and measure experimentally. These rate coefficients inform kinetic models that, when solved, describe the time evolution of chemical species to simulate real world processes. A computational model provides both qualitative and quantitative information about a chemical system and how it responds to changes in environment and time.

Even though computational modeling might fill some gaps that are not accessible via experiments, it has its own limitations for systems with such complexity as the drying process of linseed oil. Because linseed oil triglycerides have more diverse functionality and reactivity than monomers in classical polymers, it is difficult to directly apply polymer reaction engineering tools to model their polymerization process. The diversity of chemical species and their size even pose a challenge to the storage of chemical species in the memory of a computer. Moreover, the diverse chemistry that happens on and between triglycerides and fatty esters explodes the number of

possibilities for intermediate and product species, prohibiting manual reconstruction of a detailed reaction scheme.

This section features existing modeling techniques ranging from calculations of the rate parameters on the quantum scale to modeling macroscopic properties of the material.

2.6.1 Calculating Rate Parameters

If a kinetic rate constant is known experimentally for a specific reaction, it is typically used directly as a first priority over estimation methods. However, it is not uncommon, especially for radical chemistry and complex systems, that experimental rate coefficients are not available for every reaction. One option is then to use computational approaches to approximate a kinetic rate constant: quantum chemical calculations, transition state theory and kinetic correlations.

2.6.1.1 Quantum Chemical Calculations

Quantum chemical calculations (QCC) consider the energy contributions from different modes to determine the energy required to overcome the reaction barrier and transform a reactant into the product. These results and transition state theory (TST) can then derive a theoretical rate constant for a reaction. For a 7-carbon chain with two unsaturations, Szori et al. evaluated the energy requirements for hydrogen abstraction to initiate autoxidation from the methylene position.[100] The work also compared the energy requirements of allylic to the bis-allylic hydrogen abstraction. Applied to ethyl linoleate as a model molecule, Oakley et al. used quantum chemical calculations and TST to determine the mechanism for epoxide formation and aldehyde evolution from β-scission reactions.[36,80] These calculations helped refute mechanisms proposed in literature and support a novel pathways to the formation of hexanal. QCC was successfully applied in the field of catalysis to uncover the reaction between hydroperoxides and Co-EH,[33] as well as in the

works of Pfaendtner et al.[70,101] to estimate rate parameters for other hydrocarbon reactions relevant to oil chemistry.

2.6.1.2 Kinetic Correlations

For short-lived intermediates it can be difficult to measure concentrations over time or get precise data for understudied reactions. Kinetic correlations rely on the thermodynamic similarity between reactions with similar chemistry, such as two hydrogen abstraction reactions, to correlate the enthalpy of reaction to activation energy. Evans-Polanyi correlations, also attributed to Bell and Semenov[102] are linear free-energy relationships. Correlations are developed by including both experimental and theoretical measures for values characterizing the kinetics and thermodynamics of members of specific reaction families. For each reaction family, the transfer coefficient, or a measure of the relative position of the intermediate along the reaction coordinate, is assumed to be identical, and the pre-exponential factor *A* is also assumed to be the same. Using kinetic correlations has advantages in an automated scheme where a reaction type can be identified, and just the rate coefficient of reaction *k* has to be calculated and correlated to the activation energy E_a to be used in the Arrhenius equation:

$$k = A\ exp(-\frac{E_a}{RT}) \tag{2.1}$$

Relevant to linseed oil chemistry is condensed-phase oxidation of hydrocarbons, and there is a collection of kinetic correlations for families and sub-families.[70,101] Oakley et al. studied the radical epoxidation reaction using theoretical calculations and identified subfamilies. They cautioned broad application of reaction families and kinetic correlations, as finer nuances in the local chemistry become significant in the resulting kinetic rate constant as determined from the correlation.[36] For reactions with unknown enthalpies of reaction, group-contribution methods can

be used to estimate standard enthalpies of formation, and other thermodynamic properties, from local molecular structures. Common methods include the Joback method[103] and Benson group additivity,[104] the latter used by Oakley et al.,[19] drawing group values from empirical data tables and selected quantum chemical calculations.

2.6.2 Existing Models

Having calculated rate parameters, computational models of multiple reactions can be constructed to capture the behavior of the concentrations of chemical species as a function of reaction conditions. Nowadays, there exist several microkinetic models describing the drying process of linseed oil and its model systems using different levels of detail, as well as finite element models describing the propagation of cracks caused by the formation of metal soaps. These models are discussed in the section below.

2.6.2.1 Kinetic Model on Functional Groups

The very first deterministic model of the drying process of linseed oil was developed by Iedema et al.[105] A deterministic model is typically a system of ordinary differential equations (ODEs), one for each chemical species or functional group describing a homogeneous system as a function of time. Containing no stochastic aspect in its solution, the model is solved numerically, and the solution describes the change in the concentration of species over time. The first model of linseed oil was constructed in terms of functional groups, includes 70 reactions and is sensitive to the presence of drier. The model describes the main steps of an autoxidation mechanism, and its outcome is validated with the experimental results on the total peroxide content and oxygen uptake.

2.6.2.2 Modeling Polymer Formation

The classical understanding of polymers is based on Flory's extensive work, further developed by Stockmayer, giving the Flory-Stockmayer theory on highly functional molecules, which describes the gel point based on functional group conversion.[106,107] However, this theory assumes that all functional groups are equally as reactive and the monomers do not change, which is not the case for oils. In the work by Kryven et al.,[83] the authors model the formation of a linseed oil polymer network as a random graph that accounts for the Euclidean distance between monomers while connecting them. This implies that two monomers that are far apart have lower probability to be connected. Moreover, the authors connect the notion of steric hindrance of the monomer incorporated in the polymer to the centrality of a node in a network, making monomers with more crosslinks less accessible for further reactions. The formation of crosslinks is modeled as a stochastic process using Markov Chain accelerated Gillespie Monte Carlo,[108] which uses a randomly generated number to select the next reaction event to occur within a scaled time-step of weighted reaction probabilities. Because of the stochastic nature of the model results, these are averaged over several runs and provide the information about gel point transition, molecular size distributions and length of linear fragments. Assuming simple chemistry dictated by functionality of fatty esters in linseed oil as an example, the authors demonstrate novel stochastic approach for modeling molecular networks, which allows applying network theory tools for the analysis of resulting polymers.

2.6.2.3 Rate-based Automated Reaction Network Generation

Several microkinetic models for curing of ethyl linoleate were developed by Oakley et al.[18,19,109] In studying a chemical system at a range of length and time scales, microkinetic modeling

is a multiscale method to span this range by describing chemistry through elementary reactions with no assumption made about the rate-determining step.[110] In the earliest work related to oils by Oakley et al.,[18] the model includes 160 explicit species of EL taking part in 400 autoxidation reactions. The reaction mechanism is transformed into the system of differential equations, which is solved with the kinetic Monte Carlo method. Then, in the following work,[109] a model up to tetramers with 68,197 species and over a million reactions is constructed using automated reaction network generation approach. This approach algorithmically transforms reactants into products and is used to uncover explicit reaction steps of complex chemistry.[111,112] As the resulting system is intractable due to the number of species and size of the ODEs, a reduced model up to hexamers pruning insignificant species determined by rates of formation yields a system of 1384 species and 2898 reactions.[19]

2.6.2.4 Monomer Approach

Orlova et al.[17] followed the work of Oakley et al.[19] and developed a similar kinetic model based on the same reaction families including the latest findings on β-scission and epoxidation.[36,80] The automated reaction network generation methodology transforms initial monomers into further oxidation products and crosslinked species. The advancement in this model is the application of the monomer approach, according to which polymer network is modeled as a random graph in terms of its unique constituents of the size of monomers. The methodology reconstructs explicit structures of monomers with their adjacent crosslinks (alkyl, ether, peroxy) without explicitly connecting them to their neighbors. The number of these monomer constituents of a polymer is finite; thus, such a representation of a polymer allows modeling time evolution of functional groups in infinitely large polymers without imposing any cutoff on their sizes. Concentrations of

each monomer are solved for over time, and lumped functional groups can be compared to experimental values showing good agreement. Polymer species are reassembled using findings in random graph theory from the work by Kryven et al.[83] to obtain the molecular weight distribution of soluble fractions of the polymer and predict temporal formation of the insoluble fraction.

2.6.2.5 Chemo-mechanical Modeling

The chemo-mechanical model has been developed by Eumelen et al.[113] predicting crack formation in the paint surface due to growth of metal soap crystals. Modeling of the chemical process of metal soap formation is coupled with a finite element model, which describes paint around the metal soap as a homogeneous continuum. The growth of the metal soap starts from a nucleus of pre-defined size, which interacts with saturated fatty esters and metal ions on its interface with paint. This process is described by the reaction diffusion equation, and its solution provides the change of saturated fatty ester concentration and the change in volume fraction of the crystalline metal soap. The growth of the metal soap causes the mechanical strain in the paint layer and may result in crack formation, which is modeled using finite element method. Varying the parameters in the simulation shows that crack formation is sensitive to the mismatch of stiffness between the metal soap and paint, strain due to the formation of the metal soap crystal and the reaction rates between metal ions and saturated fatty esters forming ionomers and their subsequent crystallization. Interestingly, the initial size of the nucleus affects only the moment of appearance of the crack but does not influence the amount of cracks.

2.7 Future Directions

Most of the models described above do not simulate polymers moving in physical space, which is necessary to obtain certain physical properties like elasticity and glass transition

temperature. Molecular dynamics and reactive molecular dynamics simulations do offer such possibilities to the field of modeling of oil polymerization. However, these modeling techniques are not yet feasible due to the computational limitations. The limitations arise due to the size and complexity of linseed oil molecules or even its model systems. Modeling polymerization of linseed oil with molecular dynamics would also allow tracking the reactions in space as well as exploring more realistic calculations of such properties as packing density, radius of gyration, gel point, Young's modulus, etc. This has already been demonstrated on the polymer network generation by a diacrylate.[114]

Modeling chemical reactions often requires knowledge of the detailed reaction mechanism of elementary reaction steps. Thus, exploring the studies that have been performed reveals the existence of a number of uncertain chemical reactions that have not been investigated in detail. Bis-allylic hydrogen abstraction has been explored in the presence of metal drier;[33] however, evidence exists that initiation also happen without a drier.[27,53] Hypotheses ascribe this initiation to impurities in oil or to a reaction with singlet oxygen, but none of these have been scientifically confirmed as of writing this review. Russell termination is disputed to be a feasible disproportionation mechanism that occurs in linseed oil-types of systems[37,77] due to a high barrier for the recombination of secondary alkylperoxyl radicals producing ketones. Hence, more thorough investigation is needed to uncover the formation of ketones, which are known to be stable products of autoxidation process.[56] Epoxide ring opening is underexplored, as there is evidence of this reaction taking place from the observed slow decrease in the epoxide signal in NMR measurements carried out by Muizebelt et al.[34]

There is ample room for growth in computational modeling activities of the autoxidation and degradation of linseed oil and related drying molecules. The complexity of the kinetic models is an obvious challenge to improvement. Exploring beyond ethyl linoleate and other single fatty esters to trilinolein or mixtures of fatty acids is necessary to arrive at simulating linseed oil. Also, incorporating light, diffusion effects, other catalysts and pigments is necessary for real-world applications and implications.[5,115]

There is still a great need to link chemical changes on the molecular level to macroscopic, physical changes observed in linseed oil films. This requires work in understanding physical interactions between chemical moieties and potentially more coarse-grained approaches like that of finite element analysis.[113] Additionally, developing models that can realistically predict phenomena on long time scales such as degradation is pertinent to the understanding of aging mechanisms and the impact of different factors like diffusion, light and heat.

2.8 Conclusion

With the improvement of computing power, modeling the polymerization of oils becomes an attractive research topic. In this review, we provide a detailed description of chemical processes occurring in oils together with their chemical kinetics. This review is focused on the polymerization and degradation of linseed oil and its model systems in the context of drying and degradation of oil paint. The work provides an overview of chemical processes happening during the drying process of linseed oil including recent findings in β-scission and epoxidation mechanisms. The description of the reaction mechanism includes chemical kinetics data, which have been estimated computationally or experimentally in past works and are relevant to computational modeling.

Common analytical techniques exploring the drying and degradation of oils provide a vast amount of data, which can be used to validate computational models. Meanwhile, models overcome some of the experimental limitations and are able assist the interpretation of experimental results. The review provides an overview of existing computational models related to oils and their chemistry. Models vary in their complexity and level of detail ranging from studying individual reactions with QCC and extending up to chemo-mechanical models simulating cracks in a paint layer.

Numerous reaction pathways in autoxidative drying of oils are explored in great detail, while other reactions still need thorough explanation. In this review, we highlighted reaction pathways, which lack detailed exploration of elementary reaction steps and their kinetic parameters, suggesting these as an interesting subject for further experimental or computational investigation. This review summarizes the key information needed to carry out computational modeling on linseed oil and its model systems, making the exploration of the degradation of the binding medium of oil paint less invasive for our cultural heritage.

Chapter 3 Insight into Polyethylene and Polypropylene Pyrolysis: Global and Mechanistic Models

Pyrolysis of polyolefins has been proposed as a potential resource recovery strategy by converting macromolecules into valuables fuels and chemicals. Due to variations in possible backbone structures, chain length distributions, and arrangements of pendant groups, their decomposition behavior via pyrolysis can be complicated. In the present work, a review of historical data and empirical models for two distinct polyolefins, polyethylene (PE) and polypropylene (PP), is provided followed by a comparison to recent mechanistic models. The characteristic sigmoidal behavior of linear polymer decomposition is captured with global, lumped-species, and mechanistic models of high-density polyethylene. The polyethylene model was extended to simulate PP using the same reaction families and reaction family parameters, but with distinct rate coefficients that accounted for the difference in the structure of PP with its pendant methyl groups compared to PE as manifested through heats of reaction embedded in the Evans-Polanyi relationship, $E_a = E_0 + \alpha * \Delta H_{rxn}$. The change in structure and its associated kinetic parameters resulted in no sigmoidal conversion, consistent with experimental reports for atactic PP. This suggests that mechanistic modeling could be an important complement to global model studies to understand when other effects are at play in the pyrolytic decomposition of polymers such as polypropylene.

Material in this chapter is reproduced from the following peer-reviewed article: Harmon, R. E.; SriBala, G.; Broadbelt, L. J.; Burnham, A. K. Insight into Polyethylene and Polypropylene Pyrolysis: Global and Mechanistic Models. *Energy & Fuels* **2021**, *35* (8), 6765–6775.

3.1 Introduction

Hydrocarbon polymers are now a pervasive product of our industrial age to the point that they are a significant environmental pollution problem. Although there are active efforts to increase recycling in the polymer form, they are also a potential source of energy in general and liquid fuels in particular due to their favorable molecular structure. For example, single-use plastics can be converted to naphtha, opening an avenue to integrate plastics as a feedstock in petroleum refineries.[116] Liquid fuels have a higher value per weight than when used either by combustion in raw form or after conversion to syngas. Some have even proposed mini-pyrolysis units to generate fuel oil locally for cooking stoves in developing parts of the world.[117] This use could have beneficial environmental and health benefits as long as halogenated polymers were excluded.

In addition, oil and gas are formed in the subsurface by pyrolysis reactions that occur over millions of years. While this is not a typical perception of pyrolysis conditions, petroleum geochemists have developed chemical reaction models for these reactions based on laboratory pyrolysis experiments. Some well-preserved algal kerogens have linear structures that give sigmoidal conversion character similar to that of linear polymers,[118] while others have branched and crosslinked structures that require distributed reaction models.[119] Also, understanding how secondary reactions change as a function of time, temperature, and pressure can help understand the reliability of petroleum generation and cracking reactions.[120]

Conversion of polymers to any new product requires an understanding of how time, temperature, and pressure affect the product distribution and quality as a function of molecular structure, including weak links, branching, and crystallinity. Included in this goal is understanding how compositional variations in the feedstock affect the conditions for optimum product quality

and value. The current work is motivated to address that issue. It also follows in the spirit of our previous contribution addressing cellulose pyrolysis.[121]

Process modeling has historically taken various approaches, which might be described approximately in terms of three classes: global kinetic models, lumped-species pseudo-mechanistic models, and true mechanistic models.[122] In this paper, we first review the experimental data from literature for polyethylene (PE) and polypropylene (PP), which are two very common commodity polymers, and later explore connections and discrepancies among those three approaches for the thermal degradation of polymers.

3.2 Lumped-species and Global Kinetic Models

True mechanistic models for polymer pyrolysis contain hundreds of species and thousands of reactions. In lumped-species models, the mechanism is reduced to several species and perhaps a dozen reactions, depending on the material and application. Global kinetic models further simplify the reaction network to one or two reactions with a global stoichiometric product distribution. Mechanistic details are lost through this progressive simplification, but if done well, the resulting models capture the most important aspects of the reaction mechanism.

Polyolefin polymers decompose by a free-radical chain reaction mechanism. The fundamentals of free-radical chain reactions date back to Rice and coworkers[123,124] at about the same time that PE started being produced commercially. Excellent work on thermal decomposition of polyolefins was conducted in the 1940s and 1950s, much of which was reported in 1953 in the National Bureau of Standards Circular 525.[125] Kinetic concepts first presented in that document are applied in this paper. Specifically, the reaction may be either deceleratory or sigmoidal, depending on the polymeric structure and the details of its decomposition mechanism. By

deceleratory, we mean that the rate of decomposition is at its maximum value at the initial time for isothermal conditions. In contrast, a sigmoidal reaction profile starts with a small rate at the initial time and then rises to a maximum rate before declining to zero as the material is consumed.

The overall decomposition of a long hydrocarbon chain, be it in petroleum or a polymer, is described generally by:

End initiation: $P_n \rightarrow R_{n-1} + R_1$

Random initiation: $P_n \rightarrow R_{n-i} + R_i$

Hydrogen abstraction: $R_i + P_n \rightarrow P_i + R_n$

β-scission: $R_n \rightarrow P_{n-j} + R_j$

Depropagation: $R_n \rightarrow R_{n-1} + P_1$

Termination by disproportionation: $R_i + R_j \rightarrow P_i + P_j$

Termination by recombination: $R_i + R_j \rightarrow P_{i+j}$,

where P_i is a dead polymer chain of length *i*, and R_j is a radical of length *j*. Here, depropagation is listed as a separate reaction from β-scission to show explicitly the formation of monomers, but it is rigorously a β-scission reaction. Furthermore, in more detailed mechanistic treatments of polymer pyrolysis developed by Broadbelt and coworkers,[126–129] the reverse of β-scission, i.e., radical addition, is also included, and backbiting reactions such as 1,5- and 1,4-hydrogen transfer are also incorporated.

There are some variations in this formalism in the literature. For example, Simha and Wall[130] do not consider termination by recombination, and Bouster et al.[131] do not distinguish between random and end initiation. In the most detailed mechanistic treatments currently available, however, the highest degree of detail possible is maintained so that reactivity and structure are

explicitly linked.[126,127,129] Because mechanistic models can be challenging to develop and solve, various simplifications have been invoked. For example, Simha and Wall used their limited mechanism to develop statistical models on how molecular weight evolves with time. Starting with an initial chain length of N and picking a threshold chain length, L, for volatilization, they obtained

$$1 - \alpha = (1 - x)^{L-1} \left[\frac{(N-L)(L-1)}{N}\right] \tag{3.1}$$

where x is the fraction of bonds broken and α is the fraction volatilized. Burnham et al.[118] used qualitative arguments to draw links among this equation, the Prout-Tompkins equation,[132] and its extended form with a non-integer growth coefficient.[133] Further, Sanchez-Jimenez et al.[134] derived a more rigorous relationship between α and x:

$$\mathrm{d}\alpha/\mathrm{d}t = kL(L\text{-}1)x(1\text{-}x)^{L\text{-}1} \tag{3.2}$$

where k is the reaction rate constant. In the conventional notation of thermal analysis, the reaction rate is usually expressed as a rate constant times a simple function of conversion ($\mathrm{d}\alpha/\mathrm{d}t = k\, f(\alpha)$), so

$$f(\alpha) = L(L\text{-}1)x(1\text{-}x)^{L\text{-}1} \tag{3.3}$$

For L=2, this equation is the standard logistic (Prout-Tompkins) model. The shape of a plot of $f(\alpha)$ versus α is approximately independent of L, but the overall reaction rate increases, because fewer bonds must be broken to form a volatile fragment. If the reactivity of the remaining material were the same as the original, $f(\alpha)$ would equal 1-α, a first-order reaction, so the amount of deviation from first order is a measure of the change in reactivity of the remaining material.

Bouster et al.[131] approach the solution a little differently and derive the relation (again, in thermal analysis notation):

$$f(\alpha) = (1\text{-}\alpha)[1\text{-}(1\text{-}\alpha)^{2b}]^{1/2} \tag{3.4}$$

where b for polypropylene[135] also has an Arrhenius form, $b = b_o \exp\left(\frac{E_b}{RT}\right)$.

Out of the solid-state decomposition literature come the JMAEK[136–139] and Prout-Tompkins[132] models, and the following briefly summarizes the description presented earlier for cellulose pyrolysis.[121] The JMAEK model is a random nucleation and geometric growth model in which the reaction rate increases with the growing reaction interface but eventually declines as the reaction volumes converge. In thermal analysis formalism, it is given by

$$f(\alpha) = p(1-\alpha)[-\ln(1-\alpha)]^{(p-1)/p} \tag{3.5}$$

where p is a growth dimensionality. The Prout-Tomkins model is simply the empirical application of the standard logistic equation to sigmoidal reactions. It has been used with both linear and logarithmic time. More interesting, it can be related to a first-order autocatalytic reaction which, after generalization and simplification, gives the extended Prout-Tompkins (ePT) equation[133]

$$f(\alpha) = (1-\alpha)^n[1-q(1-\alpha)]^m \tag{3.6}$$

where n is a reaction order and m is a growth coefficient that is approximately equal to p-1 for similar reaction profiles. The parameter q approximately equals $1-k_1/k_2$, where k_1 is the rate coefficient for the initiation (nucleation) reaction, and k_2 is the rate coefficient for the propagation (growth) reaction.[140] The ratio k_2/k_1 is called the autocatalytic strength and correlates with the tendency of the reaction to run away if it is exothermic and combined with poor heat dissipation.

3.2.1 Global Kinetic Analysis of Polyethylene Decomposition

Chemical kinetic studies of PE have a long history, with the most extensive work being in the 1950s at the National Bureau of Standards and reviewed by Flynn and Florin.[141] These early isothermal studies established that linear PE had a maximum reaction rate at 20-40% conversion, with the latter being at the highest temperature, 420 °C. However, these experiments were

conducted in a vacuum, which enhances volatilization, so caution is warranted when applying these conclusions to relatively rapid heating rates at atmospheric pressure.

Westerhout et al.[142] reviewed the literature and commented that most workers inappropriately use a simple nth-order reaction. Their data in N_2 at atmospheric pressure confirm the NBS results that a maximum volatilization rate occurs at about 30% conversion for isothermal heating of high-density (linear) PE, which requires some sort of sigmoidal reaction model.

Rates of thermal decomposition of an unspecified high-density polyethylene (HDPE)[143] were obtained in 1996 using a Pyromat instrument[119] with a flame ionization detector. Replicates were run at heating rates of 0.97 and 50.5 °C/min to ensure precision, and a single run at 6.8 °C/min verified the interpolation of the reaction profile shape. Those data were fitted to the ePT model using q = 0.99, and the results are shown in Table 3.1 and Figure 3.1. The extended Kissinger method[133] uses profile width and asymmetry to estimate m and n and an adjusted value of A for the ePT model, and those values were used as initial conditions for the nonlinear optimization on measured reaction rates. Allowing n to be optimized enabled a significantly better fit due to the asymmetry of the reaction profile. The activation energies are in the middle of the range reported in the literature.[144]

Table 3.1. Extended Prout-Tompkins kinetic parameters for HDPE.

Parameter	**Extended Kissinger**	***n* constrained**	***n* optimized**
A, s^{-1}	1.965×10^{15}	1.886×10^{15}	1.715×10^{15}
E_a, kJ/mol	246.4	246.3	247.0
m	0.64	0.562	0.464
n	0.94	1.00	0.824
r.s.s. of rates[a]	---	2.04	1.59
r.s.s. of conversion[b]	---	0.463	0.353

[a]sum of squares of normalized rate residuals
[b]sum of squares of normalized cumulative residuals

Although there is no universally accepted method of calculating uncertainties from nonlinear regression as exists for linear regression, comments about the uncertainty in A and E_a are appropriate. First, the standard error in E_a from Kissinger's analysis is only ±0.2 kJ/mol, and the corresponding correlated change in A is 3%. These values represent the statistical uncertainty only and not the effects of any systematic errors, such as a non-constant error in temperature calibration as a function of temperature, so the true error is larger by some unknown factor. For nonlinear regression, the uncertainties of all four fitted parameters are correlated. Constraining E_a to 246.6 kJ/mol increases the r.s.s. of rates by 0.1% and decreases the r.s.s. of conversion by 4.5%. This result points out an additional uncertainty aspect that the regression results will depend on whether on optimizes on reaction rates, conversion, or a combination of both. For the purposes of this paper, there is certainly no significant difference in the three E_a values in Table 3.1.

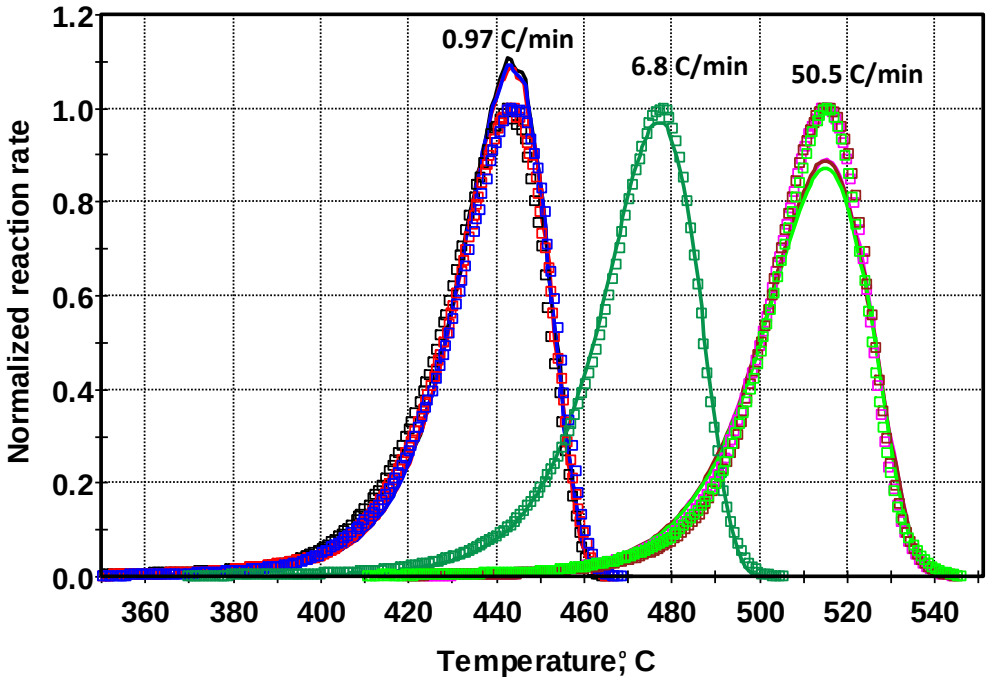

Figure 3.1. Comparison of measured[143] (shown as points) and calculated (shown as lines) reaction rates with repeated runs at 0.97 °C/min and 50.5 °C/min heating rates for thermal decomposition of HDPE using parameters optimized, including reaction order.

Scaled master plots have been a standard way of examining kinetic models for decades. Recently, Gotor et al.[145] presented various methods that can be applied to both isothermal and ramped heating experiments. The most useful method in terms of being able to discriminate various mechanisms is

$$\frac{f(\alpha)}{f(0.5)} = \frac{\mathrm{d}\alpha/\mathrm{dt}}{\mathrm{d}\alpha/\mathrm{dt}_{\alpha=0.5}} \frac{\exp\left(E_a/RT\right)}{\exp\left(E_a/RT_{0.5}\right)} \tag{3.7}$$

where the reaction rates are normalized at half conversion and scaled for arbitrary thermal histories by the apparent activation energy.

The normalized reaction rate plot calculated using Equation 3.7 is shown in Figure 3.2. The calculated curve used the parameters in Table 3.1 that were optimized for *n*. The experimental maxima are at about 30% conversion at 0.97 °C/min (lower reaction temperature) and 40% at 50.5 °C/min (higher reaction temperature). This trend is the same as observed by Bouster et al.[131] for polystyrene and PP. A related breakdown of a single activation energy model is reflected in the reaction profiles becoming narrower in Figure 3.1 relative to the ePT model as the heating rate increases. This result indicates that the temperature dependence is more complex than can be modeled by a single activation energy model, so caution should be used when extrapolating outside the range of calibration. Even though the maximum rate occurs at different conversions for isothermal conditions, it occurs at 0.64 conversion at all heating rates, with an overall standard error of 0.015. Consequently, even though Kissinger's method is known to breakdown sometimes,[146] that does not appear to be the case here.

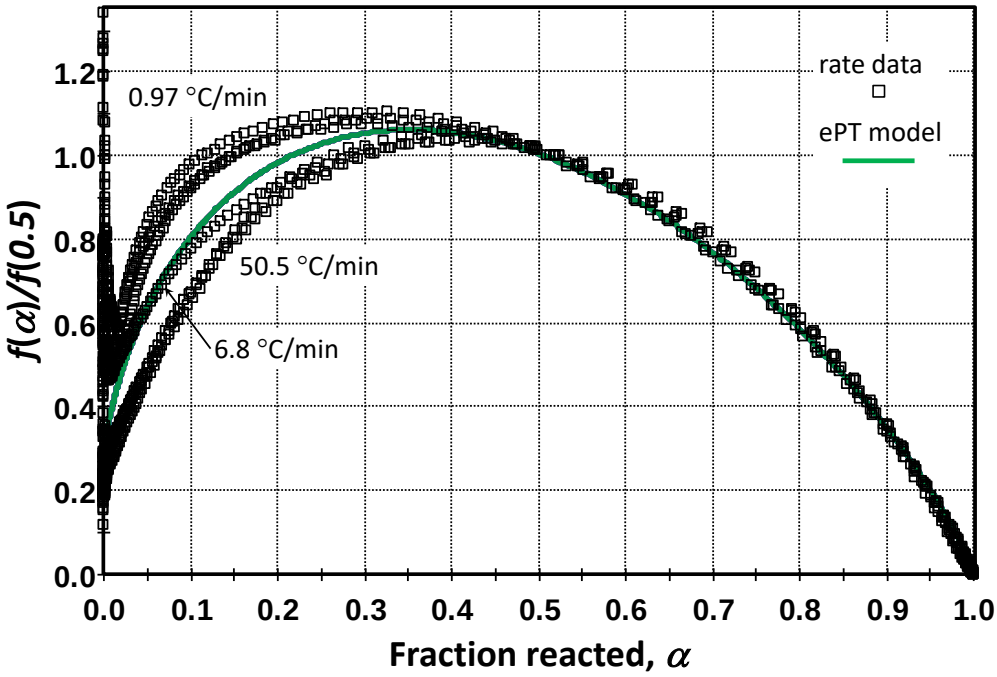

Figure 3.2. Normalized reaction rate plot for HPDE at three different heating rates, 0.97 °C/min, 6.8 °C/min and 50.5 °C/min. The 0.97 °C/min and 50.5 °C/min lines cluster above and below the calculated curve, respectively.

Polyethylene decomposition kinetics vary due to the amount of branching and possibly other factors. The degree of branching affects the number of secondary and tertiary carbon atoms, but it is also reflected in the density and crystallinity. More chain linearity and fewer weak links lead to a narrower reaction profile. Of course, the reaction profile can also be affected by additives and heat and mass transfer effects, so comparison with literature data must be interpreted cautiously.

A survey of the literature indicates that the LLNL Pyromat reaction profiles in Figure 3.1 and in Burnham and Braun[143] are narrower than most others in the literature. Specifically, the delta T between 10 and 90% conversion are 37 and 34 °C, respectively, for low-density polyethylene (LDPE) and HDPE. These values are compared in Figure 3.3 to profile widths estimated from

published reaction profiles[144,147–154] as a function of T_{max} at 10 °C/min for 15 determinations in addition to the Pyromat measurements. The HDPE samples tend to have higher T_{max} values and narrower profile widths, although there is considerable scatter due to digitization and calibration issues. For the five cases in which one lab studied both materials, the T_{max} values averaged 4 °C higher, and profile widths averaged 6 °C narrower for HDPE. Obviously, a much better relationship could be determined by a single laboratory measuring a set of samples having a range of densities.

The 20 °C temperature range of T_{max} in Figure 3.3 indicates a large variation in reactivity for different polyethylene samples. Even allowing that 5-10 °C of that range is due to temperature calibration errors and variations in peak shape, the remaining 10-15 °C range is substantial.

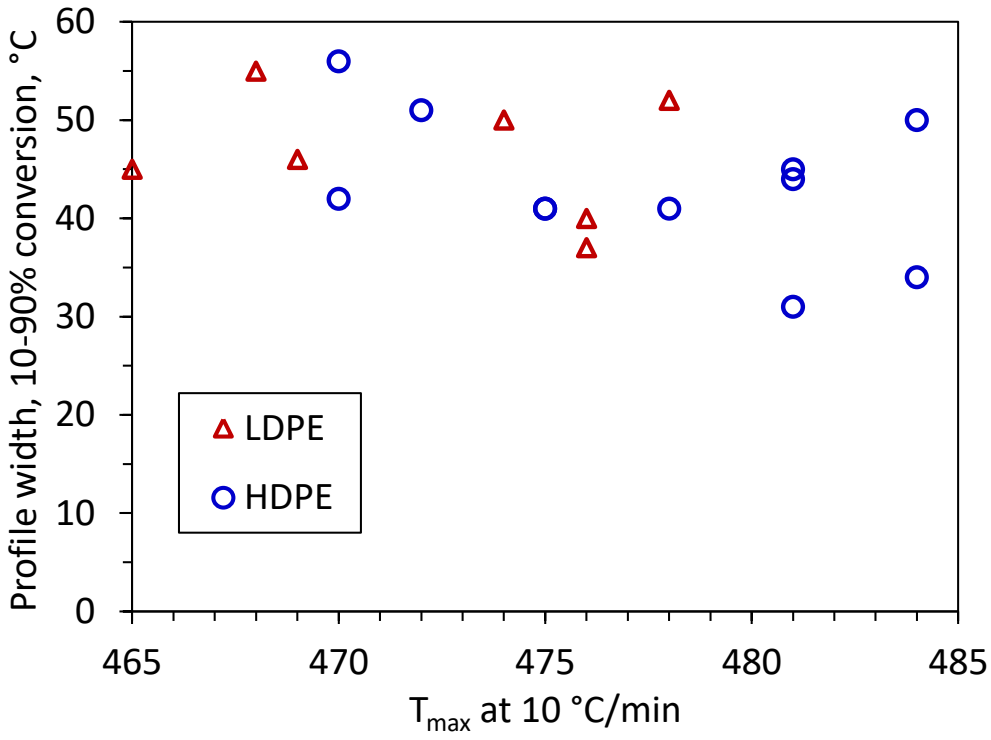

Figure 3.3. Plot of pyrolysis reaction profile widths[144,147–154] as a function of the temperature of maximum reaction when LDPE or HDPE is heated at 10 °C/min.

For a typical E value of 245 kJ/mol, every 5 °C shift corresponds to a change in the reaction rate of 30%. A plausibly real range of 15 °C in T_{max} implies a 2.3× variation in the time required to pyrolyze PE at a constant temperature.

A particularly interesting data set is from Budrugeac,[147] who reports both isothermal and ramped heating experiments. Of course, the isothermal experiments have initial ramps, and 5-10% of the reaction occurs during those ramps. A rigorous stepwise approach to determine the polymer conversion during ramp-up is detailed further in the mechanistic PE model section. Also, in our regression analysis, that is not a problem, because the analysis integrates through the exact thermal history. Results for a set of models of varying complexity are shown in Table 3.2. The reaction profile is both narrow and skewed to low temperature, which suggests a single reaction is not adequate. These properties are reflected in the *m* and *n* values of the extended Kissinger analysis of the ramped experiments. Optimizing either *m* or *n* to all experiments simultaneously to both rates and fractions reacted gave equally good fits. A better fit was obtained by fitting both *m* and *n* simultaneously but with a physically unrealistic value of *m*. A far better fit was obtained using two reactions. The initial parameter *q* was 0.99 in all cases.

Table 3.2. Extended Prout-Tompkins kinetic parameters for HDPE analyzed by Budrugeac.[147]

Parameter	Extended Kissinger	optimize *m*	optimize *n*	optimize *m*,*n*	1st rxn = 15% 2nd rxn = 85%
A1, s^{-1}	3.92×10^{14}	1.877×10^{15}	9.78×10^{14}	1.600×10^{15}	1.58×10^{9}
E1, kJ/mol	239.7	247.2	246.0	249.1	161.1
m1	0.51	0.186	0.000	-0.034	0.000
n1	0.87	1.00	0.557	0.518	0.826
A2, s^{-1}					3.46×10^{15}
E2, kJ/mol					249.0
m2					0.464
n2					1.000
r.s.s. of rates	---	10.2	10.1	3.96	1.18
r.s.s. of conversion	---	0.91	0.91	0.196	0.098

A comparison of measured and calculated conversion values at ramped and isothermal conditions for the two-reaction model (two independent, parallel, extended Prout-Tompkins reactions, with 15% and 85% relative contributions) is shown in Figure 3.4. Although the model tends to lag the data a little at the highest conversions for both the ramped and isothermal experiments, the agreement is excellent overall. The two-reaction model is also consistent with the normalized reaction rate plot shown in Figure 3.5. Above a fraction reacted of 0.2, the data tend to follow an ePT reaction model with $m \approx 0.5$. However, at lower conversions, the normalized reaction rate tends to level off and then rise sharply as conversion approaches zero.

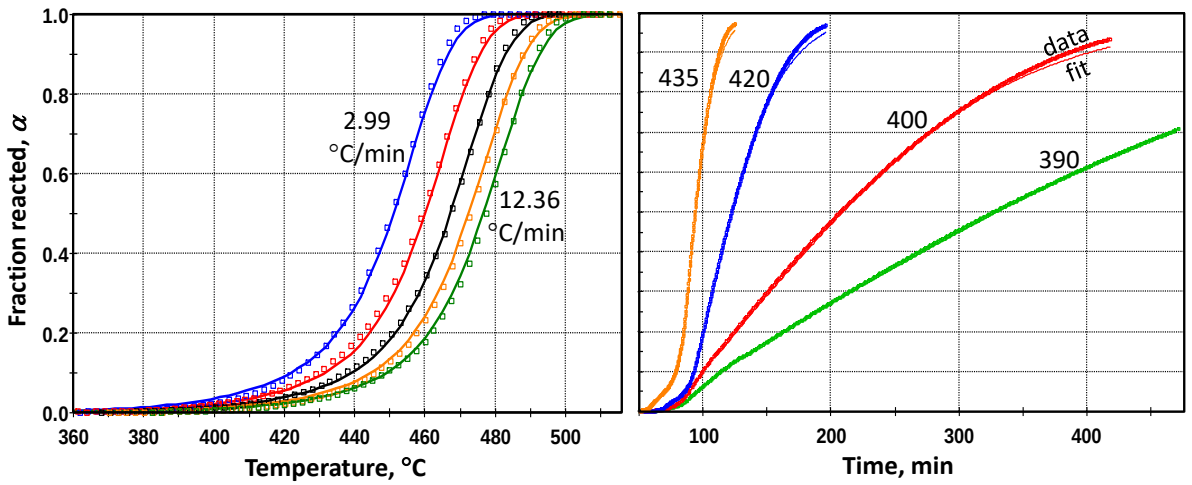

Figure 3.4. Comparison of calculated conversions (lines) for the two-reaction model in Table 3.2 with data (points) from Budrugeac[147] at heating rates of 2.99, 4.98, 7.44, 9.88, and 12.36 °C/min and nominally isothermal temperatures from 390 to 435 °C.

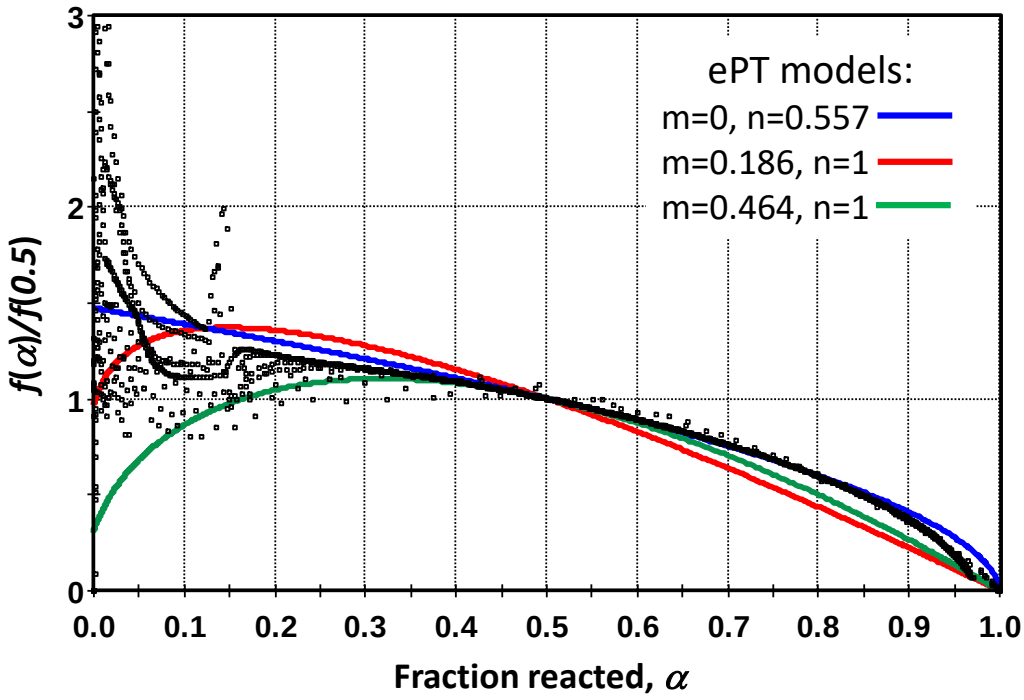

Figure 3.5. Normalized reaction rate plot for both the ramped and isothermal experiments of Budrugeac.[147] The three colored lines are single reaction models using parameters from the three nonlinear regression models in Table 3.2. The anomaly at $\alpha \approx 15\%$ was a momentary thermal excursion in one of the isothermal experiments.

Comparing these results with others in the literature, it seems that there is a variable amount of labile material even in nominally high-density PE. The sample analyzed by the Pyromat instrument seems to have the lowest concentration of this labile material, which leads to a sharper reaction profile. The PE used by Budrugeac seems to be typical of commercial HDPE. The temperature of the peak reaction rate of these two materials is very similar.

3.2.2 Global Kinetic Analysis of Polypropylene Decomposition

Although there are many papers on the thermal decomposition of PP, an early paper by Amorim et al.[135] provides data at both isothermal and ramped heating conditions for 85% isotactic PP. That data was digitized and analyzed by Kinetics2015 using Friedman isoconversional,[155]

Kissinger,[156] and ePT methods. The digitized data was shifted by 5 minutes to account for reactor heat-up time. The isoconversional results varied somewhat for the different heating regimens, but the general result is that E_a was about 235 kJ/mol over 30-70% conversion and more erratic at high and low conversion, as is typical for that method. Kissinger's method gave E_a=236 kJ/mol and A=5.60×10^{14} s^{-1}. The reaction profile was only 63% as wide as a first-order reaction using the Kissinger A and E_a values. The profile asymmetry was 0.68, about the same as a first-order reaction. Using the simple algorithms in Burnham,[133] an initial estimate of m=0.61 was derived. Subsequent nonlinear regression of the ramped and isothermal data separately and together gave the results in Figure 3.6, and the resulting kinetic parameters are consistent with the simpler methods. Reaction order n and initiation parameter q were constrained to 1.0 and 0.99, respectively, in all cases. The parameters from fitting all data simultaneously would likely give the most reliable estimate for an arbitrary thermal history.

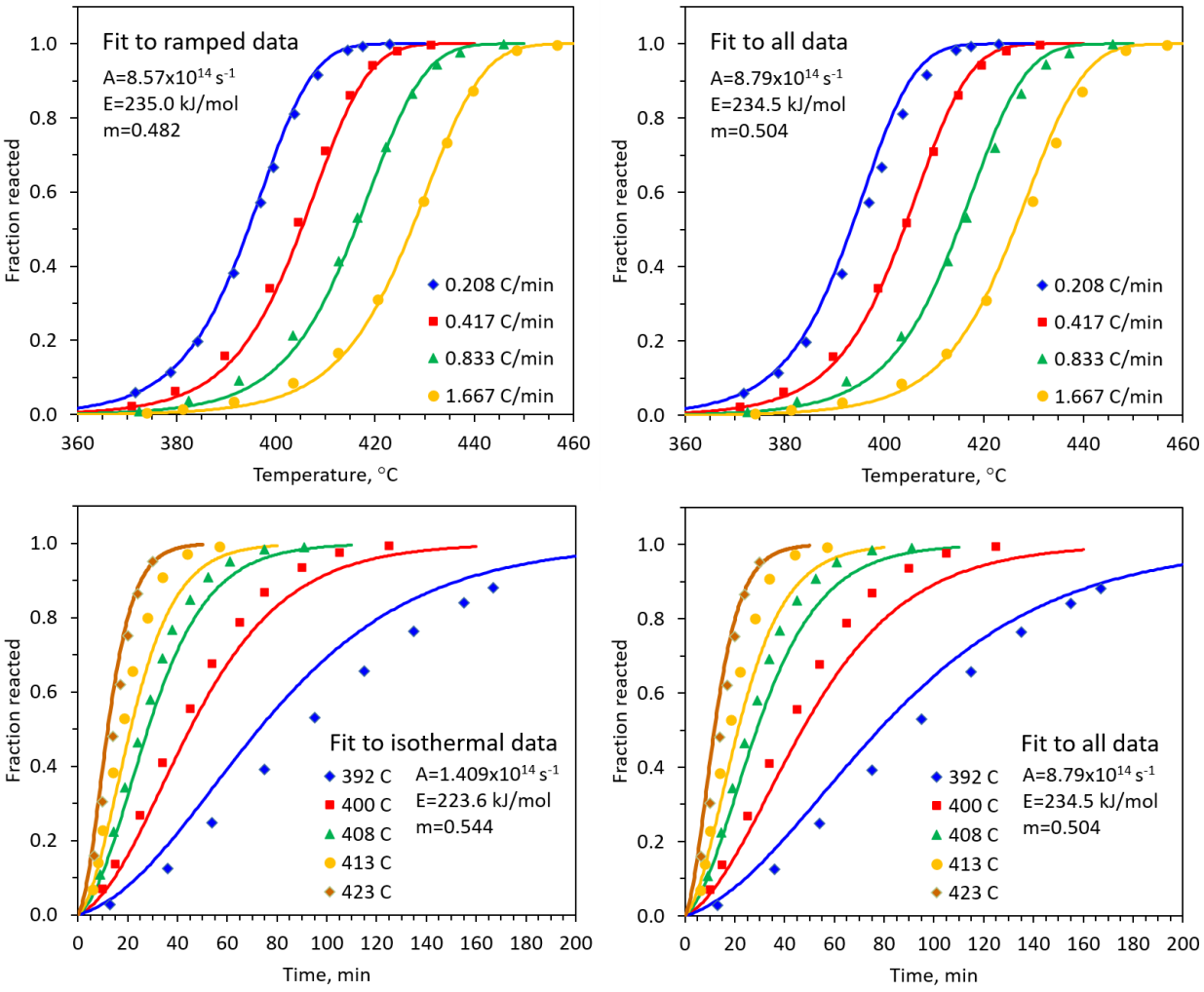

Figure 3.2. Fits of the ePT model to the PP thermal decomposition data of Amorim et al.[135] Experimental data are shown as points, and fits are depicted using lines.

Figure 3.7 uses Equation 3.7 to compare all the data from Amorim et al.[135] to the curves calculated from the ePT parameters derived by nonlinear regression of all data. In addition, Figure 3.7 shows curves from three other sigmoidal models calculated simply from their functional form.

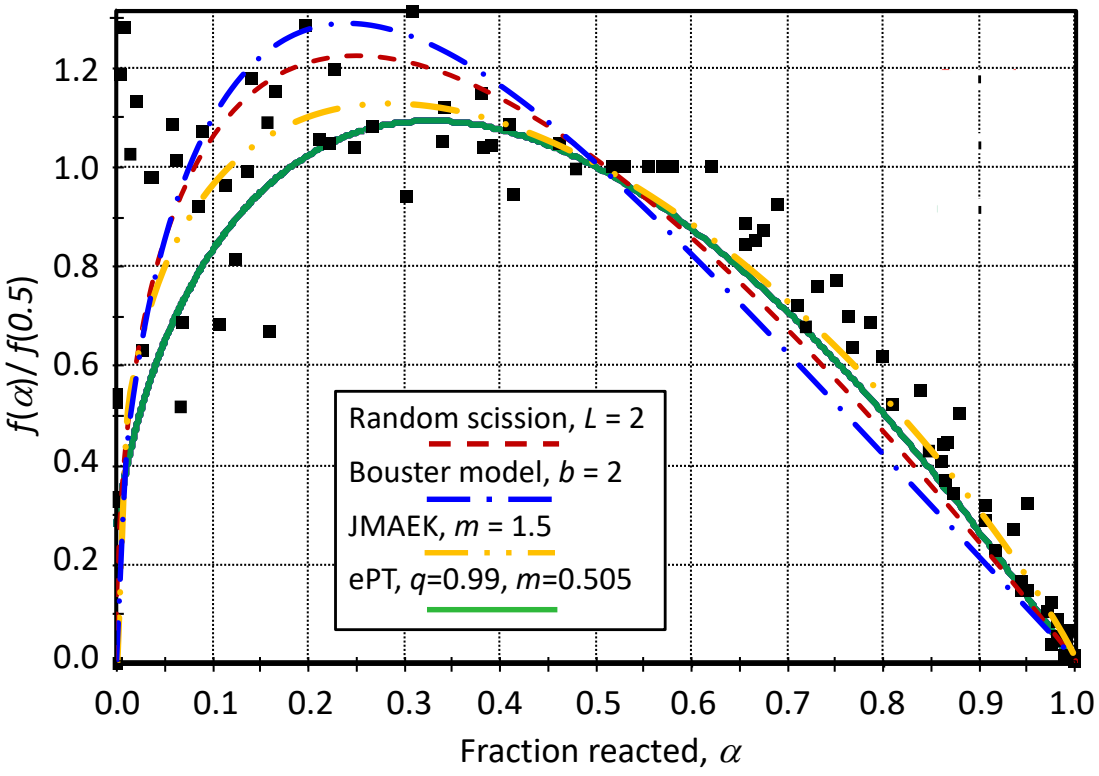

Figure 3.7. Comparison of observed (points) and calculated (lines) normalized reaction rates, where the former have been calculated for ramped heating using Equation (3.7) from the data of Amorim et al.[135]

All models agree qualitatively with the measured results. Each model curve can be changed somewhat by adjusting the relevant shape parameters.[121] For example, changing the random scission chain length, L, from 2 to 8 drops the maximum by 4% and shifts it from 0.25 to 0.28. Similarly, changing the Bouster parameter, b, from 2 to 1.5 decreases the maximum by 5% and shifts it from 0.24 to 0.26. Recall that b has an Arrhenius form, and Bouster et al.[131] found that E_b

was negative and *b* decreased from 2.57 at 331 °C to 1.20 at 380 °C for polystyrene. Amorim et al.[135] found similar values and trends for PP.

The two-parameter ePT model is the most flexible. Changing *m* to 0.25 shifts the curve maximum to 0.18, and changing it to unity causes the curve to be symmetric about 0.5 conversion. Decreasing *n* causes the maximum to be shifted to higher conversion, and increasing *n* causes the opposite shift. Using *n*=0.8 causes the normalized rate to agree well for conversion greater than 0.5, but reaction profile width as well as peak shape must be matched, which leads to other parameter constraints.

3.3 Mechanistic Models

Pyrolysis of polymers, PE and PP in particular, involves a wide variety of reactions leading to a broad product distribution. As mentioned previously, mechanistic models are characterized by detailed reaction mechanisms involving hundreds to thousands of elementary reaction steps and reactive species. Such models allow for detailed product distribution studies based on thermodynamics and kinetics of the underlying reactions, quantifying the short oligomers and small molecules that can be measured experimentally as they are formed from a variety of reaction pathways. It is also possible to track the extent of depolymerization in terms of polymer chain length and molecular weight distribution.

Discrete models based on methods such as kinetic Monte Carlo (kMC) enable tracking of every elementary reaction and the reactant and product species at each time-step. However, it can become complex and computationally intensive to build such models for the pyrolysis of polymers with longer chain lengths. Continuous distribution kinetic models[157,158] involve lumping of polymeric and free-radical species populations that are tracked according to the moments of their

distributions and are less computationally expensive. Although the detailed structural information of the degrading polymer is lost, these models can still provide its molecular weight distribution and structural detail at the level of the types of chains that are tracked (e.g., chains with unsaturated groups, chains with weak links, etc.). Vinu and Broadbelt[110], and Zhou, Broadbelt and Vinu[159] presented a detailed overview of the continuum models for polymer pyrolysis. In brief, the population balance rate equations are solved by applying the method of moments to determine the concentration, mean, and spread of similar polymer species that are grouped by specific features but not their chain length, which is tracked as distributions according to moments. The details of the model formulation, rules used for the different reaction families in the generalized mechanism above, and other specific details are outlined in the reviews.[158,110]

While the diversity of reactions and the level of detail that is tracked in mechanistic models are its strengths, they present challenges because a rate coefficient needs to be specified for each distinct reaction in the model. Therefore, a hierarchical approach to specifying rate coefficients is used, leveraging structure-reactivity relationships. The Evans-Polanyi kinetic correlation,[102] given as $E_a = E_0 + \gamma * \Delta H_{rxn}$, specifies the activation energy of individual reactions from the enthalpy of reaction and two reaction family parameters, E_0 and γ, an intrinsic barrier and transfer coefficient, respectively. In addition, each reaction in a reaction family shares the same Arrhenius pre-exponential factor. Using these correlations, temperature-dependent rate coefficients can be calculated using the Arrhenius equation, $k = A*exp(-E_a/RT)$. The combination of the mechanistic formulation of the reactions and their rate coefficients with reactor design equations that describe the reactor of interest allows for the interrogation of reaction pathways at the mechanistic level.

3.3.1 Mechanistic Analysis of Polyethylene Decomposition

The model developed by Levine and Broadbelt[129] was employed to obtain mechanistic insights into PE pyrolysis. The reaction family parameters in the model of Levine and Broadbelt are summarized in Table 3.3. The model was used to simulate the experimental data of Westerhout et al.,[142] corresponding to isothermal HDPE pyrolysis at 440 °C. When the model parameters were used without adjustment, the overall rates compared to the experimental data were slightly low. Given that the pre-exponential factors are representative values, it is feasible to adjust them slightly within the bounds set by transition state theory, particularly since Levine and Broadbelt developed their model against data collected in closed batch reactors in which secondary or tertiary reactions may be more prevalent. Specifically, $A_{H\text{-}abs}$ and $A_{\beta\text{-}scission}$ were selected for slight adjustment. In general, $A_{H\text{-}abs}$ increased the initial rate of conversion of PE, while an increase in $A_{\beta\text{-}scission}$ increased the overall conversion. Moreover, higher $A_{H\text{-}abs}$ values significantly lowered the end-chain radical concentrations and led to a faster production of low molecular weight (LMW) radical species. On the other hand, higher β-scission rates increased the concentration of these LMW radical species, which explains the increase in overall conversion. The final values of $A_{H\text{-}abs}$ and $A_{\beta\text{-}scission}$ adjusted against the data of Westerhout et al.[142] are summarized in Table 3.3.

The model with the rate parameters validated against the data of Westerhout and coworkers was then used without any further adjustment in parameters to predict a different data set, the experimental data reported by Budrugeac[147] under quasi-isothermal conditions (Figure 3.8). The model simulations were performed with a stepwise temperature profile that mimics the quasi-isothermal temperature profile. It can be observed from Figure 3.8 that there was negligible conversion predicted by the model during the temperature ramp which is in good agreement with

Budrugeac's data. The overall trends in the temperature dependence are captured very well, with a slight underproduction of the rate at the lowest temperature and times. Notably, though, the sigmoidal character of PE pyrolysis is clearly observed, manifesting at temperatures as low as 400 °C and persisting even at higher temperatures.

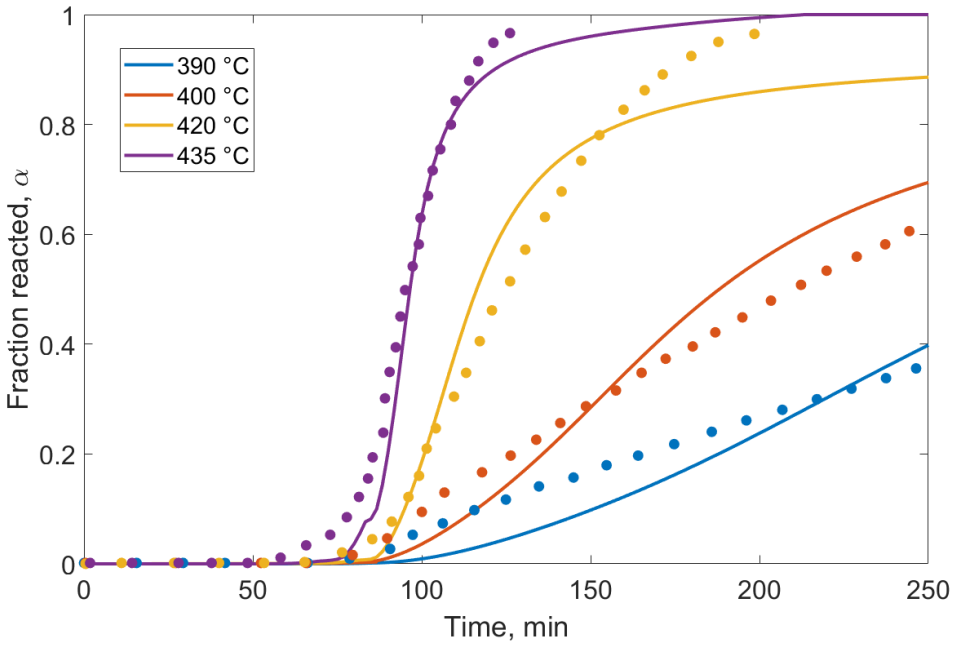

Figure 3.8. Comparison of predictions of conversion from the HDPE mechanistic model (lines) and the experimental data reported by Budregeac.[147]

The detail inherent in the mechanistic model allows a quantitative analysis of the observed sigmoidal character. Kinetic chain length, calculated as the ratio of the rate of radical propagation to the rate of initiation, is shown for PE in Figure 3.9 for a wide range of pyrolysis temperatures. The longer the kinetic chain length, the longer a free radical can react before terminating. The sigmoidal decomposition of PE stems from the slower rate of radical initiation relative to the dominating rate of propagation comprised of an accumulation of more-stable mid-chain and primary end-chain carbon radicals, thus accelerating the conversion of the polymer fraction to

LMW products. Additionally, as the temperature increases, the rate of initiation has a stronger temperature dependence (higher E_a) and increases more than that of propagation, thus lowering the ratio and shortening the chain length. Although the detail is not shown here, it is important to note that the rate of initiation and the rate of propagation are not simply a result of one reaction each, but instead are calculated from the rates of tens to hundreds of individual elementary steps. Thus, the overall rates represented in Figure 3.9 as a single kinetic chain length changing as a function of time and temperature can be dissected in even greater detail if desired, allowing the dominant rates of each family to be identified and related to the specific radical classes or chain types that are contributing most significantly. Furthermore, the evolution of individual low molecular weight products is also explicitly provided by the model. Results are not shown here since the focus of this work is on conversion and global conversion measures, but temporal yields of products as a function of time and temperature are output by the model.

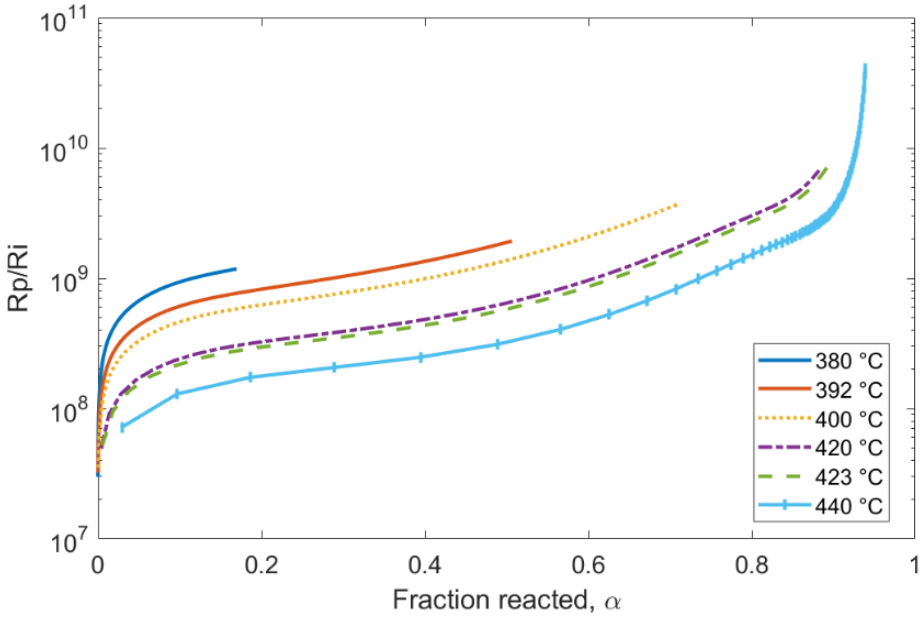

Figure 3.9. Variation in HDPE kinetic chain length, R_p/R_i, as a function of fraction reacted at temperatures over the range of 380-440 °C.

Table 3.3. Reaction family parameters used in mechanistic models of PE and PP. Bolded values are adjusted in this work. [a]

Reaction type	**Frequency factor, *A* (s^{-1} or L mol^{-1} s^{-1})**	**Intrinsic barrier, E_0 (kcal mol^{-1})**	**Transfer coefficient, γ**	**Representative ΔH_{rxn} for PE (kcal/mol)**
Chain fission	1.00×10^{16}	2.3	1	87.4
Allyl chain fission	5.50×10^{13}	2.3	1	72.9
Radical recombination	1.10×10^{11}	2.3	0	-87.4
Disproportionation	1.10×10^{10}	2.3	0	-
End-chain *β*-scission	1.29×10^{13}	11.4	0.76	22.3
Mid-chain *β*-scission	5.35×10^{14} **8.00×10^{14}**	11.4	0.76	23.0
β-scission to LMWS	2.33×10^{13} **8.00×10^{14}**	11.4	0.76	22.0
Radical addition	2.88×10^{7}	11.4	0.24	-23.0
Hydrogen abstraction	2.75×10^{8} **5.00×10^{8}**	12.0	-	-1.57
1,4-Hydrogen shift	1.58×10^{11}	-	-	-
1,5-Hydrogen shift	1.82×10^{10}	-	-	-
1,6-Hydrogen shift	1.05×10^{10}	-	-	-
1,7-Hydrogen shift	3.00×10^{9}	-	-	-
x,*x* + 3-hydrogen shift	1.00×10^{11}	-	-	-
x,*x* + 4-hydrogen shift	1.26×10^{10}	-	-	-
x,*x* + 5-hydrogen shift	7.24×10^{9}	-	-	-

[a] Rate parameters are taken from Levine and Broadbelt.[129]

3.3.2 Mechanistic Analysis of Polypropylene Decomposition

The global analysis of PP decomposition kinetics revealed interesting differences in the rate signatures for isotactic versus atactic PP. The orientation of methyl groups along the backbone of PP impacts the crystallinity of the polymer on the macroscale. Isotactic or semi-crystalline polypropylene (IPP) has regular order in that the pendant methyl groups are aligned, whereas atactic or amorphous polypropylene (APP) has a random steric structure.[160] Translating the physical structure to chemical behavior, IPP has clearly sigmoidal isothermal conversion, just as HDPE does. However, APP has a first-order decomposition rate, as demonstrated by Amorim et al.[135]

To isolate the effects of chemical structure and physical influences, polypropylene decomposition was studied *in silico* by using the PE mechanistic model and accounting for the difference that –[CH_2–$CH(CH_3)$]– repeat units in PP compared to –[CH_2– CH_2]– repeat units in PE would have on the intrinsic kinetics. That is, the introduction of branched carbon atoms influences bond strengths and the heats of reaction for the elementary steps underlying the mechanistic model, and thus, the same reactions in PE and PP all naturally have different rate coefficients, influencing the relative rates of all the reactions in the model. Following the methods of Kruse et al.[127] who built a comprehensive PP pyrolysis model, the reaction family parameters (pre-exponential factors and Evans-Polanyi parameters) from the HDPE model were used without adjustment, but the heats of reaction for individual reactions were calculated based on the structure of the species specifically contained in the PP model. As seen in Figure 3.10, the variation of reaction rate with conversion of PP is noticeably deceleratory. This behavior is a hallmark of APP as noted above and is in sharp contrast to the IPP pyrolysis behavior in Figure 3.6.

The mechanistic model is agnostic to tacticity and takes into account the difference between HDPE and PP based on monomeric structural differences alone as captured in differences in enthalpies of reaction. For radical initiation via chain fission, PP has a higher rate constant than HDPE due to the lower enthalpy of reaction and, consequentially, the lower activation energy. However, both polymers have approximately the same rate of radical propagation, so HDPE has an overall longer kinetic chain that results in higher reactivity over time as radical concentration accumulates. PP appears to become less reactive as it degrades due to the initial high rate of radical formation from chain fission, lowering the ratio of propagation to initiation. This may be a matter of degree, such that the PP pyrolyzed in this model has unhindered radical initiation via bond

fission, thus lowering this kinetic chain length. This suggests that further effects from structural differences such as tacticity manifest independently from differences in the structure of the backbone monomers, resulting in distinct variations in observed reaction kinetics. By controlling for one of these factors, the effect of chemical structure alone was identified and shown to be profound. This result also suggests that taking physical differences imparted by tacticity (i.e., IPP versus APP) into account would be important. Chen and coworkers[161] also highlight the importance of intermolecular effects such as chain mobility and viscosity on the apparent activation energy, where isotactic polystyrene has an enhanced thermal stability relative to atactic polystyrene. A similar phenomenon may be at play with PP, where APP has a lower viscosity and thus greater chain mobility compared to IPP, thus increasing the rate of radical diffusion and propagation throughout the melt sample.

While a global model can easily be fit to capture these differences, they do not provide the insight offered here by the mechanistic foundation of the more detailed model based on monomer identity, backbone composition, and elementary steps. Additionally, the purity of the literature samples used are unknown. It is possible that remnants of polymerization catalysts or oxygen are present in the polymer, especially for PP which is highly sensitive to oxidation, particularly in the amorphous phase.[162] Kruse and coworkers[127] included weak peroxide links to mimic structural defects in a modified version of the PP model used here to accelerate radical initiation and found that weak-link fission does increase the rate of radical initiation, but at temperatures above 350 °C carbon-carbon bond fission dominates. More detailed models could include further oxidative degradation,[163] such as reactions found in the autoxidation of condensed-phase hydrocarbons.[14,101]

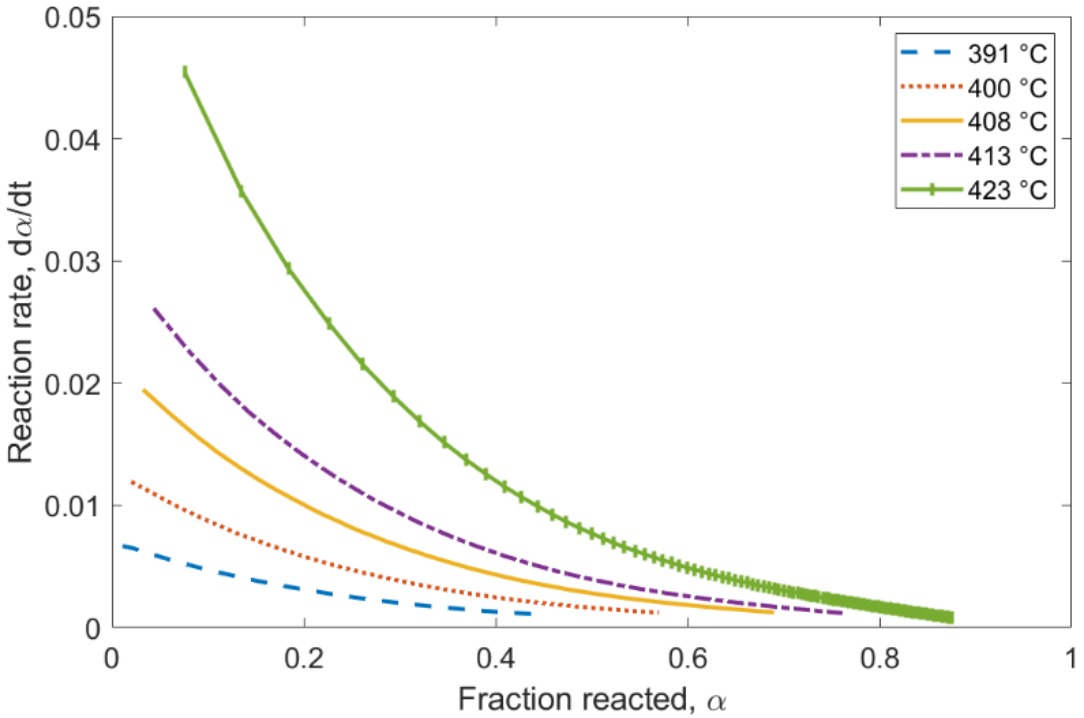

Figure 3.10. Predictions from the mechanistic model of variation of the reaction rate, dα/dt, of PP decomposition as a function of fraction reacted, α.

3.4 Conclusions

Isothermal and ramped thermal analysis of PE and PP are modeled with global, lumped, and mechanistic methods. Lumped and global models can capture experimental results with strong agreement, but mechanistic models offer insight into the effect of structural characteristics on the intrinsic kinetics of polyolefin pyrolysis. Detailed analysis of relative rates of reaction of tens to hundreds of elementary steps can be used to understand the origin of macroscopic measures such as sigmoidal character of the conversion as a function of time. The mechanistic model was able to toggle this behavior by modifying only the monomer structure of the polymeric backbone and its attendant effect on the rate coefficients through heats of reaction for individual elementary steps. This analysis shows that other characteristics such as tacticity would need to be layered on top of

these chemical structural effects, which may be best incorporated with kMC, which tracks individual chains and even can account for spatial effects. The results from studying PE and PP here fall in the expected trend of polyolefins from HDPE to LDPE to PP regarding backbone branching and effects.

A final note is that while the mechanistic models provide detailed product information, it was not given here because it is difficult to harmonize thermal analysis and product measurements with the required detail for comparison to the model. Thus, the authors encourage future experiments to collect high-quality thermal data and measure product yields in the same experiments. For example, the pyrolysis of HDPE has hundreds of products, and mechanistic models are inherently compatible with this level of detail, so it would be useful to do thermogravimetric analysis (TGA) with detailed product analysis.

Chapter 4 Chemical Kinetics, Deterministic Modeling and Analysis of Experimental Data of Model Oil Curing

A deterministic mathematical model is used to identify and quantify the complex kinetics of a fatty acid ester, ethyl linoleate, during the autoxidative drying process. The model was developed previously and is based on the monomer approach applied to automated reaction network generation (ARNG). In the chapter, the kinetic parameters of the main reaction families are estimated on the basis of new experimental data of various nature: normalized FTIR spectra of ethyl linoleate with TiO_2 cured at 70 ^oC. A sensitivity analysis is presented linking the dynamics of experimentally observed properties, like peroxide values, to particular reactions, like the decomposition of hydroperoxides. Also, a detailed study is reported of the attribution of a number of specific monomeric compounds that are dominant in the ESI-MS results to a few of the millions of reactions simulated by the ARNG model. The distribution of various types of crosslinks is analyzed and compared to ESI-MS peak data on dimers.

4.1 Introduction

Oil paints are complex, chemical mixtures. For many years, the drying oils that comprise the binder portion of paints have been studied under ambient conditions using a variety of approaches, both experimental and computational.[7,19,164–166] Drying oils, such as linseed oil, cure via autoxidation, a free-radical polymerization process through which oxygen adds to the oils after an initiation event. Subsequent oxidative reactions occur that diversify the distribution of products and crosslink the fatty acid tails of triglycerides into dense, polymer networks.[56,93,167,168] Simplified systems have also been studied that capture representative reactivity without the variation in unsaturation as found in drying oils.[34,96,169] Fatty acid esters are also reasonable model molecules for synthetic alkyd coatings, as they form mainly oligomers and extend the investigation of the curing of coatings beyond traditional, bio-based oil origins.[31,170–172]

This work follows the recent advancements in computational modeling using a monomer approach with automated reaction network generation (ARNG) applied to the curing of complex drying oils by Orlova and colleagues.[17] At its foundation, monomer chemical graphs are modified based on reaction families until no more unique monomers are found. The concentrations for these monomer fragments or their functional groups are solved with a continuum kinetic model. After the simulation and the monomer concentrations are solved, polymeric species can be assembled using random graph theory to connect all the "half-bonds" on monomers until it is a fully converged system. This is an effective method for infinite polymers such as those in crosslinked, network polymers. However, the original model was not tuned to real data. In fact, it is challenging to validate a complex system with many species using a complicated model. One question that can

be addressed is if there exist main trends that are determined by a few parameters, and what is the overall sensitivity of the reactive system.

Within this chapter, a summary of computational and experimental measures is given. An analysis of the sensitivity of key conversion measures to reaction types is denoted, and final optimized kinetic parameters are listed for lumped hydrogen abstraction rates, hydroperoxide decomposition, and radical termination. Finally, an analysis of electrospray ionization-mass spectrometry (ESI-MS) mass spectra peaks is performed in both positive and negative modes to identify the overlap between model-generated monomers and dimers and where the model still lacks in its chemical space. This chapter demonstrates the capacity of a kinetic model to elucidate chemical detail once again, with added complexity.

4.2 Methods

4.2.1 ARNG Model

The kinetic model follows the framework by Orlova et al.[17] To summarize this model, an automated reaction network generator seeks reactive patterns (Figure A.1), transforms the chemical graph, and checks the uniqueness of the product. All of this is happening on monomer fragments rather than whole chemical species graphs that would become infinite in size.

A system of ordinary differential equations is assembled for each monomer fragment, and the rates of change in concentration are determined by a rate coefficient (experimentally found or derived via the Arrhenius equation). The concentrations of each monomer fragment and the respective reactive patterns or functional groups of interest are calculated and can be summed for comparison with experimental results.

Rather than crosslinking into larger polymers, the fragments only maintain the position of a crosslink and its type, in addition to other local functional groups. One advancement made to this model since publishing is the directed edges for the monomers to distinguish crosslinks made by radical-radical termination reactions (non-directed edges) and radical-to-conjugated double bond addition reactions (directed edges), depicted in Figure 4.1. This distinction may influence the global polymer properties that are inferred from the crosslink distribution using the random graph model.[16,83,173] Although modeling the polymer network formation is beyond the scope of this chapter, the sensitivity of crosslink and polymer network gel formation to some certain rate coefficients is considered here (see Figure 4.15).

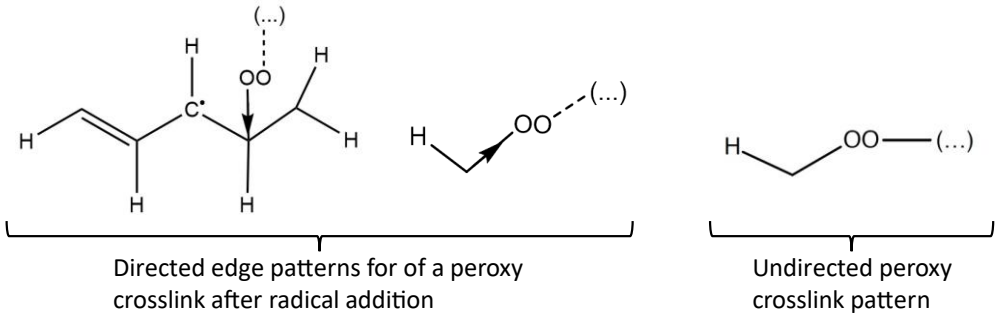

Figure 4.1. Directed and undirected edges on monomer fragments. Reactive patterns correspond to those found in the Appendix.

4.2.2 Mechanisms

Included in this model are the following autoxidation reactions for a free-radical polymerization summarized in Table 4.1. It should be noted that beyond these specific reactions, there are reactions of secondary products where reactive patterns are identified to account for greater complexity. The model extends beyond the reactions used by Orlova et al.[17] in the study of the catalyzed and uncatalyzed autoxidation of EL by including more reactions with the highly reactive hydroxyl radical (radical addition, H-abstraction from bi-allylic position). Termination and radical addition reactions oligomerize the system. Three types of crosslinks are possible: alkyl, ether, and peroxyl.

Table 4.1. Autoxidation reaction families and their respective rate coefficients at 70 °C. Values with an asterisk were optimized.

	Reaction Family	**Functional Group Representation**	***k* [1/s]**	***k* [L/mol*s]**
Initiation	Primary initiation	$I + O_2 \rightarrow IOO.$		$1\ 10^{-3}$ *
	Secondary initiation by initiator radical	IOO. + EL bi-allylic H → IOOH + R.		$1\ 10^{8}$ *
	ROOH Decomposition	ROOH → RO. + .OH	$4.5\ 10^{-5}$*	
	Peroxyl Crosslink Decomposition	ROOR' → RO. + R'O.	$8\ 10^{-7}$*	
Propagation	O_2 Addition	O_2 + R. → ROO.		$1.2\ 10^{8}$
	ROO. H-Abstraction of bi-allylic H	ROO. + R'H → ROOH + R'.		160*
	RO. H-Abstraction of bi-allylic H	RO. + R'H → ROOH + R'.		160*
	R. H-Abstraction of bi-allylic H	R. + R'H → RH + R'.		42*
	HO. H-Abstraction of bi-allylic H	.OH + R'H → H_2O + R'.		42*
	ROO. from aldehyde R(O)H	ROO. + R'(O)H → ROOH + R'.(O)		80*
	RO. from aldehyde R(O)H	RO. + R'(O)H → ROH + R'.(O)		80*
	R(O)OO. from aldehyde R(O)H	R(O)OO. + R'(O)H → R(O)OOH + R'.(O)		80*
	HO. from aldehyde R(O)H	HO. + R'(O)H → H_2O + R'.(O)		80*
	β-scission, Type 1	RO. → R(O)H + R'.	240*	
	β-scission from dimer, Type 2	RO. → R(O)H + R'.	100*	
	ROO. Addition to conjugated dienes	ROO. + //\// → ROOR'.		1000*
	RO. Addition to conjugated dienes	RO. + //\// → ROOR'.		2800*
	HO. Addition to conjugated dienes	HO. + //\// → HOR'.		2800*
	Radical Epoxidation	RO. → R(O)R	.0720	
Termination	R. + R. Recombination	R. + R'. → RR'		$2\ 10^{8}$*
	RO. + RO. Recombination	RO. + R'O. → ROOR'		$2\ 10^{8}$*
	RO. + R. Recombination	RO. + R'. → ROR'		$2\ 10^{8}$*
	ROO. + R. Recombination	ROO. + R'. → ROOR'		$2\ 10^{8}$*
	ROO. + ROO. Recombination	ROO. + R'OO. → ROOR' + O_2		$2\ 10^{8}$*
	ROO. + ROO. Russell termination	ROO. + R'OO. → ROH + R(O)H + O_2		$2\ 10^{8}$*
Oxidation	Baeyer-Villiger	R(O)OOH + R'C(O)H → 2 RC(O)OH		$7\ 10^{-3}$*

4.2.3 Experimental

FTIR: An experimental study was conducted with ethyl linoleate and coated rutile titanium dioxide. The sample was heated on a hot plate at 70 ^{o}C during spectrum collection under normal lab atmosphere (50% relative humidity and 23 ^{o}C). ATR-FTIR spectra were collected on a Frontier spectrometer (PerkinElmer) equipped with a heated diamond GladiATR module (PIKE Technologies). Spectra were collected every 12 s at 4 cm^{-1} resolution. Concentration profiles of functional groups at particular wavelengths were normalized, so only their shape carries information.

ESI-MS: The same system of ethyl linoleate (Sigma-Aldrich) and coated rutile TiO_2 (Tronox CR-826) was used for conducting drying experiments. The EL sample was heated for 146 hours without light, and samples were taken at 2.7, 5.7, 24, and 146 hours. The extractable fraction, mainly of monomers and dimers, was studied by direct-injection ESI-MS measurements taken in both positive and negative modes. Methods for measurement and peak analysis follow those published in the Orlova et al. study of triolein drying.[92]

4.3 Results

4.3.1 Identification of Kinetic Mechanisms Using the ARNG Model

Here, the effect of selecting more mechanisms on the number and type of different species is discussed. It is observed that the addition of the two scission mechanisms increases the number of monomer fragments from 300 to 800, but the addition of peroxyl crosslink decomposition yields a dramatic increase to 4,000. Any catalytic drier is assumed to be absent, but its inclusion would increase the number of monomer fragments even more (though this case is not treated in the scope of this work).

4.3.2 Sensitivity Analysis

Using a reduced model focused on key reactions in the polymerization process, indicated by the shaded rows in Table 4.1, kinetic rate parameters are optimized for validation against experimental data. The reduced model is validated with the full model afterwards. This is then followed by a discussion of specific experimentally-observed variables and their sensitivity and attribution to particular mechanisms.

4.3.2.1 Conjugated and Non-conjugated Double Bonds (EL Conversion)

The reduced model is fitted to the normalized FTIR profile in Figure 4.2a, resulting in the optimized values listed in Table 4.1. As the rate of abstraction of the bi-allylic hydrogen atom increases, the rate of consumption of the reactant molecule, ethyl linoleate, increases. A rate constant of 160 L/mol·s results in qualitative, and even relatively good quantitative, agreement of the model results with the sigmoidal conversion of EL observed experimentally. To note, an artificial delay time of 1.7 h is added to the model to account for any induction of oxygen and the non-catalytic nature of the system, as the experimental oil lacks a drier. A strong agreement between the model results and the experimental data persists at 160 L/mol·s for conjugated double bonds in Figure 4.2b.

This fitted rate constant for H-abstraction is 20 times greater than that reported in literature for peroxy radical abstraction from a bi-allylic H atom.[76,174] Additionally, it is 10^4 orders of magnitude lower than what would be determined using a reaction family approach to calculate specific rates for elementary reaction steps.[18,70,100] Having optimized using a lumped abstraction rate reduces the computational expense while also sacrificing model insight and reaction rate specificity that can be achieved using linear free energy relationships and group contributions.

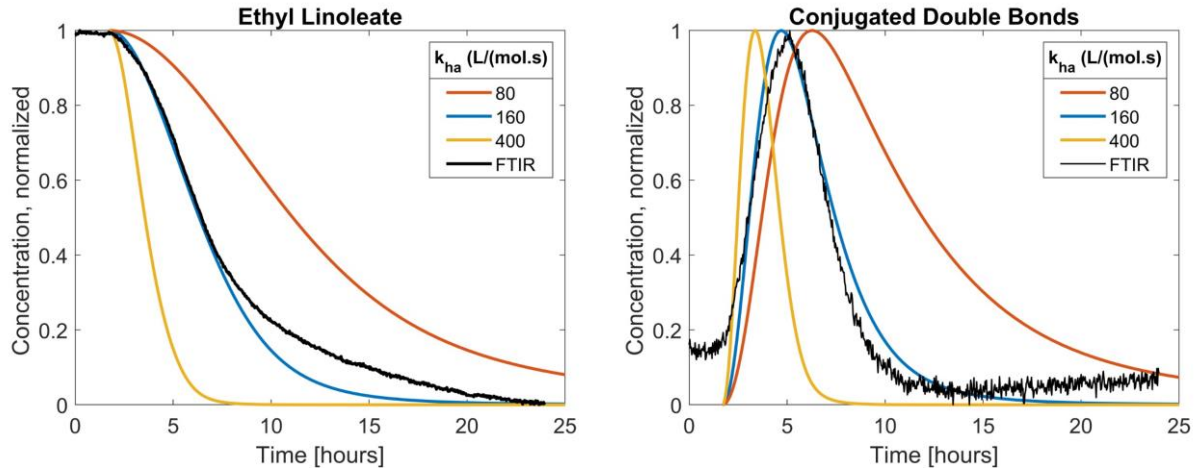

Figure 4.2. a) Sensitivity of ethyl linoleate conversion and b) conjugated double bonds to H-abstraction rate overlayed on normalized FTIR absorbance intensity for cis-alkenes at 3010 cm^{-1} and conjugated alkenes at 987 cm^{-1}, respectively.

3.2.2 Peroxide Decomposition

The unimolecular decomposition of hydroperoxides has a similar effect on the profile of EL conversion and concentration of conjugated double bonds, as found in Figure 4.3.

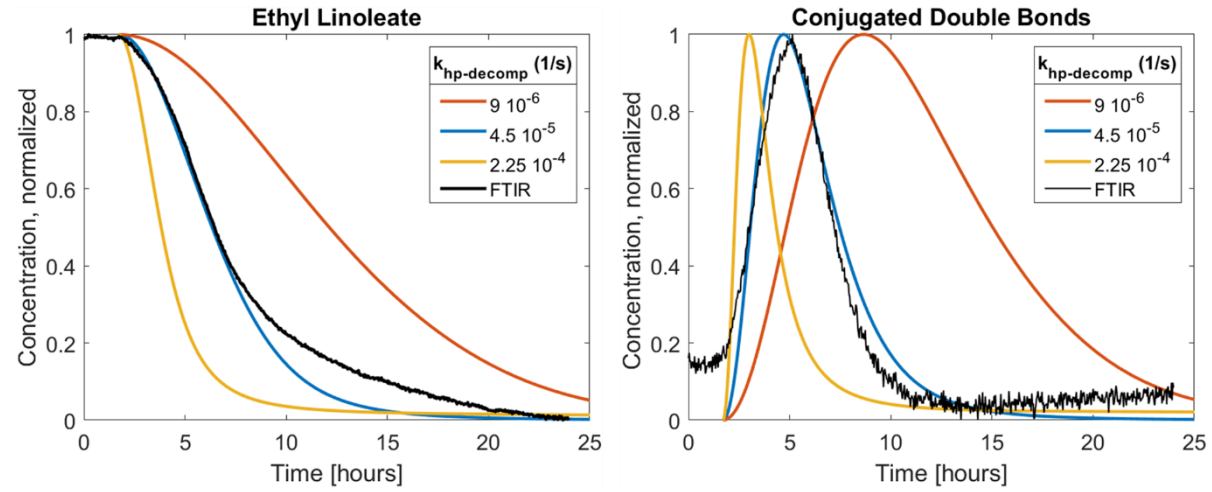

Figure 4.3. a) Sensitivity of ethyl linoleate conversion and b) concentration of conjugated double bonds to hydroperoxide decomposition overlayed on normalized FTIR absorbance intensities for cis-alkenes at 3010 cm^{-1} and conjugated alkenes at 987 cm^{-1}, respectively.

The optimal, fitted rate coefficient for this reaction is 4.5 10^{-5} s^{-1} . Intuitively, decreasing the rate of hydroperoxide decomposition would slow the conversion of EL, as it is a key in propagating radicals and breaking open the reaction network to further reactions to form radicals that can abstract from EL and eventually terminate.

However, this optimized rate parameter is unreasonable at ambient and slightly elevated conditions. According to the reaction families relevant for condensed-phase oxidation of hydrocarbons by Pfaendtner and colleagues[70] and a group additivity calculation for the heat of reaction, the rate coefficients are 10^{-5} to 10^{-11} orders of magnitude smaller than the optimized value, summarized in Table 4.2. This brings into question the uncatalyzed nature of the system. Cobalt and other metal driers are often used to catalyze the autoxidation process by overcoming the barrier for hydroperoxide decomposition. For a system without any appreciable drier, and the reported inertness of coated rutile TiO_2,[4] the spontaneous fission is not competive, nor is another plausible pathway of bimolecular interaction of hydroperoxides with an abstractable hydrogen which yields alkyl and alkoxy radical and water as products. Thus, an open question exists on other reasonable answers to the artificially inflated rate of hydroperoxide decomposition.

Table 4.2. Rate coefficient comparisons for hydroperoxide decomposition at 70 °C. Reaction parameters from Pfaendtner et al.[70]

Reaction Type	**A [1/s] or [L/mol·s]**	**E_0 [kcal/mol]**	**α_{fwd}**	**ΔH_{rxn} [kcal/mol]**	**E_a [kcal/mol]**	**k [1/s] or [L/mol·s]**
ROOH Fission	1 10^{13}	0	1	44.24	44.24	6.45 10^{-16}
ROOH Bimolec. Decomposition	1 10^{6}	24.6	-0.09	5.84	24.07	4.56 10^{-10}
Optimized ROOH Fission (Table 4.1)						4.5 10^{-5}

For common experimental measures such as peroxide value (PV),[29,93] sensitivity to hydrogen abstraction and ROOH decomposition is given in Figure 4.4. As hydroperoxides are formed downstream from EL conversion, increasing the rate of H-abstraction does increase the formation of hydroperoxides in the reduced model. Conversely, a slower rate of ROOH decomposition builds the ROOH concentration over time due to the mass balance of the formation by peroxyl radical H-abstraction and decomposition into hydroxyl and alkoxyl radicals. Both profiles follow those PV profiles found in literature samples[27] for different oil systems and temperatures which would also affect the rate coefficients.

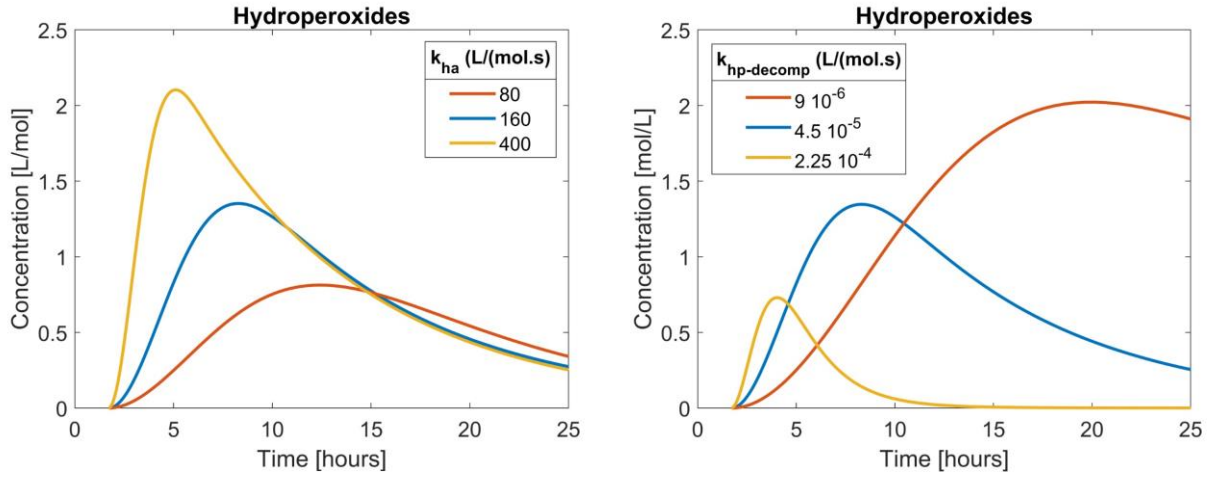

Figure 4.4. a) The sensitivity of the concentration of ROOH to the rate of hydrogen abstraction and b) ROOH decomposition.

3.2.3 Oxygen Uptake

For another common measure, O_2 uptake can be deduced from the model. Figure 4.5 denotes the sensitivity to H-abstraction. Intuitively, the faster H-abstraction occurs, the more rapid an alkyl radical is formed, onto which an O_2 molecule can add, and conversely, slowing this profile decelerates the cumulative O_2 uptake. An important note is that Oyman et al.[29] compared the catalyzed and uncatalyzed oxygen uptake at 21 ^{o}C. The profile, plotted additionally onto Figure

4.5, shows that the profile for the elevated curing of EL with TiO_2 does not follow the low oxygen uptake, but rather the appearance of a manganese drier. Thus, further investigation into the impact of coated TiO_2 should be considered with respect to the drying profile.

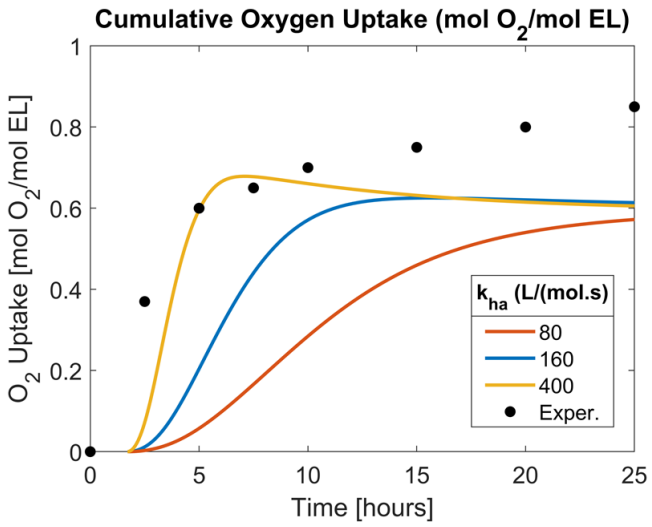

Figure 4.5. a) Cumulative oxygen uptake relative to molar concentration of ethyl linoleate over 25 hours and varied with hydrogen abstraction rates. b) Oxygen uptake profiles taken from Oyman et al.[29] for the catalyzed and uncatalyzed oxidation of EL.

3.2.4 Volatiles

Another well-studied measurement during the oxidation of EL is volatile formation, particularly hexanal and pentanal.[29,80] In Figure 4.5a, one observes a strong sensitivity of hexanal to β-scission of dimer. Assuming that the GC-MS data[80] for hexanal production are representative for the present case of EL polymerization, the optimized value of $k_{scission2}$ can be assessed at 10 1/s with relatively high certainty. Here, again a strong sensitivity of pentanal to Russell termination is observed, such that an optimized value of 2 10^8 L/(mol·s) is relatively certain. Note that Russell termination also strongly influences the fraction of trifunctional crosslinks and that a higher rate suppresses such crosslinks and, consequently, gel (polymer network) formation (see Figure 4.15).

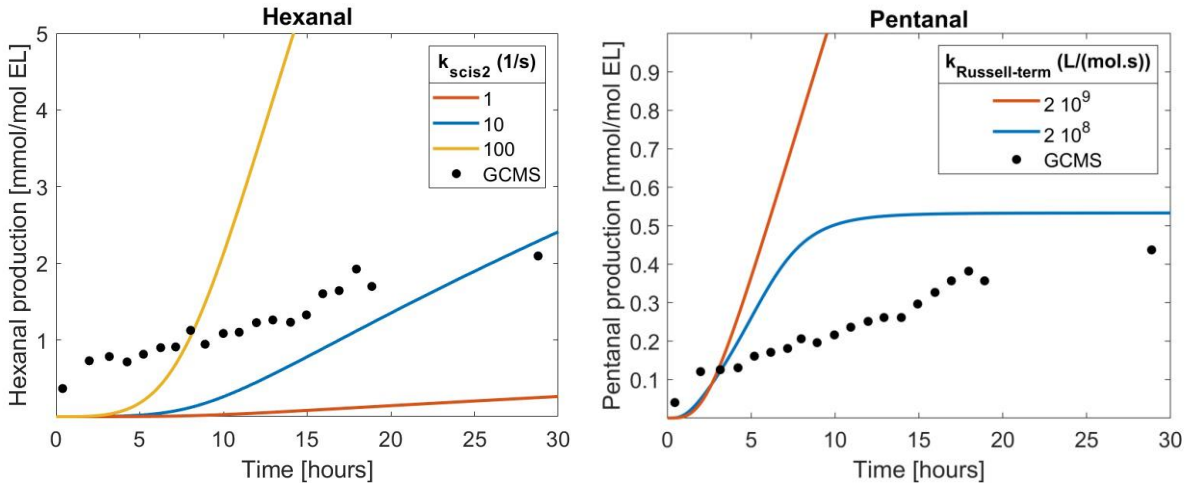

Figure 4.6. a) Effect of varying the rate of β-scission Type 2 (from dimer, see Table 4.1) on hexanal production. b) Effect of varying the rate of Russell termination on pentanal production.

4.3.3 ESI-MS Analysis

Non-radical, monomeric species from ARNG are used to identify individual *m/z* observed in the ESI mass spectrum. Relative peak intensities of the masses of the ESI spectrum identified as monomers are plotted.

The full ARNG model includes 307 monomers up to 406.2 g/mol (species with 3 hydroperoxides, 1 alkene, and an ester) and 79,207 dimers, with the smallest dimer being a species with 144.1 g/mol. Both are depicted in Figure 4.7.

The ESI mass spectrum (both positive and negative modes) counts 4,090 peaks at *m/z* ratios up to 470 g/mol in the monomer region and 5,170 peaks at *m/z* ratios up to 870 g/mol in the dimer region for ethyl linoleate. Each peak in the positive or negative mode is associated to a molecular weight (MW) by subtracting the weight of the attached Na^+, Ac^- or NH_4^+ ion, or adding the weight of a proton to deprotonated molecules. Thus, each peak in the positive mode results in 3 ESI

molecular weights, and each peak in the negative mode has 2 ESI molecular weights. The MW of monomers or dimers predicted by ARNG falling in a tolerance of 0.15 *m/z* around each ESI values are collected. Thus, an ESI product-peak may become matched to one or more model-predicted monomers or dimers.

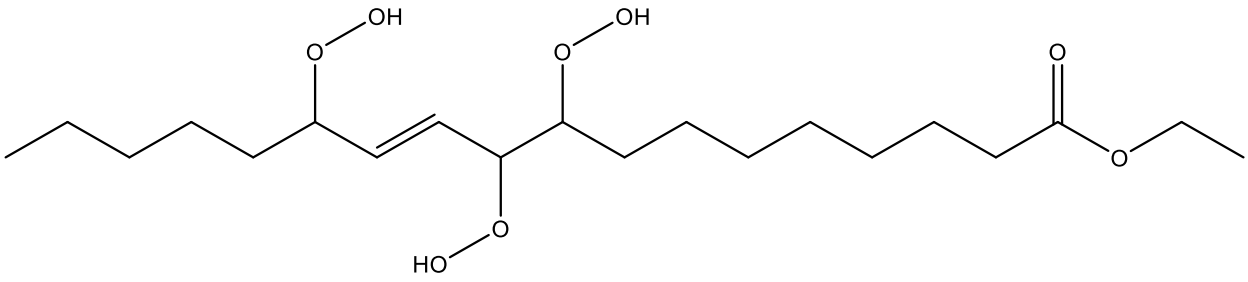

Largest Monomer, MW = 406.25 g/mol

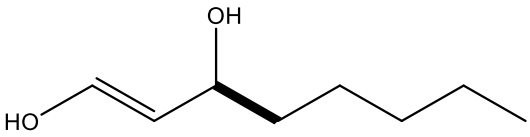

Smallest Dimer, MW = 144.21 g/mol

Figure 4.7. The largest monomer and smallest dimer identified in the ARNG model. The thick bond denotes alkyl crosslink for the dimer.

This methodology gives 579 possible monomer matches and 21,550 dimer matches. Both model-predicted molecules and ESI mass peaks may appear more than once. Within the 579 monomer matches, 280 unique ESI mass peaks out of 4090 are present and 182 out of 307 are predicted molecules. For instance, there are two isomeric monomers with MW of 104.011 g/mol. These masses match with six different ESI peaks, so there is a multiplicity with a total of 12 matches. Within 21,550 dimer-matches, 602 out of 5170 unique ESI peaks are present, and 8321 out of 79,207 are predicted molecules.

The matched peaks ('identified' peaks) are now assigned the MW of the closest model-predicted molecule. A matched peak may become associated to more than one model species MW. To avoid that, the peak counts of this peak appear multiple times in the MW spectrum. The simplest form of a multiplicity correction could be to divide the peak counts by the number of model's MW values. Instead, concentrations were used of the molecules to which a matched peak was identified. Thus, the measured peak counts are distributed among the model MW in proportion to the model-predicted concentrations.

For example, peak 1770 has an *m/z* of 157.13 and a peak count of 416. This peak is matched to model-predicted MW of 134.02 and 156.12 g/mol. Out of the 307 monomers, three (numbers 252, 274 and 297) have a MW of 134.02 g/mol, and two (numbers 164 and 200) have a MW of 156.12 g/mol. From the concentrations of these five different monomers, it is decided that the fraction going to MW of 134.02 g/mol is 0.36 and the fraction for the MW of 156.12 g/mol is 0.64. So, in the MW spectrum, the peak count of 134.02 g/mol is 0.36 x 416 peaks = 150, and that of 156.12 g/mol is 266.

The procedure is carried out for both monomers and dimers. The MW of model-predicted dimers is obtained from the monomer units predicted by ARNG that each posess only one crosslink of the same type, x (x_a, x_e, or x_p: alkyl, ether or peroxy). This monomer unit is denoted by a superscript x,1, and the calculated concentration of these species is $c_i^{x,1}$. It should be realized that the monomer units with just one crosslink are not linked only to monomer units with just one crosslink, but they may be connected to di- and tri-crosslinked monomer units. The probability for any monomer unit with just one crosslink to form a dimer follows as:

$$p^{x,1} = \frac{c(x_a=1,x_e=0,x_p=0)}{c(x_a=1,x_e\geq 0,x_p\geq 0)+\sum_{x_a=2}^{3} x_a c(x_a,(x_a=1,x_e\geq 0,x_p\geq 0)} \tag{4.1}$$

The concentration of the x-type dimers can then be determined by:

$$c_{i,j}^{x} = p^{x,1} c_i^{x,1} \, c_j^{x,1} / \sum_j c_j^{x,1} \tag{4.2}$$

where *i* and *j* are the monomers that compose dimer species. In the case of the directed crosslinks convention used to denote crosslinked formed via radical addition to an alkene, a similar argument holds. The monomer units making up this type of dimer are a pair of outgoing and ingoing crosslinked edges. Here also, the fact that a monomer unit may crosslink with another that has multiple crosslinks would be accounted for using the probability expression formulated above.

The peaks positively identified by ARNG as monomers and/or (there may be overlap) dimers are collected in an MW histogram with an interval of 0.15 g/mol. Within each interval, the peak counts (corrected for multiplicity) are summed up. In intervals with both monomers and dimers, the peak count is distributed in proportion to the model-predicted concentrations of those monomers and dimers.

Figure 4.8 shows the ESI mass spectra results of peak intensity of monomers after 146 hours of heating EL. A noise level around 10^{-4} in relative peak intensity is identified. Though a substantial part of the peaks above the noise level could be positively matched to monomers predicted by the ARNG model, at least 10 high intensity peaks could not be identified, suggesting more mechanisms are active than what are accounted for in the full model.

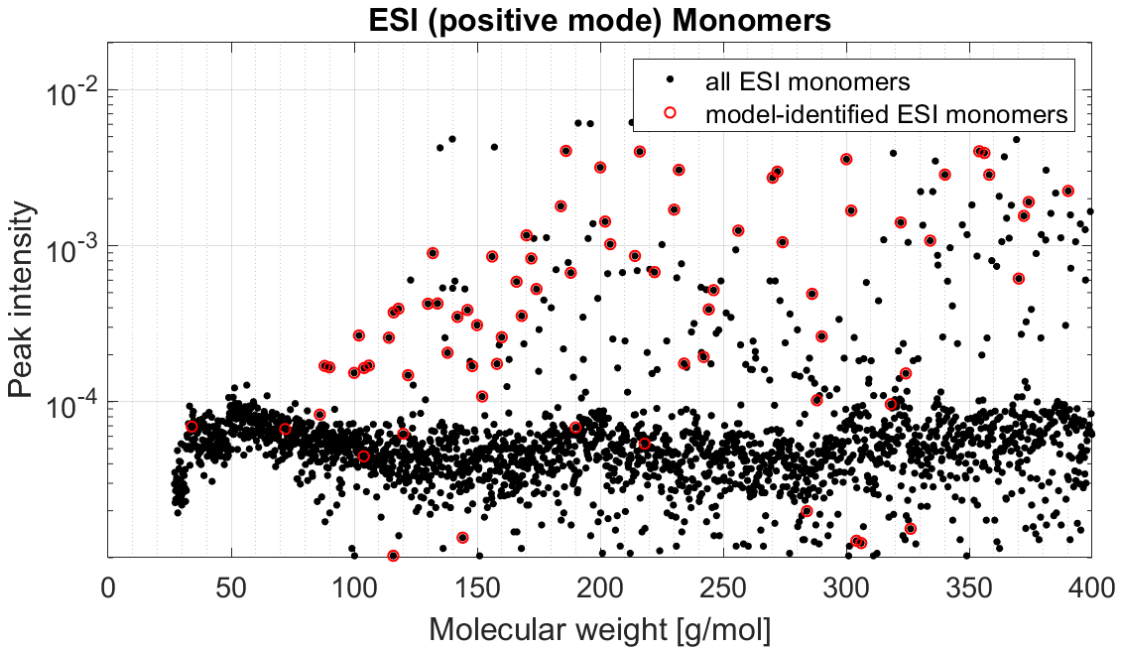

Figure 4.8. ESI molecular weight spectrum showing measured peak intensity vs molecular weight (rather than *m/z*) of monomers. Red circles are peaks that could be matched to model-predicted molecular weight products and corrected for calculated concentrations.

Figure 4.9 shows the ESI mass spectrum for the dimer species up to the heaviest dimer at 775 g/mol. Agreement with the model is more complete with the identified species; however, peaks at the low and high end of the dimer range are not identified. This also suggests greater fragmentation into smaller molecules, such as products deriving from allylic H-abstraction, which is not incorporated in this model.

Similar trends are found in the negative mode, but they are excluded from this work for brevity and can be found instead in the Appendix.

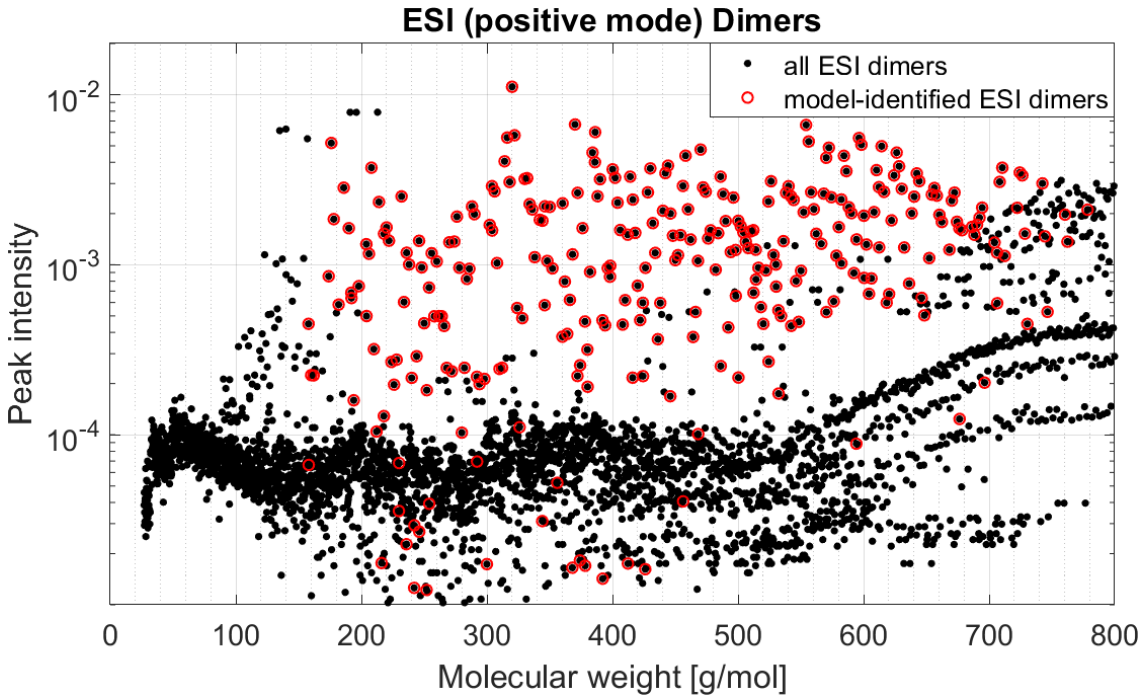

Figure 4.9. ESI molecular weight spectrum showing measured peak intensity vs molecular weight (rather than *m/z*) for dimers. Red circles are peaks that could be matched to model-predicted products and corrected for calculated concentrations.

4.3.4 Quantitative Results: ESI-MS and ARNG Model Comparison

The ESI MW spectrums do show a difference in peak counts of various model-identified species. An important question is to which extent the peak counts of species are proportional to the real concentration of that fragment species. The ESI-MS analysis allows one to compare the peak counts to the predicted counts, with both techniques having the same mass resolution. The ESI peak counts are compared to the model-predicted concentrations in Figure 4.10.

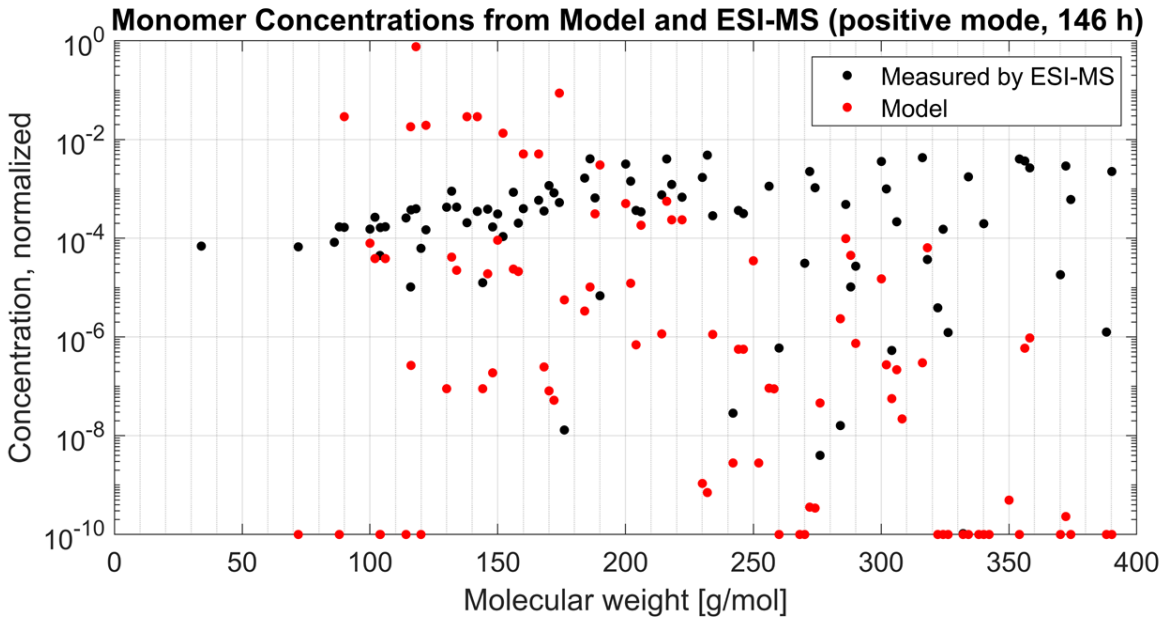

Figure 4.10. Comparison between measured peak counts and model concentration for the curing of ethyl linoleate, with an emphasis on the monomer and dimer regions.

Peak intensities vary within three orders of magnitude. When discarding 'noise' (peaks < 10^{-4}) a variation of two orders of magnitude is seen. The ARNG model shows that the variation of concentrations of the same model-identified monomers is much larger. This discrepancy between ESI-MS and ARNG suggests that peak intensity of fragment species is far from linear with their real concentration. Therefore, the focus turns to trends over time in peak intensity as compared to model-predicted trends. The combination of ESI-MS and the ARNG model allows one to do this as they have similar resolution, identifying individual species within an MW resolution of 0.15 g/mol.

ESI-MS product analysis was performed on ethyl linoleate at four times: 0, 2.7, 5.7, and 146 hours. Figure 4.11 displays the time trends for monomers identified by ARNG. The arrows highlight monomers with consistent upward or downward peak intensity trends in time. This suggests that the ESI-observed trends provide quantitative information on the relative

concentration behavior of the identified small species. Of the 22 consistent trends, 15 are in agreement with the ARNG model results, indicated by the black arrows in Figure 4.11. For example, a monomer identified with a mass of 172 g/mol has an increasing trend in intensity. The model-predicted concentration profile is shown in Figure 4.12 and supports this increase in peak intensity from ESI measurements over 146 hours.

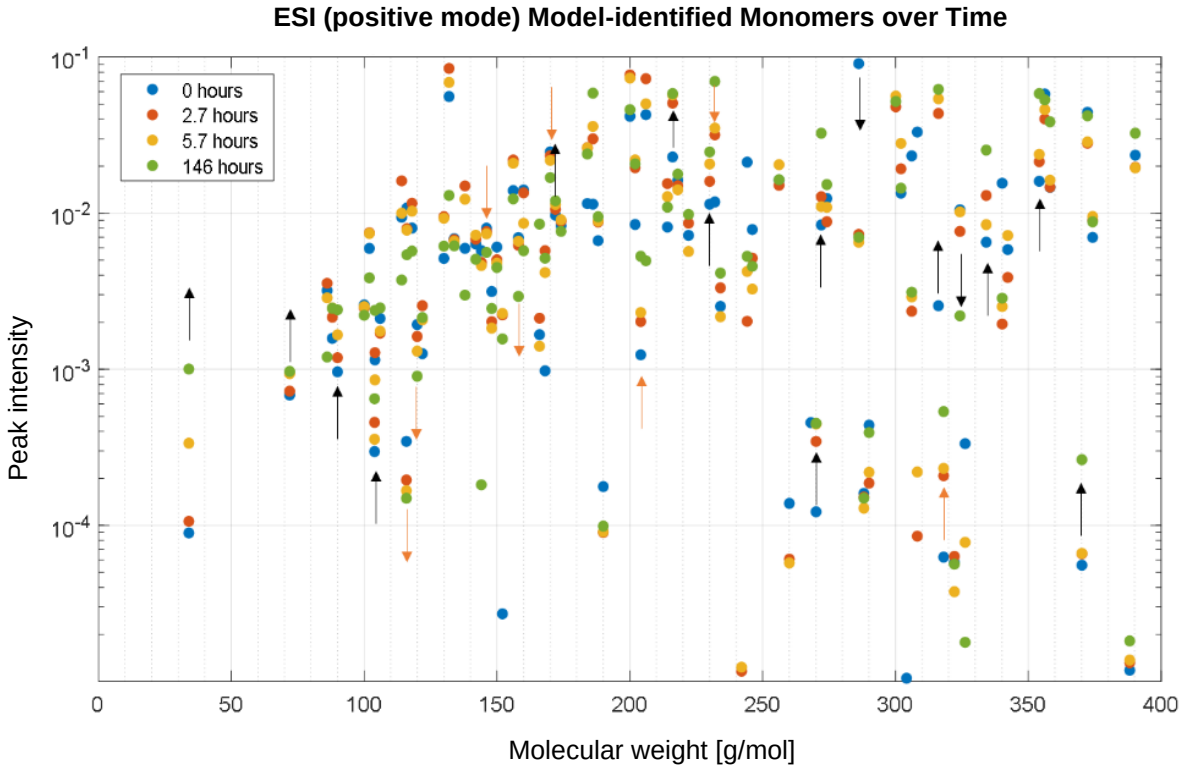

Figure 4.11. A time-series of peak intensities for monomers in the ESI-MS positive mode at 0, 2.7, 5.7, and 146 hours. The arrows indicate consistent trends in the time-evolution of peaks. Black arrows are in agreement with ARNG model results, and red arrows mark disagreement.

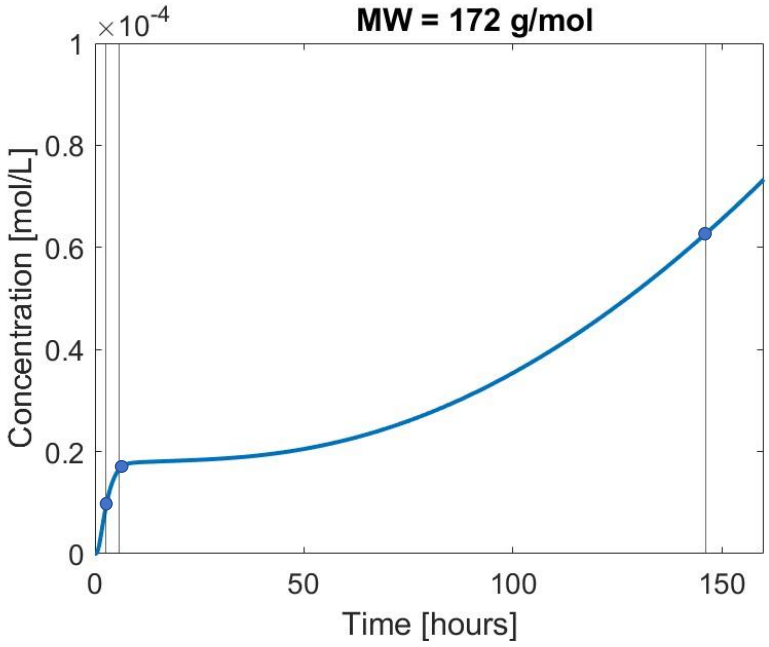

Figure 4.12. The concentration profile of species with a molecular weight of 172 g/mol according to the model showing an increase in concentration or peak intensity.

The same analysis can be performed on the time-evolution of dimer peak intensities, as shown in Figure 4.13. A noticeable trend exists among the distribution of dimers. Smaller dimers tend to decrease in peak intensity in time, while larger dimers tend to have an increasing peak intensity. A possible explanation for this observation is the volatility of smaller dimers at the experimental conditions. A further analysis was performed on the dimers identified in the experiment. The types of crosslinks between the dimers were summed (Figure 4.14a). However, the peaks of all crosslink types overlapped significantly. The kinetic model can help tease out the overlapping dimer peaks. The model predicts peroxy and ether crosslinks are in similar amounts, but alkyl crosslinks were 10^5 lower in concentration (Figure 4.14b). The data suggests that alkyl crosslink concentration may still be significant, despite a model correction for overlapping dimer peaks. It also shows a decrease in alkyl crosslinks in time, whereas peroxy crosslinks increase.

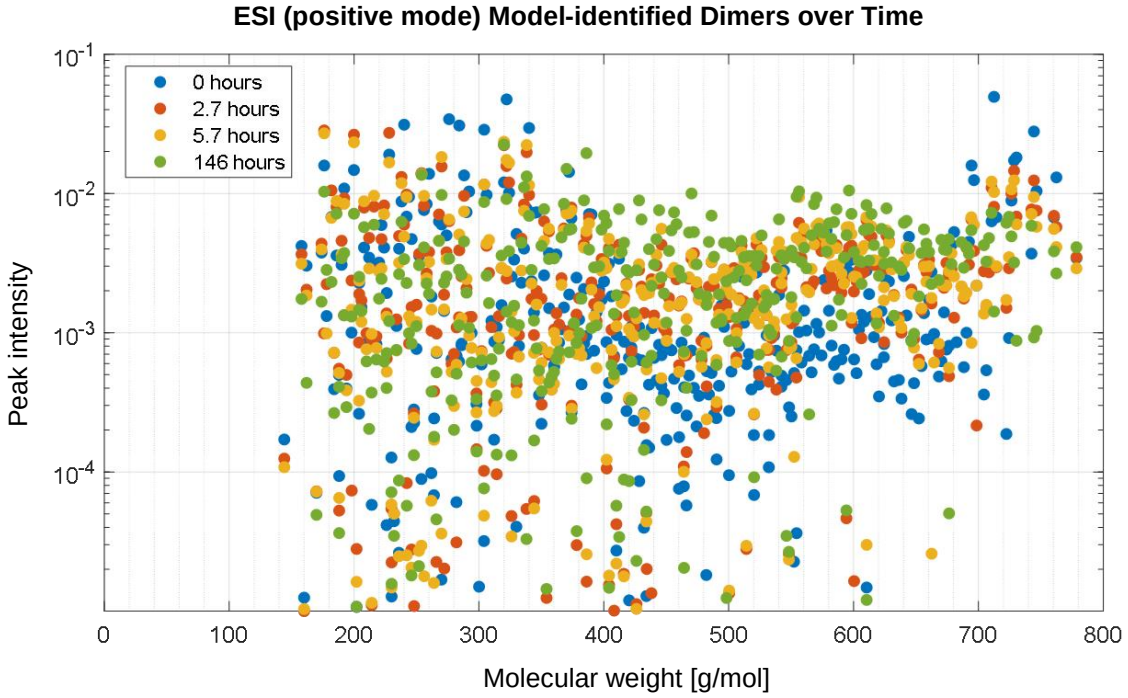

Figure 4.13. ESI molecular weight spectrum for dimers at 0, 2.7, 5.7, and 146 hours.

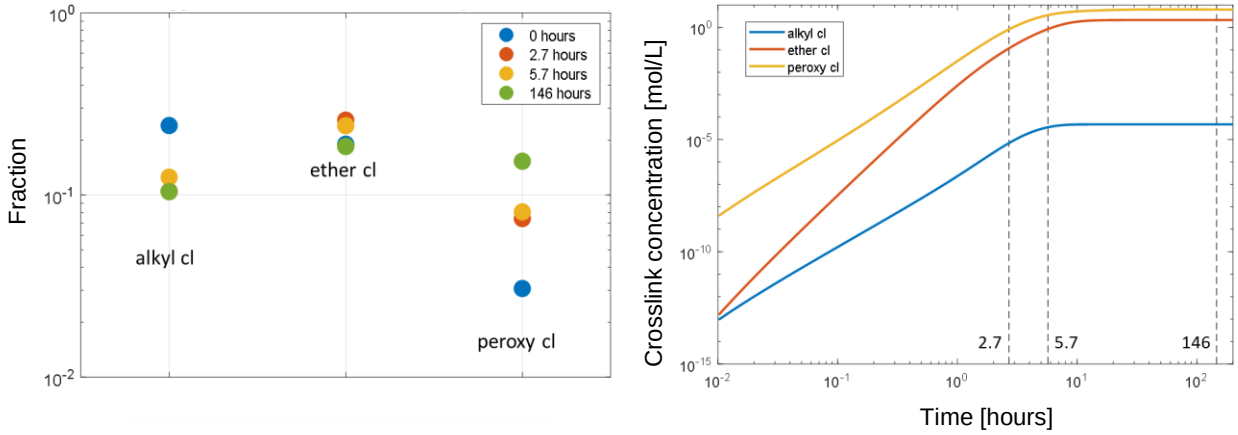

Figure 4.14. a) Crosslink types from ESI-MS-identified dimers, corrected by the model. b) Crosslink types from the kinetic model over time.

4.3.5 Crosslink and Polymer Network Formation

Although modeling the polymer network formation is beyond the scope of this chapter, a brief sensitivity analysis of crosslink and polymer network (gel) formation to some rate coefficients will conclude this chapter. Polymer network computations have been made by an existing random graph model.[17] While Figure 4.14b shows the crosslink *type* distribution, Figure 4.15a shows the crosslink *functionality* distribution. The fraction of trifunctional crosslinks that are responsible for branching and network formation is shown in Figure 4.15b. Figure 4.15c clearly elucidates that the fraction of trifunctional crosslinks is decisive for the formation of the gel fraction: the fraction of the polymer that is present as a polymer network. Figures 4.15b and 4.15c also clearly show the strong impact of the peroxy crosslink decomposition rate coefficient on trifunctional crosslinks and network formation. Interestingly, Russell termination also has a strong influence on gel formation; although still a (low) fraction of trifunctional crosslinks is present in the high RT-case, no polymer network is formed at all in that situation.

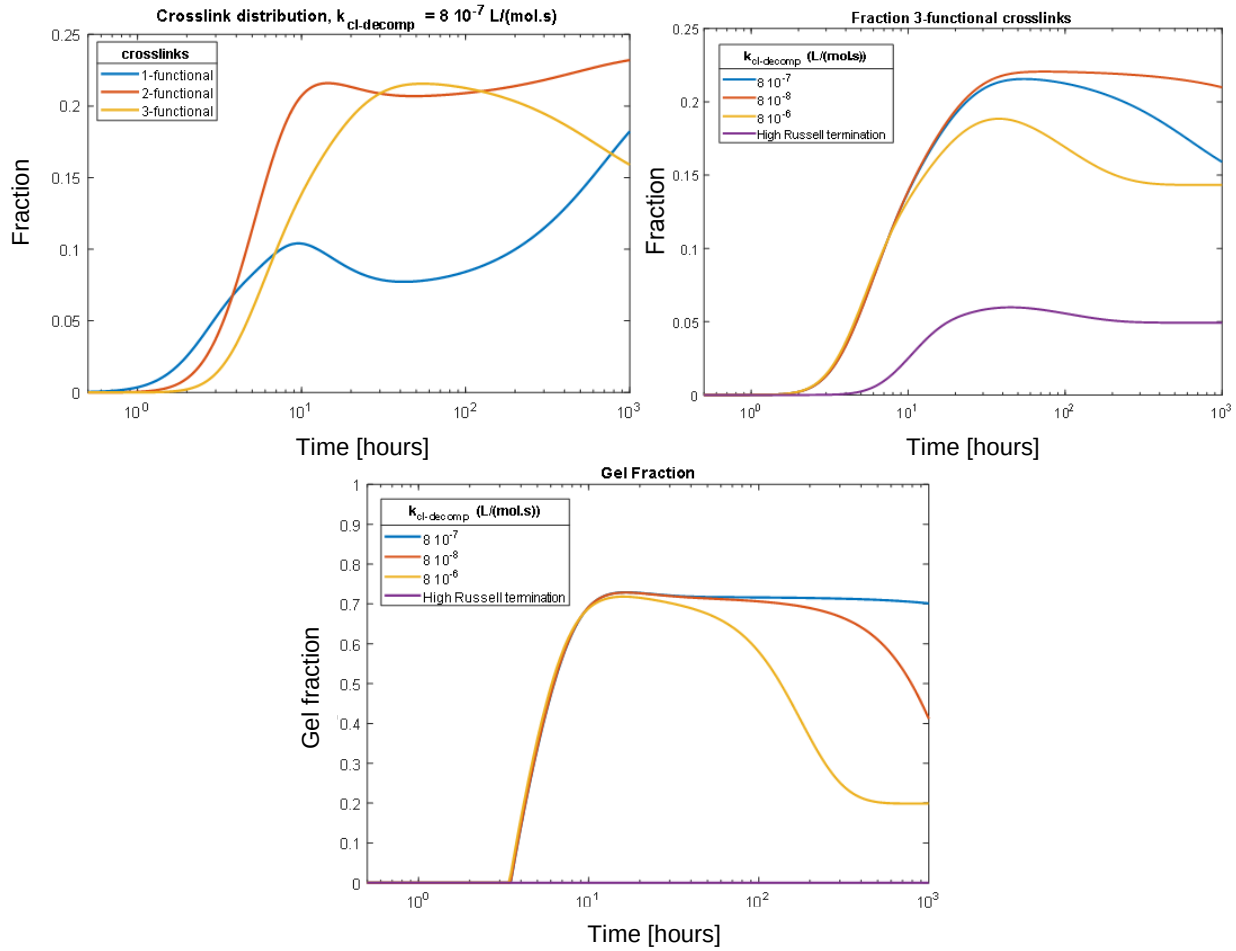

Figure 4.15. Effect of crosslink decomposition and Russell termination on crosslink functionality and polymer network gel fraction. (Top-left) Distribution of crosslink functionality. (Top-right) influence of crosslinking decomposition rate and Russell termination on fraction of trifunctional Crosslinks (reference value Russell termination: k_{RT} = 2 10^8 L/(mol·s), high value: k_{RT} = 2 10^9 L/(mol·s). (Bottom) Gel fraction for various conditions as calculated from the Random Graph model.[17] Gel point in all low-RT cases at 3.5 h; stronger gel fraction decrease with higher $k_{cl\text{-}decomp}$; no gel formation at all for high Russell termination.

4.3.6 Reaction Path Analysis

An analysis of the reaction network can be used to elucidate the pathway to highly oxidized products found experimentally. For example, the species hex-2-ene-6-t1,1,4-triol with MW = 174.13 g/mol (shown in blue in Figure 4.16) is present in the mass spectrum. This triol is identified by the full model, but not by the reduced model that lacks peroxide crosslink decomposition.

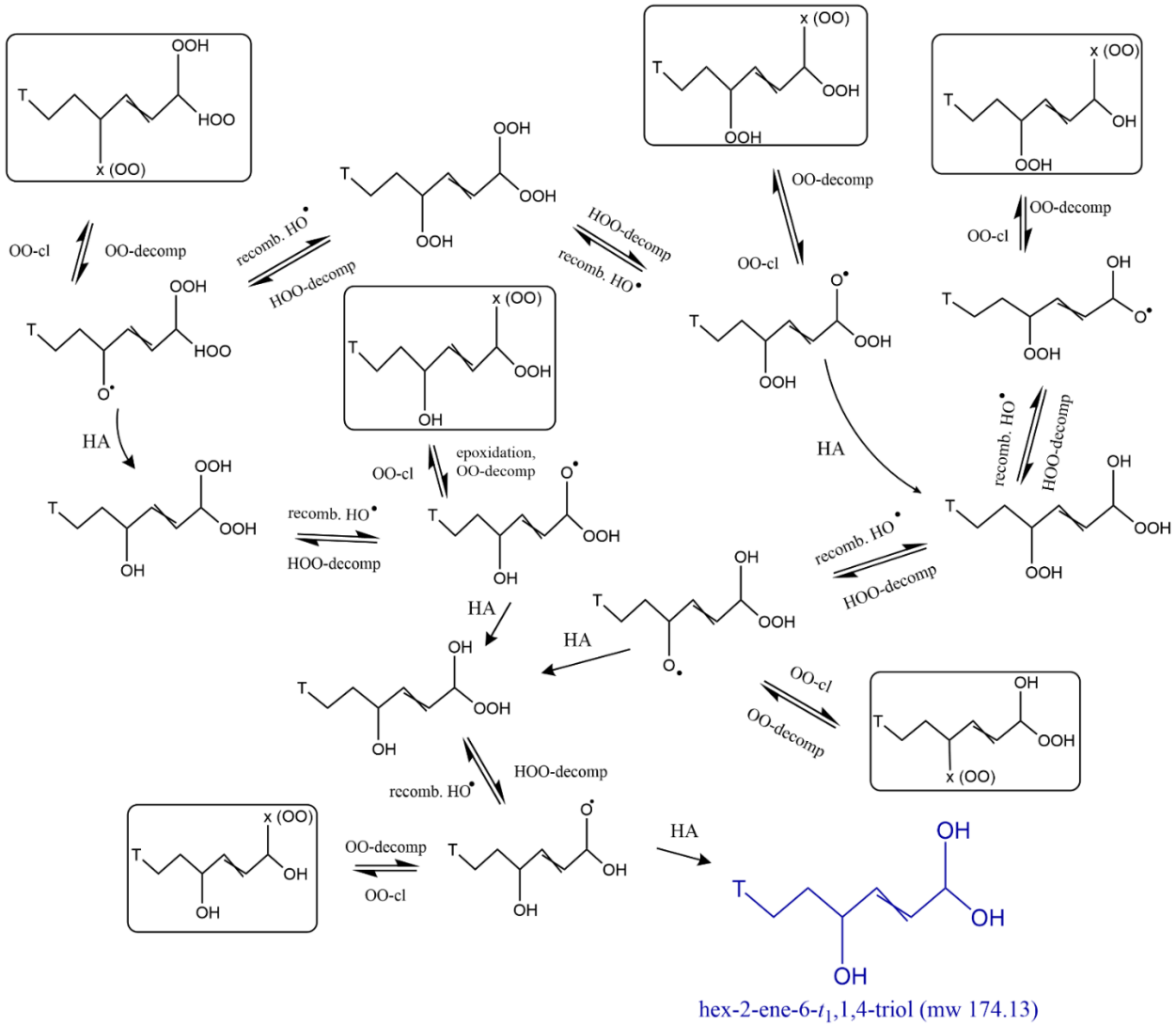

Figure 4.16. Analysis of the reaction path to particular peaks identified in ESI mass spectrum.

According to the model, this is a non-reactive species as it only has alcohol groups and cannot further react with the chemistry included. This part of the reaction network in Figure 4.16 shows all possible pathways leading to the triol starting from six different species (in rectangular frames) that all are connected to other monomers through peroxy crosslinks. Since the reduced reaction scheme does not allow for peroxy-crosslink decomposition, it is deduced that the triol can only be produced by virtue of that reaction pathway.

4.4 Conclusions

An analysis on the basis of individual small molecules is possible. Hence, optimizing the rate coefficients to improve the agreement of the model to experiments on the basis of individual species is possible. This underscores the necessity for refined adjustment of rate coefficients using methods such as group contribution theory and linear free energy relationships to approximate specific reaction kinetics. It must be noted that knowing what the model is used for motivates the need for refined or global parameters. For instance, when knowing the mechanism to reach a particular chemical species or moiety is important, a detailed kinetic model is needed. However, if only global properties are being studied, a looser approximation may be sufficient. Also, it would be more practical for other applications to focus on the reactivity of functional groups rather than specific species, especially for polymer systems and comparisons with methods such as FTIR. This underscores the balance of accuracy and expense in time, detail, and resources to get the answer.

Chapter 5 Multifunctional Monomer Stochastic Modeling Framework Applied to the Autoxidation of Ethyl Linoleate

Traditional oil paint binding media are comprised of triglycerides with varying degrees of unsaturation. These oil molecules cure through autoxidation, a free-radical polymerization process, into a dry film. Physical experiments fail to provide sufficient detail to understand the many competing reactions, so microkinetic modeling, a computational tool, is used to offer insight into the dynamic chemical system. Previous work studied the use of automated reaction network generation to enumerate the possible chemical species and ordinary differential equations to solve evolution of concentrations in time. However, from a case study of a fatty acid ester, ethyl linoleate, it turns out that the complexity and scale of full triglycerides are generally too great for a tractable solution. This research implements kinetic Monte Carlo simulation with a multifunctional monomer-based representation of the chemical species to handle the diversity and scale of polymer evolution. In a case study, ethyl linoleate, a doubly unsaturated fatty acid ester, undergoes simplified autoxidation. This work demonstrates that the monomer-based stochastic approach is effective at capturing both key and peripheral species without a combinatorial explosion as seen previously with rule-based automated reaction network generation. By studying how oil paint dries on the molecular level, macroscopic detail can emerge related to the composition, reactivity, and stability of a paint film over time.

5.1 Introduction

One of the greatest challenges of modeling the polymerization of drying oils is the limit of storing and computing each polymeric species. A crosslinked polymer approaches unity as it cures, but the polymer microstates are innumerable because of the vast number of reactions and combinations from polymerization and autoxidation. For example, Oakley et al. found that a deterministic ethyl linoleate (EL) curing model which only permitted up to tetramers yielded 68,197 species and 1,087,360 reactions but was intractable to solve.[109] As a result of this limit, the large chemical system still lacks the diversity of larger oligomers and is not fully representative of curing triglycerides in a drying oil, the ultimate goal. There are too many species to store within the computer memory and solve the stiff system of differential equations. Using a stochastic method allows for the probabilistic search in chemical space for species using their propensity to react instead of generating all possible combinations that may be insignificant.

Another challenge is the complexity of the monomer and resulting polymer, highlighting the need for balance between molecular detail and efficiency. The classical understanding of polymers is based on Flory's extensive work, further developed by Stockmayer, giving the Flory-Stockmayer theory on highly functional molecules, which describes the gel point based on functional group conversion.[106,107] However, this theory assumes that all functional groups are equally reactive and the monomers do not change. In the case of drying oils, there is great diversity in products and reactivity of functional groups. There are no repeat units because of oxidation and multiple functionality. Thus, it is imperative to devise a way to capture the distribution of functional groups throughout the polymeric species because the chemical detail is important for stability of the polymer film.

Several efforts have preceded by lumping based on molecular weight by only counting the number of crosslinks that captures physical properties, like gel point.[83,175] However, chemical detail is lost. The ultimate goal of the following work is to develop a model that retains more topological characteristics and reactivity to better understand a film's curing and aging chemistry. There is complexity in multiple sites for crosslinking, different types of crosslinks, oxidation chemistry, and free-radical polymerization. With regards to monomers with multiple functional sites and radicals, Kurdikar et al. studied the simulation of multifunctional polymerization and proceeded with lumping.[176] A similar approach by Orlova et al.[16] was crafted as a "monomer approach" that focused on modifying monomer units through applied reaction rules and tracking evolution of functional groups.

Thus, this chapter demonstrates a method that sufficiently overcomes these challenges and surpasses the previous computational barriers reached by researchers. This work is motivated by research questions raised in how paint dries at the molecular level and its impact on the later stability of films in hardening and degradation phases. A generic framework is presented for multifunctional polymers, and its application is demonstrated with a case study of the autoxidation of ethyl linoleate (EL), a model molecule for triglyceride-based drying oils. Special considerations were made when applying this framework to the complex, reactive system and are presented to the reader to communicate what may be necessary when applying the framework to other systems.

5.2 Methods

There are three main features of the multifunctional monomer-based framework described in this chapter: monomer and polymer graphs store detailed chemical information; on-the-fly species generation diversify from the reactants; and lumped reaction-type stochastic simulation solves for functional group concentrations in time.

5.2.1 Monomer and Polymer Graphs

Chemical graphs are a common and useful tool to represent molecules. Graph nodes are the atoms, and the edges between nodes are the covalent bonds between them. This information can be stored in an adjacency matrix and a node list to identify where the connections or bonds exist in the graph.

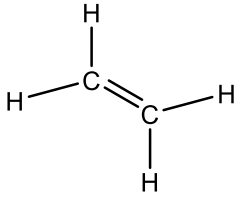

	C	C	H	H	H	H
C	0	2	1	1	0	0
C	2	0	0	0	1	1
H	1	0	0	0	0	0
H	1	0	0	0	0	0
H	0	1	0	0	0	0
H	0	1	0	0	0	0

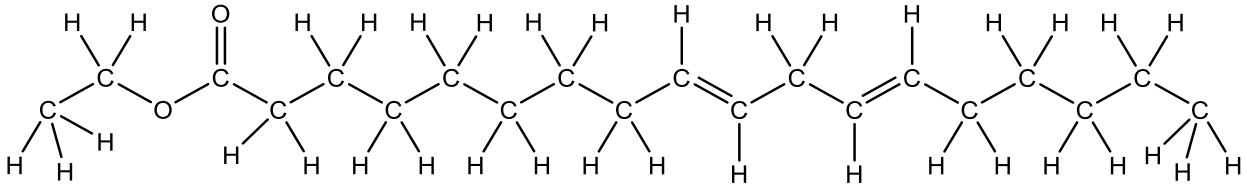

Figure 5.1. (Top) Chemical graph of ethylene and its respective atom adjacency list and connectivity matrix. (Bottom) Chemical graph of ethyl linoleate with 58 atoms, which would need a 58x58 adjacency matrix for one monomer.

Functional groups can be identified in the chemical graphs by searching the connectivity for the particular pattern of bonded atoms and modified using matrix addition based on specified reaction rules that make and break bond edges (e.g., removing a hydrogen atom for hydrogen abstraction).

On the monomer level, information can be stored about each fragment or monomer: count of how many exist at a given time, its adjacency list and matrix for the chemical graph, molecular weight, and what reactions the monomer participates in and what its product is. Also, for easy access of information, an array can be stored of what functional groups are present in the multifunctional monomer and how many it has.

For simple chemical systems such as ethane pyrolysis,[88] maintaining explicit chemical graphs for all products is feasible, as the system is self-contained and chemical species are a reasonable size. For polymer systems, there is a limit to which an explicit chemical graph is useful or feasible. Particularly for free-radical polymerization and crosslinking polymers, an infinite polymer is formed, and the combinatorial explosion of radical terminations is not possible to track. Additionally, for systems with high molecular weight monomers, such as in ethyl linoleate oligomerization, EL itself has 58 atoms (20 C, 2 O, 36 H) compared to ethene, which has 6 (2 C, 4 H), as shown in Figure 5.1. EL is already tenfold larger, and all further polymerization would increase that graph linearly. Another common way to represent polymers is through a coarse-grain representation. A polymer chain can be subdivided by functional group beads if highly complex[177–179] or by monomers like is PE/PP/PS pyrolysis with head/tail orientation.[127,129,180] Particularly for multifunctional monomers, there is a diversity in what monomers are present in the system at any time that can react and form unique polymers. A coarse-grain polymer graph can be made with

these monomers as they are identified. This can be as simple as A/B monomers, or the fragments generated using a monomer approach by Orlova and colleagues,[16,92] for example. In the monomer approach, no detail on the polymer level is maintained in time, but instead only the formation of unique monomers is generated. It is only after a simulation or at a particular time slice that a random graph approach may be used to "assemble" polymers to connect all crosslinks based on monomer concentrations at that time. This method is advantageous in that it calculates and tracks the concentration of functional groups in time, which is analogous to experimental techniques such as FTIR in which a lumped value is elucidated. Now, instead of atoms as the graph nodes, monomers are the nodes, and crosslinks are the edges between them. This can scale for systems with one type of bond between monomers or a greater variety (e.g., alkyl, ether, and peroxy crosslinks in oxidation reactions or polyurethane linkages[181]).

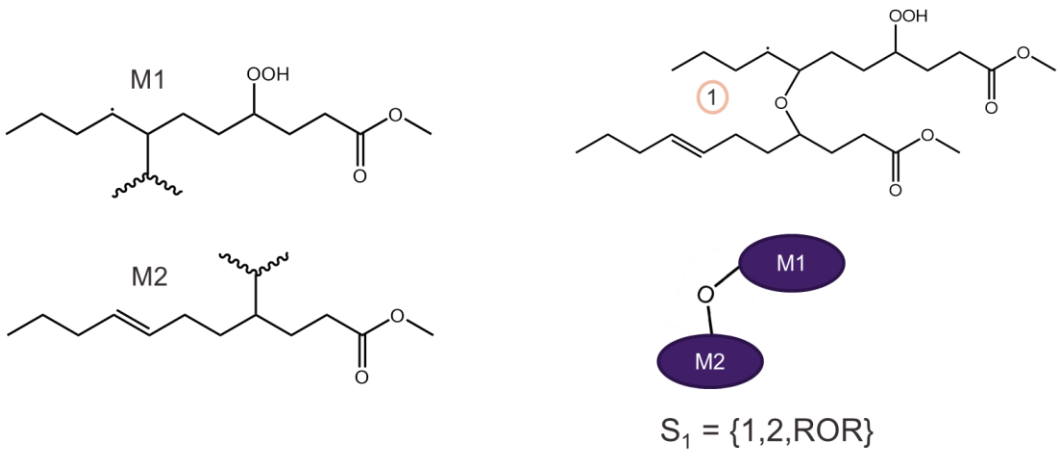

Figure 5.2. (Left) Monomer chemical graphs with multiple functional groups. The jagged lines indicate that the monomer is crosslinked at that carbon position. (Top-right) Explicit polymer species as a chemical graph. (Bottom) Coarse-grained polymer graph representation used in this work.

Like the monomer details, information about polymers can be stored during simulation, such as the count of each unique polymer, the cumulative functional groups present in the large molecules, the adjacency list and matrix of its monomer connections, degree of polymerization, molecular weight, and the distribution of crosslink types, if more than one type is present.

5.2.2 On-the-fly Species Generation

For small, self-limiting reactive systems, the entire possible chemical space can be explored by hand. However, as mentioned previously about polymer systems specifically, the possible distribution of products is too vast to identify experimentally or write out by hand. Even for EL autoxidation, a significant undertaking was made by Oakley et al. to get only to dimers and track all possible reactions and products.[18] Thus, on-the-fly generation of both polymers and monomers is advantageous to not have to enumerate potential insignificant species *a priori*. Automated reaction network generation (ARNG) is an effective tool and commonly used method for many chemical systems.[112,159,182] With ARNG, only reactant chemical graphs and the included reaction types are given at the beginning. Modifications to the chemical graphs are made at functional group graph sites each iteration until the whole chemical space is explored or a stopping point is reached. Stopping points may be time, chemical species' size, rank within the reaction network, or rate of formation.

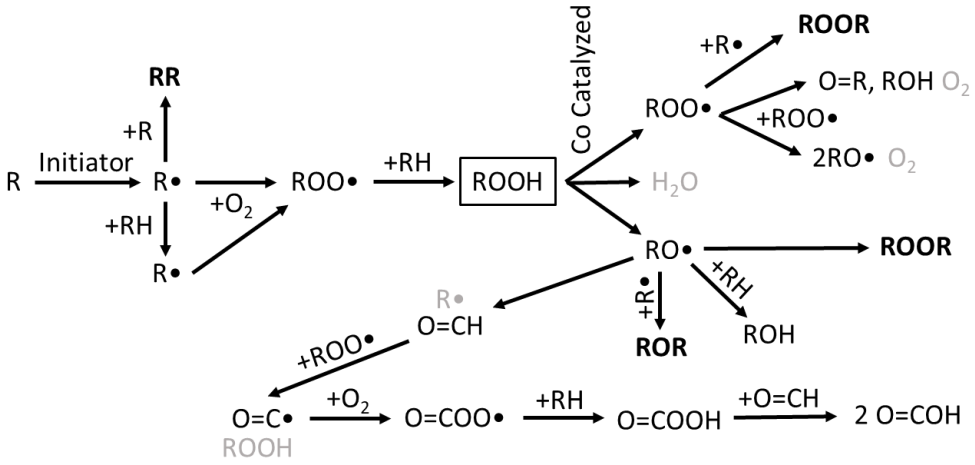

Figure 5.3. An example of a reaction network denoted by main reactive functional groups for autoxidation. Adapted from Oakley et al.[18]

5.2.3 Stochastic Simulation

A common stochastic method is kinetic Monte Carlo (kMC) simulation, an extension of the Monte Carlo method, which uses reaction probabilities and random numbers to solve problems informed by chemical kinetics. Gillespie devised the Stochastic Simulation Algorithm (SSA) which is outlined below.[108] A kMC simulation occurs in a small, finite volume and tracks explicit counts of chemical species. Within this volume is a range of 10^7-10^{12} molecules.[183] For radical systems, it is necessary to determine the minimum volume that contains at least two radicals to allow for termination reactions, as shown by Gao et al.[183] Initial states and quantities are selected by the user.

Reaction pathways can be written in two ways: each reaction between chemical species is written explicitly with a detailed rate constant, *k*, or through lumping functional groups with a representative rate constant. The former works for chemical systems where all reactants and products are known and can be fully enumerated, generally for smaller systems. The latter is best

for polymerization/depolymerization chemistry, as species are lumped based on molecular weight and different functional groups, like in polystyrene depolymerization.[184] A reaction rate for reaction *r* is calculated by multiplying reactant amount(s) by the rate constant,

$$R_r = c_{ij} N_i N_j \tag{5.1}$$

Because species are counted on a molecule basis in the kMC method, the rate constants must also be converted to a molecule basis. This is done using Avogadro's number and the system volume, resulting in the following equations and units for unimolecular and bimolecular reactions of species *i* and *j*:

$$c_i = k_i \quad [s^{-1}] \tag{5.2}$$

$$c_{ii} = \frac{2k_{ii}}{VN_A} \quad [molecules^{-1}s^{-1}] \tag{5.3}$$

$$c_{ij} = \frac{k_{ij}}{VN_A} \quad [molecules^{-1}s^{-1}] \tag{5.4}$$

where VN_A can be calculated by a scaled total number of molecules in the system, N_{TOT}, with the mole fraction, x_i, and molar density, ρ_i, of reactant components:

$$VN_A = N_{TOT} \sum_{i \in monomers,solvent} \frac{x_i}{\rho_i} \tag{5.5}$$

This scaling factor holds best when the density does not change significantly as the system evolves chemically.

Once all *N* reaction rates are calculated, the rates are summed to determine a propensity function, or the likeliness of a reaction to occur, and a random number selects the reaction.

$$p_r = \frac{R_r}{\sum_{r=1}^{N} R_r} \tag{5.6}$$

The summed rates also inform the time step with the relation:

$$\tau = \ln\left(\frac{1}{x}\right) \frac{1}{\sum_{r=1}^{N} R_r} \tag{5.7}$$

where τ is the timestep, and *x* is a uniform random number between 0 and 1. Time advances to $t = t + \tau$.

Once a reaction occurs, a stoichiometric number of molecules is added or removed from the respective species counts. The SSA iterates through a predetermined number of timesteps or until a final time is reached.

A benefit of using kMC is to overcome some issues with stiff systems or systems with many unique chemical species, where it would be infeasible to write and solve a differential equation for each. This is often the case in free radical polymerization with infinite molecular growth, as is the case in drying oil curing into a unified film. However, it should be noted that stiffness is a trait of the complex system, and stochastic simulation can still have challenges with the scale in solving.[185]

In smaller, contained simulations, an exact list of events can be pre-determined, calculating the rate of explicit species reacting with others. However, with an on-the-fly method generating new species, it would be infeasible to append this ever-growing list of reactions. As such, the rates are determined based on lumped functional group concentrations for reaction types:

$$R_{decomp} = k_{decomp}/(VN_A)N_{ROOH}N_{Co(II)} \tag{5.8}$$

$$R_{add} = k_{add}/(VN_A)N_{rad}N_{=} \tag{5.9}$$

$$R_{iso} = k_{iso}N_{=} \tag{5.10}$$

$$R_{recomb} = k_{recomb}/(VN_A)\ N_{rad}(N_{rad} - 1)/2 \tag{5.11}$$

where N_{ROOH} is the number of hydroperoxide functional groups in the system, for example. As a note, there are several factors of 2 to take into consideration when translating a kinetic model from

a deterministic to a stochastic method, and the authors direct the reader to an extensive article on the subject by De Keer and colleagues.[186]

Thus, rather than a growing list of reactions being generated and included, the reaction types are capped at a pre-determined number for which reaction types correspond to chemistry included in the model (on the order of 10-100 reaction types). Rate constants for each reaction are pre-determined. They can be derived from experiments in literature, fitted, or in Arrhenius form and temperature-dependent. The system size, N_{TOT}, must also be specified *a priori*.

Using the total number of functional groups at that time, all rates are calculated. Then a uniform random number is generated to select the reaction type that occurs.

From there, a function "PickASpecies" searches the list of all polymers that have that functional group, and then a new random number picks from the weighted distribution of those polymers to identify the reactants that will participate in that reaction event. "PickAMonomer" function then goes into the polymer and identifies a monomer within it that has the functional group of interest that will also participate in the reaction event. This method is grounded on the assumption of a homogenous, well-mixed system and equal reactivity of functional groups.

After the reactant polymers and their internal monomers are identified, a reaction rule is applied that modifies the chemical graph of the monomer. The resulting monomer is checked for uniqueness, or if it has been generated previously. If it has been identified previously, the monomer ID is reported. If not, the new monomer is added to the pool of monomers. The polymer species is updated to have this product monomer, and again a uniqueness check is performed in the same way. The final counts of the monomers and polymers participating in this reaction are updated

stoichiometrically, the total number of functional groups is updated, and the system iterates to the next time step until the final time specified is reached.

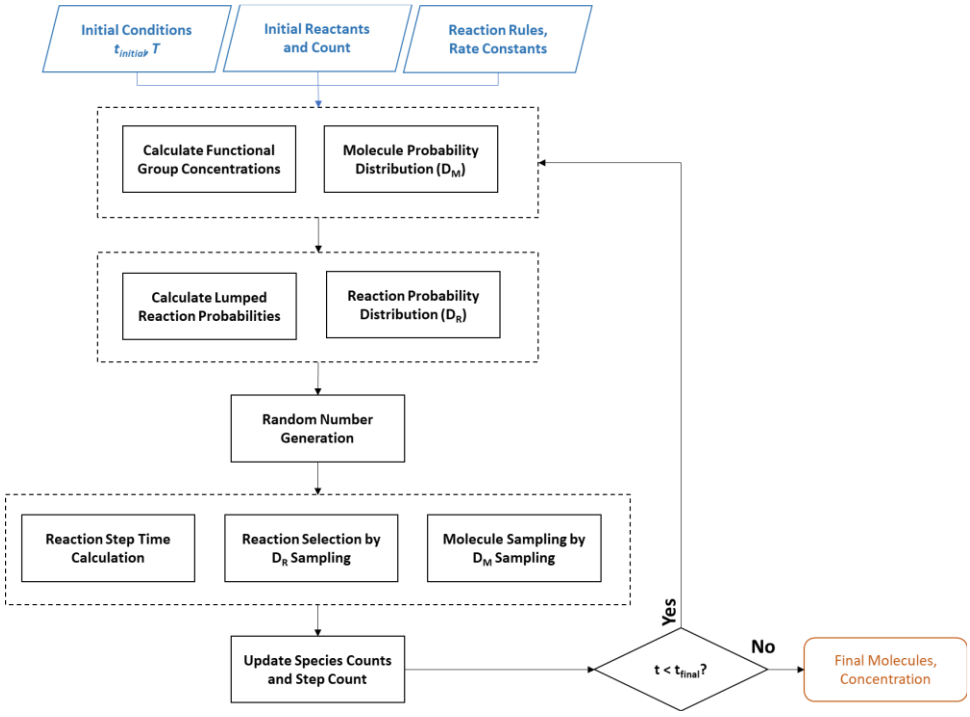

Figure 5.4. Stochastic Simulation Algorithm flowchart from starting inputs (blue) to final output (orange). Adapted from de Oliveira and Costa da Cruz.[187,188]

5.3 Case Study: Applying to the Autoxidation of Ethyl Linoleate

To the author's knowledge, this level of specificity has not yet been included in a whole model. For simpler chemical systems, lacking the chemical graph is fine, as there is not much spatial difference in the functional groups, or it is not multifunctional. However, for more larger, multifunctional monomers or polymers, such as unsaturated fatty acid esters found in drying oils, the position of functional groups along the fatty acid determines the reactivity and volatile products from scission or addition reactions.

To demonstrate the multifunctional monomer framework, it will be applied to the autoxidation of ethyl linoleate, a representative molecule for drying oils such as linseed oil with its double unsaturation along the 18-carbon fatty acid ester tail.

5.3.1 Simulation Methods

The chemistry included in this case study follows that from Chapter 4 for un-catalyzed autoxidation of ethyl linoleate. Continued work is being done to also have a direct comparison with Oakley and colleagues' study of the catalyzed autoxidation of EL.[18] Reactions in the model are summarized in Table 5.1.

The reactants and their initial concentrations are the following: ethyl linoleate molar concentration of 2.84 mol/L, cobalt(II)-ethyl hexanoate (CoEH) at 1.78 10^{-3} mol/L from Oyman's 0.07 wt% catalyst in oil,[96] and molecular oxygen at 1.58 10^{-3} mol/L at 25 ^{o}C from Choe and colleague's study of dissolved oxygen in soybean oil,[25] which predominantly has doubly unsaturated fatty tails in the triglycerides.

A system size is first calculated as 10^8 molecules, subdividing the collection of molecules proportionally with their concentrations based on VN_A scaling.

The code was written in MATLAB and builds off the base devised by Orlova and colleagues.[16,17] The automated reaction network generator, patterns, reaction family rules, and functions for graph modification were maintained. A stochastic simulation and polymer detail were layered onto the monomer approach framework already present. The code is available on GitHub.

Simulations ran on Northwestern University's high-performance computing cluster, Quest.

Table 5.1. Autoxidation reaction families and their respective rate coefficients at 70 °C. Values with an asterisk were optimized. Shaded rows are in the simplified free-radical polymerization model. White reaction rows are added to study the oligomerization pathways.

	Reaction Family	**Functional Group Representation**	***k* [1/s]**	***k* [L/mol*s]**
Initiation	Primary initiation	$I + O_2 \rightarrow IOO.$		$1\ 10^{-3}$ *
	Secondary initiation by initiator radical	IOO. + EL bi-allylic H → IOOH + R.		$1\ 10^{8}$ *
	ROOH Decomposition	ROOH → RO. + .OH	$4.5\ 10^{-5}$*	
Propagation	O_2 Addition	O_2 + R. → ROO.		$1.2\ 10^{8}$
	ROO. H-Abstraction of bi-allylic H	ROO. + R'H → ROOH + R'.		160*
	RO. H-Abstraction of bi-allylic H	RO. + R'H → ROOH + R'.		160*
	R. H-Abstraction of bi-allylic H	R. + R'H → RH + R'.		42*
	HO. H-Abstraction of bi-allylic H	.OH + R'H → H_2O + R'.		42*
	β-scission, Type 1	RO. → R(O)H + R'.	240*	
	ROO. Addition to conjugated dienes	ROO. + //\// → ROOR'.		1000*
	RO. Addition to conjugated dienes	RO. + //\// → ROOR'.		2800*
Termination	R. + R. Recombination	R. + R'. → RR'		$2\ 10^{8}$*
	RO. + RO. Recombination	RO. + R'O. → ROOR'		$2\ 10^{8}$*
	RO. + R. Recombination	RO. + R'. → ROR'		$2\ 10^{8}$*
	ROO. + R. Recombination	ROO. + R'. → ROOR'		$2\ 10^{8}$*
	ROO. + ROO. Recombination	ROO. + R'OO. → ROOR' + O_2		$2\ 10^{8}$*
	ROO. + ROO. Russell termination	ROO. + R'OO. → ROH + R(O)H + O_2		$2\ 10^{8}$*

5.3.2 Model Observations and Considerations

Several considerations were made in using the multifunctional framework to study this complex reactive system. Observations and modifications are listed in the following subsections to improve the computational efficiency of the model and should be used as inspiration for future applications of the framework to other complex systems with their own rates, concentrations, and challenges.

5.3.2.1 System Size

A main consideration is the simulation system size. For radical systems, it is crucial to have a sufficient concentration of radicals to propagate and continue the chemistry; otherwise, the solution will be artificially truncated. Gao and colleagues studied this for PMMA and other systems.[183] The pseudo-steady state approximation is made and is a reasonable assumption for many systems; however, for EL, it begins to fail if an insufficient concentration of radicals is given. As demonstrated in Figure 5.5, there is a deviation in the kMC solution and a continuum model due to the concentration of alkyl radicals being so low (10^{-10} M) and the model truncating.

For 10^8 molecules, the conversion profile for EL deviates within 1 hour, leading to a 0.79% lower concentration, rather than an error of 0.072% for 10^9 molecules and 0.0072% for 10^{10} molecules. The accuracy increases proportionally to how the system size scales. Similarly, the computation time scales with a power-law relationship, where increasing the system size tenfold increases the simulation time by 10, as shown in Figure 5.6.

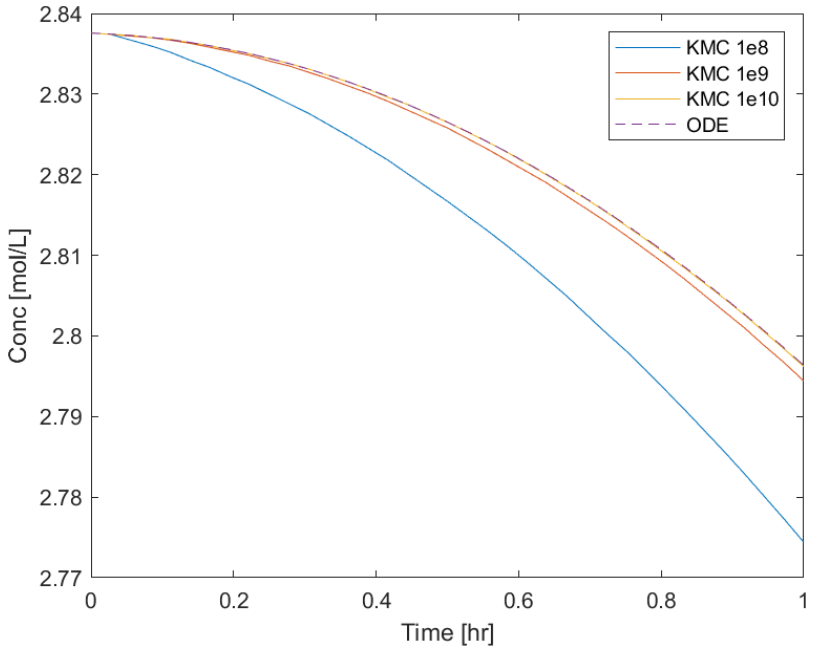

Figure 5.5. A comparison of system sizes from 10^8 to 10^{10} molecules to a continuum model of functional group conversion and the effect of artificial truncation of the stochastic model within 1 hour.

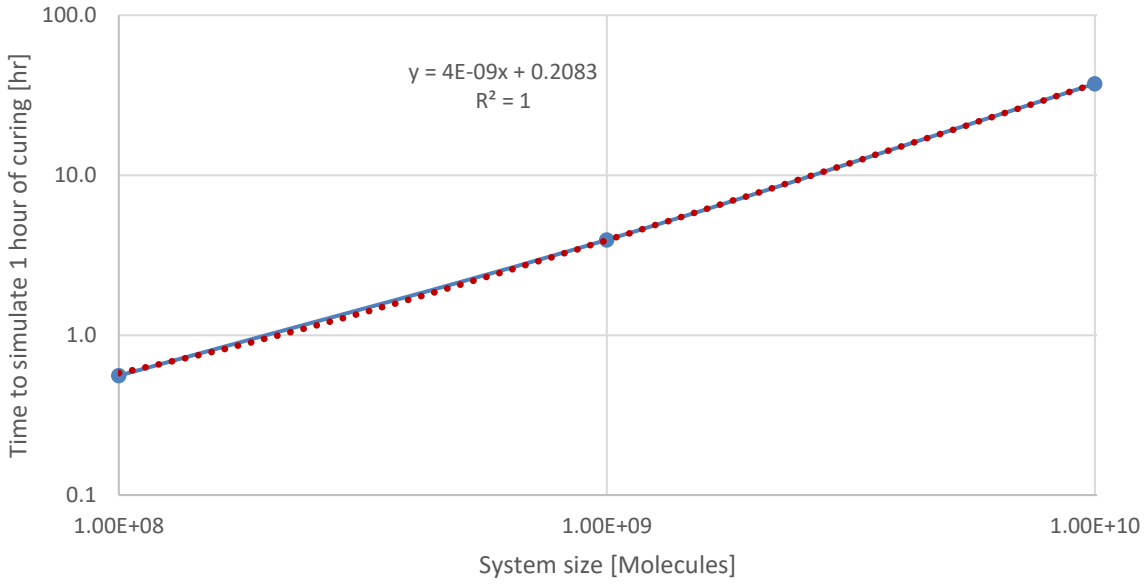

Figure 5.6. Relationship between the computational time to simulate curing and the system size. Blue dots indicate experiments at 10^8, 10^9 and 10^{10} molecules, and the red dashed line is a power-law trendline.

When extending the simulated curing time to 6 hours in Figure 5.7, a run with 10^9 molecules performs reasonably well, though there is still a 0.66% under-prediction in the conversion of EL compared to the continuum model. In order to balance computational expense and accuracy, subsequent model results reported in this chapter will be with a simulation system size of 10^9 molecules.

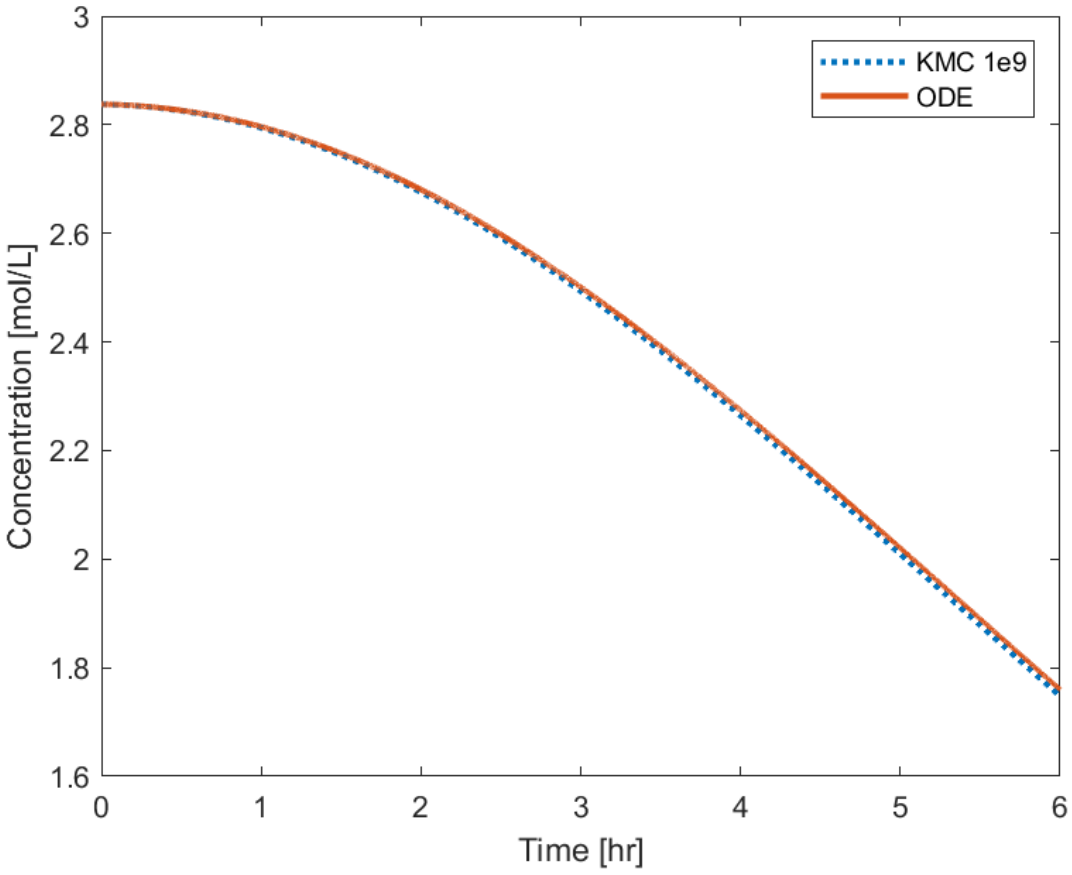

Figure 5.7. Stochastic and continuum model comparison at 6 hours for the conversion of ethyl linoleate. A slight deviation propagates over time in the stochastic model with 10^9 molecules.

3.2.2 Reaction Rates

In the autoxidation of EL, oxygen addition to an alkyl radical dominates the event distribution. As seen in Figure 5.8, within the 100 s time intervals taken, the rate of oxygen addition is 2 orders of magnitude greater than the second-most rapid reaction of peroxy radical bi-allylic H-abstraction: 1.89 10^5 molecules/s vs 3.16 10^3 molecules/s, respectively. As such, excess computational time is spent only adding O_2 because it is so frequent, rather than other productive or forward chemistry—for example, it took over 15 hours to simulate 1 hour of curing at 10^9 molecules.

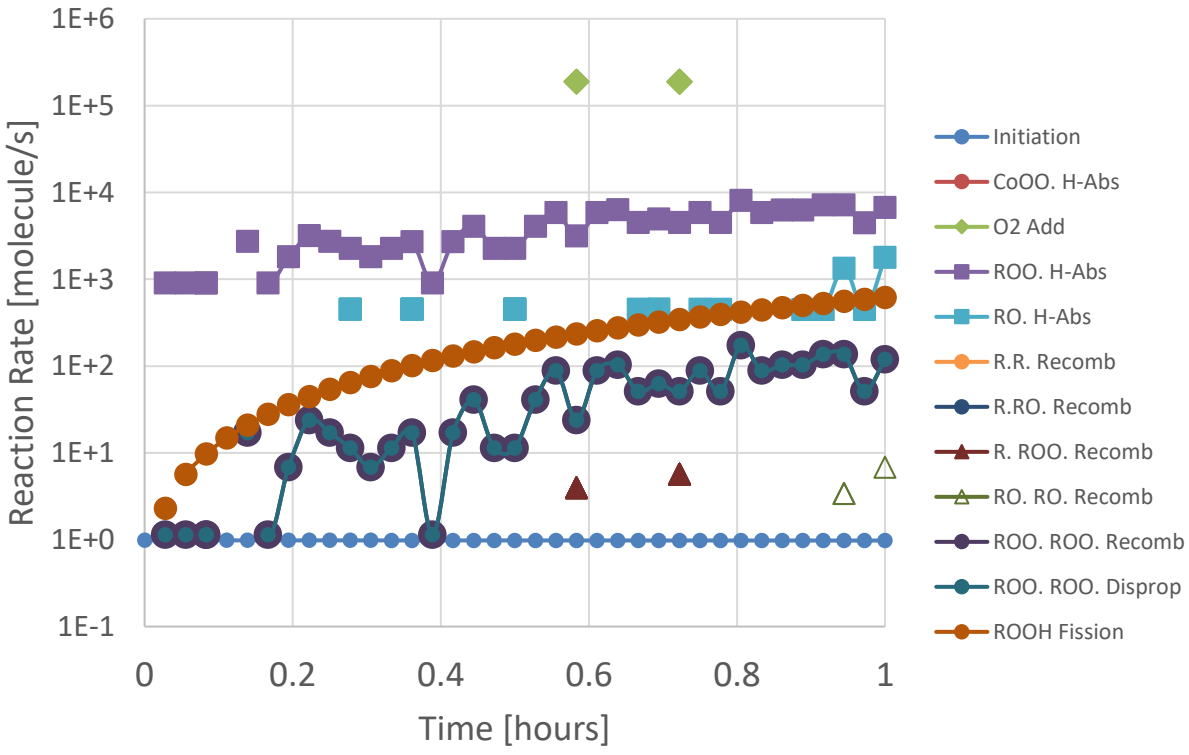

Figure 5.8. Reaction rates for reduced EL autoxidation model reaction types over 1 hour. Any disconnected points indicate non-consecutive non-zero reaction rates at the interval of 100 s.

An attempt was made to implement τ-leaping, developed by Gillespie and Petzold,[189] to "leap" over frequent, non-rare events to accelerate the simulation and use low-concentration species and their rare-event reactions as the events to step between, with more frequent reaction events summed over. However, there are several reasons this approach would not work. One reason is on-the-fly generation of species would need to be pooled and checked if unique, and then reacted due to the reaction-type events rather than specific reactions between species. An additional step would be needed to generate possible reactants and products which would then get included after each step. This is not infeasible, as a rate-based on-the-fly approach has been effective for other large systems,[112] even that of EL autoxidation.[19]

Another reason τ-leaping would not work for this particular case is that the reaction that it would try to leap or sum over is oxygen addition with an average rate of 10^5 molecules/s, but the alkyl radical as a reactant is a critical species as defined by Cao and colleagues[190] and is the limiting factor. Oxygen addition would not get summed over, since there is a chance the concentration of alkyl radicals would become negative.[190]

Thus, a simplification is made to assume immediate O_2 addition to starting alkyl radicals formed from bi-allylic H-abstraction. This has 3.75x speed-up of the system with 100% accuracy within rounding error, as it now took just under 4 hours to simulate 1 hour of curing.

This assumption of immediate O_2 addition does have an effect on the number of polymers formed, since alkyl radicals can occasionally persist and undergo self- and cross-termination with other radicals. Within 1 hour, 7 dimers were formed: 1 alkyl dimer, 3 ether dimers, and 3 peroxy dimers. The peroxy and ether dimers have a multiplicity due to the combinations of where the crosslink exists in the conjugated diene system. For the same multiplicity reasons, one would

expect 3 alkyl dimer isomers; however, the time for those particular dimers to evolve in the system begins around 1 hour, as found in the lower right corner of Figure 5.9. Additionally, the concentration of alkyl radicals is small relative to other radicals, so self-termination is exponentially less likely than cross termination with other radicals or the competing reaction of O_2 addition, as discussed.

The non-peroxy crosslinked dimers in Figure 5.9 total to concentrations ranging from 10^{-8} to 10^{-6} mol/L. The amount of ether crosslinks is much lower than the number of peroxy crosslinks, as no addition by alkoxy radicals is assumed in the simplified model, which becomes clear by comparing to Figure 4.14a in Chapter 4.

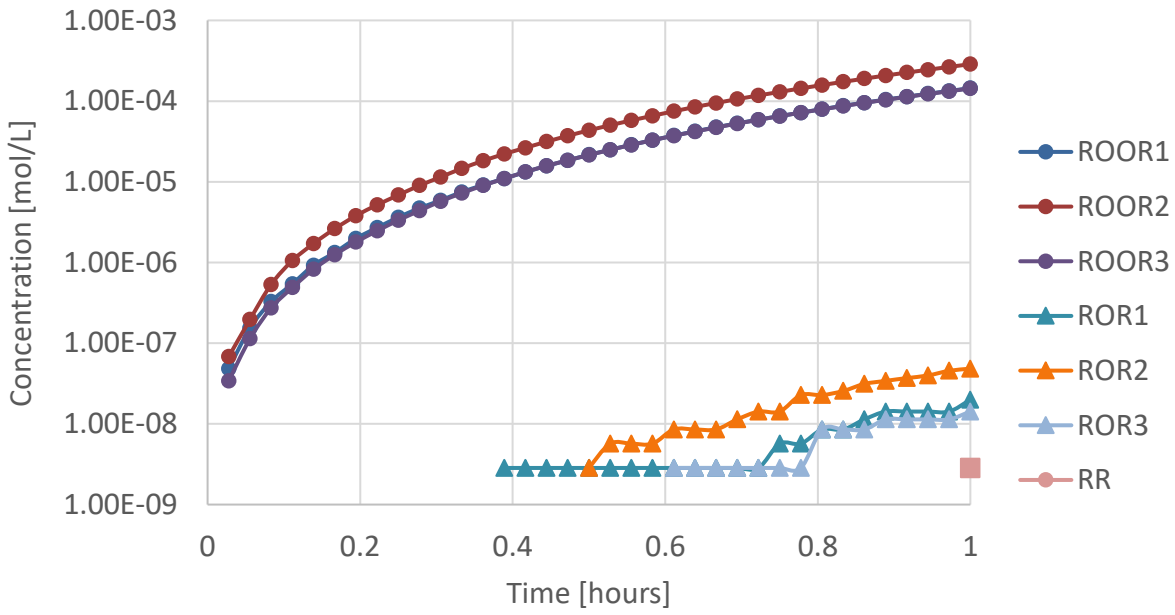

Figure 5.9. Concentration of dimers in simplified autoxidation model over 1 hour. Peroxy-crosslinked dimers are circles, ether crosslinked dimers are triangles, and alkyl-crosslinked dimer has a square marker.

3.2.3 Uniqueness Check

An analysis was made on the run-time of the simulation and inefficiencies to optimize. One point of optimization is bypassing the uniqueness check of each monomer graph after it is generated from applying reaction rules. There is a finite, small number of monomer constituents; for example, each H-abstraction from EL gives the same two possibilities (5-carbon conjugated dienes with the radical most likely on 1^{st} and 5^{th} carbon atoms). Rather than going through the intensive Ullman function to check the uniqueness of the chemical graph, a feature of the monomer object was added to the monomers of the reaction it participates in and what its product was. Then, if the flag is indicated that this monomer participated in the reaction before, the uniqueness check can be bypassed. This has a maximum speed-up to the uniqueness check of O(1) to O(*m*) where m is the number of monomers found to be unique up to that point in simulation.

5.3.2.4 Polymer Functional Groups

Another opportunity for speedup was identified in the "PickASpecies" function, in which the whole list of polymers is searched each time step for the polymers that have the functional group or pattern of interest. A simplification was made to have an array structure 1x45, where each of the 45 functional groups contains a growing array of polymers with at least 1 of that functional group pattern that is explicitly tracked. Though inefficient to append to an array, it is faster than the previous version without the improvement. However, there are still limits as the system gets larger and many unique polymers are added to each array, and the functional group array can range from O(1) to O(*p*) for the number of *p* unique polymer species in the extreme case, especially for common functional groups such as conjugated double bonds or crosslinks.

5.3.2.5 Polymer graph-modifying reactions

Since the monomer approach by Orlova et al.[16] lacks an explicit polymer that can be modified, additional routines were incorporated to the code to modify polymer graphs in the multifunctional framework.

Particularly in autoxidation, alkoxy radicals may undergo β-scission. This leads to volatile fragments that split a "monomer" unit. Depending on where crosslinks exist, the fragments after splitting may still be connected to the reactant polymer. A function was implemented to check the connectivity of scission fragments after a reaction occurred, which did not exist in the monomer approach code base, since polymer detail was not maintained.

Some reaction types also modify crosslinks, such as epoxidation or peroxy crosslink decomposition. For this reaction, a peroxy crosslink is randomly chosen from the polymer graph of a species selected to decompose in the time step. The monomers that are connected by that edge must have their chemical graphs modified to now have alkoxy radicals. A final step, similar with β-scission, is checking if the product is still a single connected component or the crosslink was critical, and now two product species exist. As a mixed case, epoxidation involving a peroxy crosslink also modifies both the polymer graph and monomer graphs.

5.3.3 Kinetic Model Extension with Radical Addition

The simplified model was extended by the remaining reactions in Table 5.1 to include radical addition to 4-carbon conjugated double bonds, hydroperoxyl radical bi-allylic H-abstraction, and the first of two β-scission pathways studied extensively by Oakley et al.[80] which forms pentanal. This extended model, which still lacks secondary oxidation and epoxidation, does allow the formation of oligomers beyond dimers.

Within 1 hour of simulated curing time, 339 unique monomer fragments were generated, and 46,192 unique polymers formed up to 11-unit species. This extension came at a computational price of nearly 2.5 days running the simulation. A particular inefficiency happens in the step of selecting reactant polymers from the growing list of species that have the functional group of interest, as mentioned in Section 3.2.4. With over 46,000 finite polymers formed only within 1 hour, this approach may be unreasonable in the infinite polymer growth when tracking explicit polymers is the objective. However, a future adaption may be in only storing polymer graphs as they form, eventually converging into a single massive component with 10^9 monomer units.

These 46,192 polymers can be lumped together by their molecular weights, simplifying down to 694 mass peaks with accumulated molar concentrations. The mass spectrum with concentration as a proxy for intensity is given in Figure 5.10, with a note of the logarithmic scale of concentration ranging from 10^{-9} to 10^{0}. Again, this underscores the importance of having a substantial simulation size, though the error in truncating artificially at early curing is small.

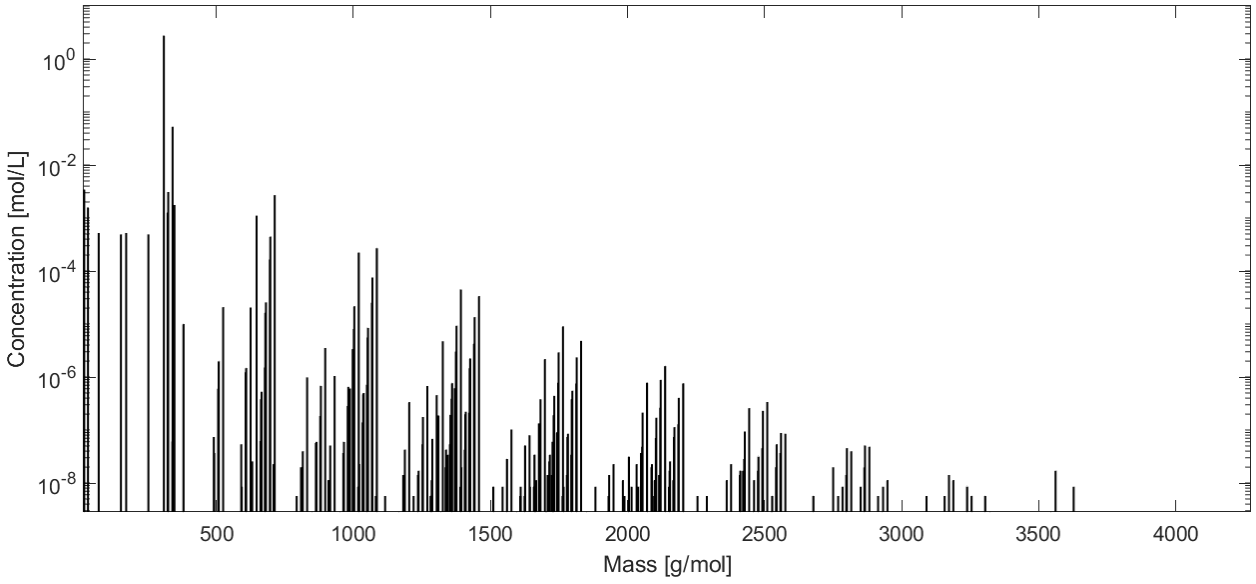

Figure 5.10. Mass spectrum of 694 polymer molecular weights, lumped from 46,192 total polymers at 1 hour of simulated EL curing at 70 °C.

Another representation for the mass distribution of the oligomers formed within 1 hour is shown in Figure 5.11. Conversion of EL monomer is still low at 1 hour, and thus further oligomers consume minor fractions of the mass distribution. For example, the oligomers beyond the hexamer limit set using a rate-based termination criteria by Oakley et al.[80] only constitute 5.77 10^{-4} % of the mass. Though this is only at 1 hour of autoxidation, the contribution of a greater number of higher molecular weight oligomers is expected. Note that obtaining the mass distribution, as shown in Figure 5.11, marks the progress in the investigation of polymer properties as compared to Orlova et al.[16] In that work, the *size* distribution was presented as computed from a Random Graph model. However, the size distribution has been estimated from the distribution of the number of monomer units in the polymers. In EL polymerization, in contrast to most industrial polymerization systems, the monomer units are of highly varying weight (see also Chapter 4). The *mass* distribution does not correspond to the size distribution in a simple manner. This illustrates the strength of the kMC-based simulations that were developed.

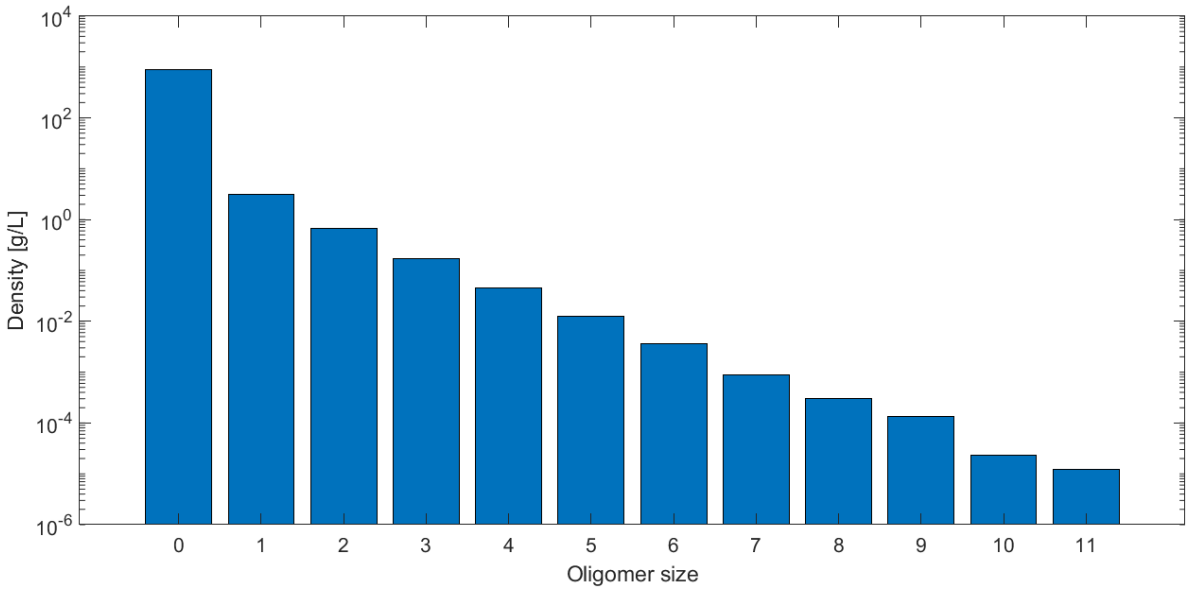

Figure 5.11. Exponential decay in cumulative oligomer masses for 1 hour of autoxidative curing of EL at 70 °C.

5.4 Conclusion

The growth in the field of polymer reaction engineering is driven by challenges in modeling complex polymer systems and the advancement of resources to manage the level of detail. This chapter puts forth a specialized framework for multifunctional, crosslinked polymers that overcomes computational barriers faced in simulating complex polymer and chemical systems by using a composite approach of graphs, on-the-fly species generation, and stochastic simulation.

Though a general framework was described, care must be taken in applying the framework to different complex systems. For example, with the autoxidation of ethyl linoleate, assumptions and simplifications must be made to efficiently simulate the chemistry due to rapid reaction rates, low radical concentrations, and the expense of checking for uniqueness in chemical graphs as novel species are generated in time. There are drawbacks to this method, but that is expected in the balance of computational expense and level of detail gained from a model like this. One can cater or tune the model to the specific bounds and rates, and the general framework is available for simple models up to complex polymers to allow further exploration of reactive polymer systems.

Further applications of the framework to triglyceride polymer hydrolysis[78,82,191,192] would be of particular interest to art conservation science and studying the factors of accelerated aging or stability of drying oil mixtures. The framework discussed in this chapter focuses on the forward chemistry and capability for polymerization, but depolymerization and fissions would be feasible and particularly useful to plastics recycling.

Chapter 6 Summary and Future Perspectives

6.1 Summary

In this dissertation, a key thread is the application of modeling techniques and the limits and advantages of different methods. Especially when dealing with complex chemical systems, it is imperative to consider the bounds and the objectives of a problem, as different methods can focus on certain measures of interest. Art inspires the pursuit of technical solutions found in the complex problems related to cultural heritage science. In the context of oil paint, Chapter 2 summarizes the chemistry and state of the field for studying oil paint and its model systems. The autoxidation of drying oils is both relevant to art and other areas, such as food science and biological systems where these unsaturated, bio-based oils are present.

Chapter 3 is placed in the broader polymer reaction engineering field studying the pyrolysis-induced depolymerization of polyethylene (PE) and polypropylene (PP). While differing from the emphasis on forward polymerization found in the rest of this thesis, this chapter demonstrates the merits of different computational models. A global model for polyolefin pyrolysis has a strong agreement to historical experimental results of the sigmoidal behavior in linear polymer decomposition. An equivalent mechanistic model for high-density polyethylene also has a strong agreement with the sigmoidal conversion. However, a model for PP pyrolysis, differing from the PE model only in the heats of reaction, does not find the same agreement; rather, it captures the deceleratory behavior of conversion for atactic-PP. Had the mechanistic model not been used for PP, non-chemical influences on the conversion of linear polymers would not have been apparent.

Looking then to drying oil chemistry, Chapter 4 takes an existing model for the autoxidation of ethyl linoleate and fits sensitive kinetic parameters to experimental data for the elevated drying of samples. The model focuses only on the formation of novel monomeric fragments rather than the oligomerization or polymerization using automated reaction network generation. Thus, this model is useful when comparing to lumped concentrations of functional groups of interest. The model does give an option for reassembling the monomer fragments into polymers using random graph theory, but this chapter instead focuses on the monomers and dimers formed and identified within ESI mass spectra to indicate where the model can be improved. Models and experiments can be a feedback loop, informing each of what is present and where further insight is necessary. For example, greater investigation in the decomposition of hydroperoxides is needed, especially for the uncatalyzed system, where a rate of decomposition that is too low, yet is calculated with common kinetic parameters, does not capture the experimental behavior. Also, the fine subdivision of reaction families is also underscored in the influence of conversion, where a lumped rate coefficient can be fitted, but the spread for different reactants varies dramatically from 10^1 to 10^8 L/mol*s.

In an effort to overcome several computational barriers reached by previous kinetic models for the autoxidation of ethyl linoleate (EL), a new multifunctional, mechanistic framework is developed that combines automated reaction network generation, monomer and coarse-grain polymer graphs, and stochastic simulation. Chapter 5 describes the method in detail for a generic system and is then applied to EL autoxidation. There is a balance struck in the chemical complexity of this system and the computational expense it takes to solve for the time-evolution of functional groups and polymer species' concentrations. Several speed-ups are identified and implemented;

however, the reality of particular reaction rates for this specific system continue to challenge the efficient simulation. The multifunctional framework does offer a new way to overcome challenges in modeling the physical aspect of polymers and challenges for complex systems.

In summary, this dissertation demonstrates the importance of computational modeling, particularly for reactive polymer systems. Challenges persist, but advances have been made in the study of complex systems.

6.2 Recommendations for Future Research

The autoxidation chemistry discussed and included in this thesis does not include further photochemistry, such as UV degradation of drying oils[193,194] or the addition of singlet oxygen.[47,195] This extension is necessary for more-detailed systems; however, there will be a penalty in the complexity and the explosion in unique polymer species. Additionally, these models also lack allylic hydrogen abstraction and focus only on the facile bi-allylic abstraction from the reactant. This would also extend the studied chemical space, but it would also grow the system to include possibly more insignificant species to capture the resonance of products and multiplicity of where the reaction network continues to grow. Also, it should be kept in mind that in this thesis, a monoglyceride, EL, has been taken as a model substance for a true triglyceride. Indeed, the final target of this research line is the full modeling of drying oils like linseed oil. As a consequence, many more reactions will have to be included, like the formation of various cyclic structures.[62]

The multifunctional framework was developed with a view of having a polymer to eventually depolymerize and study triglyceride hydrolysis that would destroy the polymer network. This future direction is of great interest and importance to art conservation scientists and other coatings research, as the period of long-term degradation is the one that is studied long after

a paint has cured. The framework is conducive to studying polymer degradation, and a parallel to it has already been implemented for simpler chemistry.

All of these refinements and extensions mentioned would extend the size of the model and lead to excess computational effort. Applying state-of-the-art model reduction techniques like those based on 'directed relation graphs'[196] or genetic algorithms[197] is one potential avenue to overcome this problem and could therefore be a topic of future research in this field.

In current times, plastics recycling is top of mind for polymer research. Particularly, what is the mixture and composition of monomers that are reconstituted into a recycled product, and how does the that impact the chemistry and mechanical properties of the new polymers. By developing a framework that can capture the diversity of monomeric fragments, the computational studies of these systems could improve and sooner address questions in theory and practice.

Additionally, it would be beneficial to build out the computational model into a functional software package. Extensive time went into building up the model, and it is appealing to have a package to roll out and be open source for others to continue to build out functionality in a controlled manner. This could also be useful for engineering education to look at the impact of temperature on product distributions and complex reactive systems, which are present in modern reactors. Also, it could be a tool for STEM outreach.

The non-invasive tools developed for cultural heritage science continue to expand and address long-standing questions in the field. The intersection of chemical engineering and art is rich with research questions, particularly modern, industrial paints, as they no longer exist as bio-based coatings and include modifiers that affect drying and physical properties of the polymer film. The long-term stability of these newer materials is only now being revealed experimentally,

and the addition of computational models in tandem may allow for deeper insights into what is happening on the molecular level to aid in conservation and intervention efforts.

References

1. Defining the conservator: essential competencies. in 1–18 (American Institute for Conservation of Historic and Artistic Works, 2003).
2. Erhardt, D., Tumosa, C. S. & Mecklenburg, M. F. Long-Term Chemical and Physical Processes in Oil Paint Films. *Stud. Conserv.* **50**, 143–150 (2005).
3. Hermans, J. J., Keune, K., Loon, A. van & Iedema, P. D. The crystallization of metal soaps and fatty acids in oil paint model systems. *Phys. Chem. Chem. Phys.* **18**, 10896–10905 (2016).
4. van Driel, B. A. *et al.* Determination of early warning signs for photocatalytic degradation of titanium white oil paints by means of surface analysis. *Spectrochim. Acta Part A Mol. Biomol. Spectrosc.* **172**, 100–108 (2017).
5. de la Rie, E. R., Michelin, A., Ngako, M., Del Federico, E. & Del Grosso, C. Photo-catalytic degradation of binding media of ultramarine blue containing paint layers: A new perspective on the phenomenon of "ultramarine disease" in paintings. *Polym. Degrad. Stab.* **144**, 43–52 (2017).
6. Cakić, S. M., Ristić, I. S., Vladislav, J. M., Stamenković, J. V & Stojiljković, D. T. IR-change and colour changes of long-oil air drying alkyd paints as a result of UV irradiation. *Prog. Org. Coatings* **73**, 401–408 (2012).
7. Clark, G. L. & Tschentke, H. L. Physico-Chemical Studies on the Mechanism of the Drying of Linseed Oil I—Changes in Density of Films. *Ind. Eng. Chem.* **21**, 621–627 (1929).
8. Carter, S. *et al.* Atomic spectrometry update: review of advances in the analysis of metals, chemicals and materials. *J. Anal. At. Spectrom.* **32**, 2068–2117 (2017).
9. Sotiropoulou, S. *et al.* Advanced analytical investigation on degradation markers in wall paintings. *Microchem. J.* **139**, 278–294 (2018).
10. Liu, P., Hall-Aquitania, M., Hermens, E. & Groves, R. M. Mapping the opacity of paint layers in paintings with coloured grounds using optical coherence tomography. in vol. 10331 103310C-10331–8 (2017).
11. Erhardt, D., Tumosa, C. S. & Mecklenburg, M. F. Natural and accelerated thermal aging of oil paint films. *Stud. Conserv.* **45**, 65–69 (2000).
12. *Global Paints and Coatings Market Report by Resin Type, Formulation, Application, and By Regions - Industry Trends, Size, Share, Growth, Estimation and Forecast, 2017-2024*. (2018).
13. Douny, C. *et al.* Linseed oil presents different patterns of oxidation in real-time and accelerated aging assays. *Food Chem.* **208**, 111–115 (2016).
14. Orlova, Y., Harmon, R. E., Broadbelt, L. J. & Iedema, P. D. Review of the kinetics and simulations of linseed oil autoxidation. *Prog. Org. Coatings* **151**, (2021).

15. Harmon, R. E., SriBala, G., Broadbelt, L. J. & Burnham, A. K. Insight into Polyethylene and Polypropylene Pyrolysis: Global and Mechanistic Models. *Energy & Fuels* **35**, 6765–6775 (2021).

16. Orlova, Y., Kryven, I. & Iedema, P. D. Automated reaction generation for polymer networks. *Comput. Chem. Eng.* **112**, 37–47 (2018).

17. Orlova, Y., Gambardella, A. A., Harmon, R. E., Kryven, I. & Iedema, P. D. Finite representation of reaction kinetics in unbounded biopolymer structures. *Chem. Eng. J.* 126485 (2020) doi:https://doi.org/10.1016/j.cej.2020.126485.

18. Oakley, L. H., Casadio, F., Shull, K. R. & Broadbelt, L. J. Microkinetic modeling of the autoxidative curing of an alkyd and oil-based paint model system. *Appl. Phys. A* **121**, 869–878 (2015).

19. Oakley, L. H., Casadio, F., Shull, K. R. & Broadbelt, L. J. Modeling the Evolution of Crosslinked and Extractable Material in an Oil-Based Paint Model System. *Angew. Chemie Int. Ed.* **57**, 7413–7417 (2018).

20. Gombrich, E. H. *The Story of Art - 16th Edition*. (Phaidon Press, 1995).

21. van den Brink, O. F., Boon, J. J., O'Connor, P. B., Duursma, M. C. & Heeren, R. M. A. Matrix-assisted laser desorption/ionization Fourier transform mass spectrometric analysis of oxygenated triglycerides and phosphatidylcholines in egg tempera paint dosimeters used for environmental monitoring of museum display conditions. *J. Mass Spectrom.* **36**, 479–492 (2001).

22. Currier, A. J. & Kagarise, I. H. Rate of Linseed Oil Oxidation with Driers. *Ind. Eng. Chem.* **29**, 467–469 (1937).

23. Hess, P. S. & O'Hare, G. A. Oxidation of Linseed Oil. *Ind. Eng. Chem.* **42**, 1424–1431 (1950).

24. Colombini, M. P., Modugno, F., Giacomelli, M. & Francesconi, S. Characterisation of proteinaceous binders and drying oils in wall painting samples by gas chromatography–mass spectrometry. *J. Chromatogr. A* **846**, 113–124 (1999).

25. Choe, E. & Min, D. B. Mechanisms and Factors for Edible Oil Oxidation. *Compr. Rev. Food Sci. Food Saf.* **5**, 169–186 (2006).

26. Meilunas, R. J., Bentsen, J. G. & Steinberg, A. Analysis of aged paint binders by FTIR spectroscopy. *Stud. Conserv.* **35**, 33–51 (1990).

27. Mallégol, J., Lemaire, J. & Gardette, J.-L. Drier influence on the curing of linseed oil. *Prog. Org. Coatings* **39**, 107–113 (2000).

28. Okan Oyman, Z., Ming, W. & van der Linde, R. Oxidation of model compound emulsions for alkyd paints under the influence of cobalt drier. *Prog. Org. Coatings* **48**, 80–91 (2003).

29. Oyman, Z. O., Ming, W., van der Linde, R., van Gorkum, R. & Bouwman, E. Effect of [Mn(acac)3] and its combination with 2,2′-bipyridine on the autoxidation and oligomerisation of ethyl linoleate. *Polymer (Guildf).* **46**, 1731–1738 (2005).

30. van Gorkum, R. & Bouwman, E. The oxidative drying of alkyd paint catalysed by metal complexes. *Coord. Chem. Rev.* **249**, 1709–1728 (2005).

31. Bouwman, E. & van Gorkum, R. A study of new manganese complexes as potential driers for alkyd paints. *J. Coatings Technol. Res.* **4**, 491–503 (2007).

32. Mallégol, J., Gardette, J.-L. & Lemaire, J. Long-term behavior of oil-based varnishes and paints. Fate of hydroperoxides in drying oils. *J. Am. Oil Chem. Soc.* **77**, 249–255 (2000).

33. Spier, E., Neuenschwander, U. & Hermans, I. Insights into the Cobalt(II)-Catalyzed Decomposition of Peroxide. *Angew. Chemie Int. Ed.* **52**, 1581–1585 (2013).

34. Muizebelt, W. J. *et al.* Oxidative crosslinking of alkyd resins studied with mass spectrometry and NMR using model compounds. *J. Coatings Technol.* **70**, 83–93 (1998).

35. Fjällström, P., Andersson, B., Nilsson, C. & Andersson, K. Drying of linseed oil paints: a laboratory study of aldehyde emissions. *Ind. Crops Prod.* **16**, 173–184 (2002).

36. Oakley, L. H., Casadio, F., Shull, K. R. & Broadbelt, L. J. Theoretical Study of Epoxidation Reactions Relevant to Hydrocarbon Oxidation. *Ind. Eng. Chem. Res.* **56**, 7454–7461 (2017).

37. Honzíček, J. Curing of Air-Drying Paints: A Critical Review. *Ind. Eng. Chem. Res.* **58**, 12485–12505 (2019).

38. Soucek, M. D., Khattab, T. & Wu, J. Review of autoxidation and driers. *Prog. Org. Coatings* **73**, 435–454 (2012).

39. Juita, Dlugogorski, B. Z., Kennedy, E. M. & Mackie, J. C. Low temperature oxidation of linseed oil: a review. *Fire Sci. Rev.* **1**, 3 (2012).

40. Yermanos, D. M. & Goodin, J. R. Effect of Temperatures During Plant Development on the Fatty Acid Composition of Linseed Oil1. *Agron. J.* **57**, 453–454 (1965).

41. van den Berg, J. D. J., Vermist, N. D., Carlyle, L., Holčapek, M. & Boon, J. J. Effects of traditional processing methods of linseed oil on the composition of its triacylglycerols. *J. Sep. Sci.* **27**, 181–199 (2004).

42. Degano, I., La Nasa, J., Ghelardi, E., Modugno, F. & Colombini, M. P. Model study of modern oil-based paint media by triacylglycerol profiling in positive and negative ionization modes. *Talanta* **161**, 62–70 (2016).

43. Stenberg, C., Svensson, M. & Johansson, M. A study of the drying of linseed oils with different fatty acid patterns using RTIR-spectroscopy and chemiluminescence (CL). *Ind. Crops Prod.* **21**, 263–272 (2005).

44. Muizebelt, W. J., Hubert, J. C. & Venderbosch, R. A. M. Mechanistic study of drying of alkyd resins using ethyl linoleate as a model substance. *Prog. Org. Coatings* **24**, 263–279 (1994).

45. Frankel, E. N., Garwood, R. F., Vinson, J. R. & Weedon, B. C. L. Stereochemistry of olefin and fatty acid oxidation. Part 1. Autoxidation of hexene and hepta-2,5-diene isomers. *J. Chem. Soc. Perkin Trans. 1* 2707–2713 (1982) doi:10.1039/P19820002707.

46. Hubert, J. C., Venderbosch, R. A. M., Muizebelt, W. J., Klaasen, R. P. & Zabel, K. H. Mechanistic study of drying of alkyd resins using (Z,Z)- and (E,E)-3,6-nonadiene as model substances. *Prog. Org. Coatings* **31**, 331–340 (1997).

47. Carless, H. A. J. & Batten, R. J. Photosensitised oxidation of model unsaturated lipid systems: (4Z,7Z)-undeca-4,7-diene and (4Z)-undec-4-en-7-yne. *J. Chem. Soc. Perkin Trans. 1* 1999–2007 (1987) doi:10.1039/P19870001999.

48. Sengupta, A. & Mazumder, U. K. Triglyceride composition of Papaver somniferum seed oil. *J. Sci. Food Agric.* **27**, 214–218 (1976).

49. Özcan, M. M., İman, C. & Arslan, D. Physicochemical properties, fatty acid and mineral content of some walnuts (Juglans regia L.) types. *Agric. Sci.* **1**, 62–67 (2010).

50. Maggio, R. M. *et al.* Monitoring of fatty acid composition in virgin olive oil by Fourier transformed infrared spectroscopy coupled with partial least squares. *Food Chem.* **114**, 1549–1554 (2009).

51. Iedema, P. D. & Kolhapure, N. H. Mathematical Methods. *Handbook of Polymer Reaction Engineering* 431–532 (2005) doi:https://doi.org/10.1002/9783527619870.ch9.

52. Mallégol, J., Gardette, J.-L. & Lemaire, J. Long-term behavior of oil-based varnishes and paints I. Spectroscopic analysis of curing drying oils. *J. Am. Oil Chem. Soc.* **76**, 967–976 (1999).

53. Lazzari, M. & Chiantore, O. Drying and oxidative degradation of linseed oil. *Polym. Degrad. Stab.* **65**, 303–313 (1999).

54. Middlemiss, R. G. & Olszanski, D. J. New Catalysts for High-Solids Coatings, Part 1. *Am. Paint Coatings J.* **78**, 43–43 (1993).

55. Muizebelt, W. J. *et al.* Aluminum compounds as additional crosslinkers for air-drying high-solids alkyd paints. *J. Coatings Technol.* **70**, 53–59 (1998).

56. Muizebelt, W. J. & Nielen, M. W. F. Oxidative Crosslinking of Unsaturated Fatty Acids Studied with Mass Spectrometry. *J. Mass Spectrom.* **31**, 545–554 (1996).

57. Mecklenburg, M. F. & Tumosa, C. S. Traditional Oil Paints: The Effects of Long-Term Chemical and Mechanical Properties on Restoration Efforts. *MRS Bull.* **26**, 51–54 (2001).

58. Baij, L. *et al.* A review of solvent action on oil paint. *Herit. Sci.* **8**, 43 (2020).

59. Sutherland, K. Solvent-Extractable Components of Linseed Oil Paint Films. *Stud. Conserv.* **48**, 111–135 (2003).

60. Phenix, A. & Sutherland, K. The cleaning of paintings: effects of organic solvents on oil paint films. *Stud. Conserv.* **46**, 47–60 (2001).

61. Berg, J., Van den Berg, K. J. & Boon, J. J. Chemical changes in curing and ageing oil paints. *12th Trienn. Meet.* 248–253 (1999).

62. Porter, N. A., Caldwell, S. E. & Mills, K. A. Mechanisms of free radical oxidation of unsaturated lipids. *Lipids* **30**, 277–290 (1995).

63. Wexler, H. Polymerization of Drying Oils. *Chem. Rev.* **64**, 591–611 (1964).

64. Kumarathasan, R., Rajkumar, A. B., Hunter, N. R. & Gesser, H. D. Autoxidation and yellowing of methyl linolenate. *Prog. Lipid Res.* **31**, 109–126 (1992).

65. Marshall, G. L. The analysis of cured drying oils by swollen state 13C-NMR spectroscopy. *Eur. Polym. J.* **22**, 231–241 (1986).

66. Delahaye, N., Saiter, J. M., Liziard, M. & Podgorski, L. Alkyd-based thermosetting resins: influences of temperature and UV radiation on curing kinetics. *J. Coatings Technol.*

67. Belhaj, N., Arab-Tehrany, E. & Linder, M. Oxidative kinetics of salmon oil in bulk and in nanoemulsion stabilized by marine lecithin. *Process Biochem.* **45**, 187–195 (2010).

68. Gunstone, F. *Fatty Acid and Lipid Chemistry*. (Springer US, 2012).

69. Halliwell, B. & Gutteridge, J. *Free Radicals in Biology and Medicine*. (Oxford University Press, 2015).

70. Pfaendtner, J. & Broadbelt, L. J. Mechanistic Modeling of Lubricant Degradation. 1. Structure−Reactivity Relationships for Free-Radical Oxidation. *Ind. Eng. Chem. Res.* **47**, 2886–2896 (2008).

71. Allen, P. E. M. & Patrick, C. R. Diffusion-controlled reactions in free radical polymerisation. *Die Makromol. Chemie* **47**, 154–167 (1961).

72. Guertin, A. T. Diffusion controlled termination in free radical polymerization. *J. Polym. Sci. Part B Polym. Lett.* **1**, 477–481 (1963).

73. Trommsdorff, V. E., Köhle, H. & Lagally, P. Zur polymerisation des methacrylsäuremethylesters1. *Die Makromol. Chemie* **1**, 169–198 (1948).

74. Norrish, R. G. W. & Smith, R. R. Catalyzed Polymerization of Methyl Methacrylate in the Liquid Phase. *Nature* **150**, 336–337 (1942).

75. Ėmanuėl′, Z. M. N. M., Denisov, E. T. & Maĭzus, Z. K. *Liquid-Phase Oxidation of Hydrocarbons*. (Plenum Press, 1967).

76. Denisov, E. T. *Liquid-Phase Reaction Rate Constants*. (Plenum Press, 1974).

77. Lee, R., Gryn'ova, G., Ingold, K. U. & Coote, M. L. Why are sec-alkylperoxyl bimolecular self-reactions orders of magnitude faster than the analogous reactions of tert-alkylperoxyls? The unanticipated role of CH hydrogen bond donation. *Phys. Chem. Chem. Phys.* **18**, 23673–23679 (2016).

78. Baij, L., Chassouant, L., Hermans, J. J., Keune, K. & Iedema, P. D. The concentration and origins of carboxylic acid groups in oil paint. *RSC Adv.* **9**, 35559–35564 (2019).

79. Fjällström, P., Andersson, B. & Nilsson, C. Drying of linseed oil paints: the effects of substrate on the emission of aldehydes. *Indoor Air* **13**, 277–282 (2003).

80. Oakley, L. H., Casadio, F., Shull, K. R. & Broadbelt, L. J. Examination of Mechanisms for Formation of Volatile Aldehydes from Oxidation of Oil-Based Systems. *Ind. Eng. Chem. Res.* **57**, 139–149 (2018).

81. Scalarone, D., Lazzari, M. & Chiantore, O. Thermally assisted hydrolysis and methylation-pyrolysis-gas chromatography/mass spectrometry of light-aged linseed oil. *J. Anal. Appl. Pyrolysis* **58**–**59**, 503–512 (2001).

82. van Dam, E. P., van den Berg, K. J., Proaño Gaibor, A. N. & van Bommel, M. Analysis of triglyceride degradation products in drying oils and oil paints using LC–ESI-MS. *Int. J. Mass Spectrom.* **413**, 33–42 (2017).

83. Kryven, I., Duivenvoorden, J., Hermans, J. J. & Iedema, P. D. Random Graph Approach to Multifunctional Molecular Networks. *Macromol. Theory Simulations* **25**, 449–465 (2016).

84. Kryven, I. Analytic results on the polymerisation random graph model. *J. Math. Chem.* **56**, 140–157 (2018).

85. Lee, J. *et al.* Scientific investigation into the water sensitivity of twentieth century oil paints. *Microchem. J.* **138**, 282–295 (2018).

86. El-Aneed, A., Cohen, A. & Banoub, J. Mass Spectrometry, Review of the Basics: Electrospray, MALDI, and Commonly Used Mass Analyzers. *Appl. Spectrosc. Rev.* **44**, 210–230 (2009).

87. Glish, G. L. & Vachet, R. W. The basics of mass spectrometry in the twenty-first century. *Nat. Rev. Drug Discov.* **2**, 140–150 (2003).

88. Broadbelt, L. J., Stark, S. M. & Klein, M. T. Computer Generated Pyrolysis Modeling: On-the-Fly Generation of Species, Reactions, and Rates. *Ind. Eng. Chem. Res.* **33**, 790–799 (1994).

89. Song, J. Building Robust Chemical Reaction Mechanisms: Next Generation of Automatic Model Construction Software. (Massachusetts Institute of Technology, 2004).

90. Battin-Leclerc, F. Development of kinetic models for the formation and degradation of unsaturated hydrocarbons at high temperature. *Phys. Chem. Chem. Phys.* **4**, 2072–2078 (2002).

91. Ranzi, E., Faravelli, T., Gaffuri, P. & Sogaro, A. Low-temperature combustion: Automatic generation of primary oxidation reactions and lumping procedures. *Combust. Flame* **102**, 179–192 (1995).

92. Orlova, Y., Gambardella, A. A., Kryven, I., Keune, K. & Iedema, P. D. Generative Algorithm for Molecular Graphs Uncovers Products of Oil Oxidation. *J. Chem. Inf. Model.* **61**, 1457–1469 (2021).

93. Oyman, Z. O., Ming, W. & Linde, R. van der. Oxidation of drying oils containing non-conjugated and conjugated double bonds catalyzed by a cobalt catalyst. *Prog. Org. Coatings* **54**, 198–204 (2005).

94. *Official Methods and Recommended Practices of the American Oil Chemists' Society*. (American Oil Chemists' Society, 1997).

95. Bonaduce, I. *et al.* New Insights into the Ageing of Linseed Oil Paint Binder: A Qualitative and Quantitative Analytical Study. *PLoS One* **7**, e49333 (2012).

96. Oyman, Z. O., Ming, W. & van der Linde, R. Oxidation of 13C-labeled ethyl linoleate monitored and quantitatively analyzed by 13C NMR. *Eur. Polym. J.* **42**, 1342–1348 (2006).

97. Proietti, N., Capitani, D. & Di Tullio, V. Nuclear Magnetic Resonance, a Powerful Tool in Cultural Heritage. *Magnetochemistry* vol. 4 (2018).

98. Blümich, B., Perlo, J. & Casanova, F. Mobile single-sided NMR. *Prog. Nucl. Magn. Reson. Spectrosc.* **52**, 197–269 (2008).

99. Catalano, J. *et al.* Review of the use of NMR spectroscopy to investigate structure, reactivity, and dynamics of lead soap formation in paintings. *Magn. Reson. Chem.* **n/a**, (2020).

100. Szori, M., Abou-Abdo, T., Fittschen, C., Csizmadia, I. G. & Viskolcz, B. Allylic hydrogen abstraction II. H-abstraction from 1,4 type polyalkenes as a model for free radical trapping by polyunsaturated fatty acids (PUFAs). *Phys. Chem. Chem. Phys.* **9**, 1931–1940 (2007).

101. Pfaendtner, J. & Broadbelt, L. J. Mechanistic Modeling of Lubricant Degradation. 2. The Autoxidation of Decane and Octane. *Ind. Eng. Chem. Res.* **47**, 2897–2904 (2008).

102. Evans, M. G. & Polanyi, M. Inertia and driving force of chemical reactions. *Trans. Faraday Soc.* **34**, 11–24 (1938).

103. Joback, K. G. & Reid, R. C. Estimation of Pure-Component Properties from Group-Contributions. *Chem. Eng. Commun.* **57**, 233–243 (1987).

104. Benson, S. W. *Thermochemical Kinetics: Methods for the Estimation of Thermochemical Data and Rate Parameters*. (1968).

105. Iedema, P. D., Hermans, J. J., Keune, K., van Loon, A. & Stols-Witlox, M. J. N. Mathematical modeling of mature oil paint networks. in *ICOM-CC 17th Triennial Conference Preprints* 8 (International Council of Museums, 2014).

106. Flory, P. J. Molecular Size Distribution in Three Dimensional Polymers. I. Gelation. *J. Am. Chem. Soc.* **63**, 3083–3090 (1941).

107. Stockmayer, W. H. Theory of Molecular Size Distribution and Gel Formation in Branched Polymers II. General Cross Linking. *J. Chem. Phys.* **12**, 125–131 (1944).

108. Gillespie, D. T. A general method for numerically simulating the stochastic time evolution of coupled chemical reactions. *J. Comput. Phys.* **22**, 403–434 (1976).

109. Oakley, L. H. Mechanistic Studies of the Autoxidative Curing of an Oil-Based Paint Model System. (Northwestern University, 2017).

110. Vinu, R. & Broadbelt, L. J. Unraveling Reaction Pathways and Specifying Reaction Kinetics for Complex Systems. *Annu. Rev. Chem. Biomol. Eng.* **3**, 29–54 (2012).

111. Broadbelt, L. J., Stark, S. M. & Klein, M. T. Computer generated reaction networks: on-the-fly calculation of species properties using computational quantum chemistry. *Chem. Eng. Sci.* **49**, 4991–5010 (1994).

112. Susnow, R. G., Dean, A. M., Green, W. H., Peczak, P. & Broadbelt, L. J. Rate-Based Construction of Kinetic Models for Complex Systems. *J. Phys. Chem. A* **101**, 3731–3740 (1997).

113. Eumelen, G. J. A. M., Bosco, E., Suiker, A. S. J., van Loon, A. & Iedema, P. D. A computational model for chemo-mechanical degradation of historical oil paintings due to metal soap formation. *J. Mech. Phys. Solids* **132**, 103683 (2019).

114. Torres-Knoop, A., Kryven, I., Schamboeck, V. & Iedema, P. D. Modeling the free-radical polymerization of hexanediol diacrylate (HDDA): a molecular dynamics and graph theory approach. *Soft Matter* **14**, 3404–3414 (2018).

115. Samain, L. *et al.* Fading of modern Prussian blue pigments in linseed oil medium. *J. Anal. At. Spectrom.* **26**, 930–941 (2011).

116. Ragaert, K., Delva, L. & Van Geem, K. M. Mechanical and chemical recycling of solid plastic waste. *Waste Manag.* **69**, 24–58 (2017).

117. Saptoadi, H. & Pratama, N. N. Utilization of Plastics Waste Oil as Partial Substitute for Kerosene in Pressurized Cookstoves. *Int. J. Environ. Sci. Dev.* **6**, 363–368 (2015).

118. Burnham, A. K. *et al.* An appropriate kinetic model for well-preserved algal kerogens. *Energy & Fuels* **10**, 49–59 (1996).

119. Braun, R. L., Burnham, A. K., Reynolds, J. G. & Clarkson, J. E. Pyrolysis kinetics for lacustrine and marine source rocks by programmed micropyrolysis. *Energy & Fuels* **5**, 192–204 (1991).

120. Burnham, A. K. *Global Chemical Kinetics of Fossil Fuels*. (Springer: Cham, Switzerland, 2017).

121. Burnham, A. K., Zhou, X. & Broadbelt, L. J. Critical Review of the Global Chemical Kinetics of Cellulose Thermal Decomposition. *Energy & Fuels* **29**, 2906–2918 (2015).

122. Klein, M. T., Neurock, M., Broadbelt, L. J. & Foley, H. C. Reaction Pathway Analysis. in *Selectivity in Catalysis* vol. 517 290–312 (American Chemical Society, 1993).

123. Rice, F. O. The thermal decomposition of organic compounds from the standpoint of free radicals. I. Saturated compounds. *J. Am. Chem. Soc.* **53**, 1959–1972 (1931).

124. Rice, F. O. & Herzfeld, K. F. The Thermal decomposition of organic compounds from the standpoint of free radicals. VI. The mechanism of some chain reactions. *J. Am. Chem. Soc.* **56**, 284–289 (1934).

125. Standards, N. B. of. *Polymer Degradation Mechanisms, NBS Circular 525*. (1953).

126. De Witt, M. J., Dooling, D. J. & Broadbelt, L. J. Computer Generation of Reaction Mechanisms Using Quantitative Rate Information: Application to Long-Chain Hydrocarbon Pyrolysis. *Ind. Eng. Chem. Res.* **39**, 2228–2237 (2000).

127. Kruse, T. M., Wong, H.-W. & Broadbelt, L. J. Mechanistic Modeling of Polymer Pyrolysis: Polypropylene. *Macromolecules* **36**, 9594–9607 (2003).

128. Kruse, T. M. *et al.* Binary mixture pyrolysis of polypropylene and polystyrene: A modeling and experimental study. *J. Anal. Appl. Pyrolysis* **73**, 342–354 (2005).

129. Levine, S. E. & Broadbelt, L. J. Detailed mechanistic modeling of high-density polyethylene pyrolysis: Low molecular weight product evolution. *Polym. Degrad. Stab.* **94**, 810–822 (2009).

130. Simha, R. & Wall, L. A. Kinetics of Chain Depolymerization. *J. Phys. Chem.* **56**, 707–715 (1952).

131. Bouster, C., Vermande, P. & Veron, J. Study of the pyrolysis of polystyrenes: I. Kinetics of thermal decomposition. *J. Anal. Appl. Pyrolysis* **1**, 297–313 (1980).

132. Prout, E. G. & Tompkins, F. C. The thermal decomposition of silver permanganate. *Trans. Faraday Soc.* **42**, 468–472 (1946).

133. Burnham, A. K. Application of the Šesták-Berggren equation to organic and inorganic materials of practical interest. *J. Therm. Anal. Calorim.* **60**, 895–908 (2000).

134. Sánchez-Jiménez, P. E., Pérez-Maqueda, L. A., Perejón, A. & Criado, J. M. A new model for the kinetic analysis of thermal degradation of polymers driven by random scission. *Polym. Degrad. Stab.* **95**, 733–739 (2010).

135. Amorim, M. T. S. P., Bouster, C. & Veron, J. Pyrolysis of polypropylene: II. Kinetics of degradation. *J. Anal. Appl. Pyrolysis* **4**, 103–115 (1982).

136. Johnson, W.A Mehl, R. F. Reaction kinetics in processes of nucleation and growth. *Trans. Am. Insitute Min.* **135**, 733–739 (1939).

137. Avrami, M. Kinetics of Phase Change. II Transformation-Time Relations for Random Distribution of Nuclei. *J. Chem. Phys.* **8**, 212–224 (1940).

138. Erofe'ev, B. V. C. R. *No*. (1946).

139. Kolmogorov, A. A statistical theory for the recrystallization of metals. *Izv. Akad. Nauk USSR Neorg. Mater.* **1**, 355–359 (1937).

140. Burnham, A. K., Weese, R. K., Wemhoff, A. P. & Maienschein, J. L. A historical and current perspective on predicting thermal cookoff behavior. *J. Therm. Anal. Calorim.* **89**, 407–415 (2007).

141. Flynn, J. H. & Florin, R. E. Degradation and pyrolysis mechanisms. in *Pyrolysis and GC in Polymer Analysis* (ed. Liebman, S.A. Levy, E. J.) 149–208 (Marcel Dekker, 1985).

142. Westerhout, R. W. J., Waanders, J., Kuipers, J. A. M. & van Swaaij, W. P. M. Kinetics of the Low-Temperature Pyrolysis of Polyethene, Polypropene, and Polystyrene Modeling, Experimental Determination, and Comparison with Literature Models and Data. *Ind. Eng. Chem. Res.* **36**, 1955–1964 (1997).

143. Burnham, A. K. & Braun, R. L. Global Kinetic Analysis of Complex Materials. *Energy & Fuels* **13**, 1–22 (1999).

144. Peterson, J. D., Vyazovkin, S. & Wight, C. A. Kinetics of the Thermal and Thermo-Oxidative Degradation of Polystyrene, Polyethylene and Poly(propylene). *Macromol. Chem. Phys.* **202**, 775–784 (2001).

145. Gotor, F. J., Criado, J. M., Malek, J. & Koga, N. Kinetic Analysis of Solid-State Reactions: The Universality of Master Plots for Analyzing Isothermal and Nonisothermal Experiments. *J. Phys. Chem. A* **104**, 10777–10782 (2000).

146. Vyazovkin, S. Kissinger Method in Kinetics of Materials: Things to Beware and Be Aware of. *Molecules* vol. 25 (2020).

147. Budrugeac, P. Theory and practice in the thermoanalytical kinetics of complex processes: Application for the isothermal and non-isothermal thermal degradation of HDPE. *Thermochim. Acta* **500**, 30–37 (2010).

148. Chao-Hsiung Wu *et al.* On the thermal treatment of plastic mixtures of MSW: Pyrolysis kinetics. *Waste Manag.* **13**, 221–235 (1993).

149. Albano, C. & de Freitas, E. Thermogravimetric evaluation of the kinetics of decomposition of polyolefin blends. *Polym. Degrad. Stab.* **61**, 289–295 (1998).

150. Kim, S., Jang, E.-S., Shin, D.-H. & Lee, K.-H. Using peak properties of a DTG curve to estimate the kinetic parameters of the pyrolysis reaction: application to high density polyethylene. *Polym. Degrad. Stab.* **85**, 799–805 (2004).

151. Kayacan, İ. & Doğan, Ö. M. Pyrolysis of Low and High Density Polyethylene. Part I: Non-isothermal Pyrolysis Kinetics. *Energy Sources, Part A Recover. Util. Environ. Eff.* **30**, 385–391 (2008).

152. Aboulkas, A., El harfi, K. & El Bouadili, A. Thermal degradation behaviors of polyethylene and polypropylene. Part I: Pyrolysis kinetics and mechanisms. *Energy Convers. Manag.* **51**, 1363–1369 (2010).

153. Das, P. & Tiwari, P. Thermal degradation kinetics of plastics and model selection. *Thermochim. Acta* **654**, 191–202 (2017).

154. Dubdub, I. & Al-Yaari, M. Pyrolysis of Low Density Polyethylene: Kinetic Study Using TGA Data and ANN Prediction. *Polymers* vol. 12 (2020).

155. Friedman, H. L. Kinetics of thermal degradation of char-forming plastics from thermogravimetry. Application to a phenolic plastic. *J. Polym. Sci. Part C Polym. Symp.* **6**, 183–195 (1964).

156. Kissinger, H. E. Reaction Kinetics in Differential Thermal Analysis. *Anal. Chem.* **29**, 1702–1706 (1957).

157. Madras, G. & McCoy, B. J. Distribution Kinetics for Polymer Mixture Degradation. *Ind. Eng. Chem. Res.* **38**, 352–357 (1999).

158. Madras, G., Smith, J. M. & McCoy, B. J. Degradation of Poly(methyl methacrylate) in Solution. *Ind. Eng. Chem. Res.* **35**, 1795–1800 (1996).

159. Zhou, X., Broadbelt, L. J. & Vinu, R. Mechanistic Understanding of Thermochemical Conversion of Polymers and Lignocellulosic Biomass. in *Thermochemical Process Engineering* (ed. Van Geem, K. M. B. T.-A. in C. E.) vol. 49 95–198 (Academic Press, 2016).

160. Natta, G. & Corradini, P. Structure and properties of isotactic polypropylene. in (eds. NATTA, G. & DANUSSO, F. B. T.-S. P. and S. P.) 743–746 (Pergamon, 1967). doi:https://doi.org/10.1016/B978-1-4831-9882-8.50057-9.

161. Chen, K., Harris, K. & Vyazovkin, S. Tacticity as a Factor Contributing to the Thermal Stability of Polystyrene. *Macromol. Chem. Phys.* **208**, 2525–2532 (2007).

162. Knight, J. B., Calvert, P. D. & Billingham, N. C. Localization of oxidation in polypropylene. *Polymer (Guildf).* **26**, 1713–1718 (1985).

163. Ryan, T. G., Calvert, P. D. & Billingham, N. C. The Distribution of Additives and Impurities in Isotactic Polypropylene. in *Stabilization and Degradation of Polymers* vol. 169 22–261 (AMERICAN CHEMICAL SOCIETY, 1978).

164. Bolland, J. L. & Gee, G. Kinetic studies in the chemistry of rubber and related materials. II. The kinetics of oxidation of unconjugated olefins. *Trans. Faraday Soc.* **42**, 236–243 (1946).

165. Pizzimenti, S. *et al.* Oxidation and Cross-Linking in the Curing of Air-Drying Artists' Oil Paints. *ACS Appl. Polym. Mater.* **3**, 1912–1922 (2021).

166. Nardelli, F. *et al.* The stability of paintings and the molecular structure of the oil paint polymeric network. *Sci. Rep.* **11**, 14202 (2021).

167. Schaich, K. M. Chapter 1 - Challenges in Elucidating Lipid Oxidation Mechanisms: When, Where, and How Do Products Arise? in (eds. Logan, A., Nienaber, U. & Pan, X. B. T.-L. O.) 1–52 (AOCS Press, 2013). doi:https://doi.org/10.1016/B978-0-9830791-6-3.50004-7.

168. Shahidi, F. K. M. S. Lipid Oxidation: New Perspectives on an Old Reaction. *Bailey's Ind. oil fat Prod.* **1**, (2020).

169. Miccichè, F., van Haveren, J., Oostveen, E., Ming, W. & van der Linde, R. Oxidation and oligomerization of ethyl linoleate under the influence of the combination of ascorbic acid 6-palmitate/iron-2-ethylhexanoate. *Appl. Catal. A Gen.* **297**, 174–181 (2006).

170. Ploeger, R., Scalarone, D. & Chiantore, O. Thermal analytical study of the oxidative stability of artists' alkyd paints. *Polym. Degrad. Stab.* **94**, 2036–2041 (2009).

171. Liu, Z., Kooijman, H., Spek, A. L. & Bouwman, E. New manganese-based catalyst systems for alkyd paint drying. *Prog. Org. Coatings* **60**, 343–349 (2007).

172. van Gorkum, R., Bouwman, E. & Reedijk, J. Fast Autoxidation of Ethyl Linoleate Catalyzed by [Mn(acac)3] and Bipyridine: A Possible Drying Catalyst for Alkyd Paints. *Inorg. Chem.* **43**, 2456–2458 (2004).

173. Schamboeck, V., Kryven, I. & Iedema, P. D. Acrylate Network Formation by Free-Radical Polymerization Modeled Using Random Graphs. *Macromol. Theory Simulations* **26**, 1700047 (2017).

174. Bateman, L. & Gee. G. Determination of absolute rate constants for olefinic oxidations by measurement of photochemical pre- and after-effects: Part I At ‘high’ oxygen pressures. *Trans. Faraday Soc.* **47**, 155–164 (1951).

175. Wang, L. & Broadbelt, L. J. Tracking Explicit Chain Sequence in Kinetic Monte Carlo Simulations. *Macromol. Theory Simulations* **20**, 54–64 (2011).

176. Kurdikar, D. L., Somvarsky, J., Dušek, K. & Peppas, N. A. Development and Evaluation of a Monte Carlo Technique for the Simulation of Multifunctional Polymerizations. *Macromolecules* **28**, 5910–5920 (1995).

177. Pervaje, A. K. *et al.* Molecular Simulations of Thermoset Polymers Implementing Theoretical Kinetics with Top-Down Coarse-Grained Models. *Macromolecules* **53**, 2310–2322 (2020).

178. Megariotis, G., Vogiatzis, G. G., Schneider, L., Müller, M. & Theodorou, D. N. Mesoscopic Simulations of Crosslinked Polymer Networks. *J. Phys. Conf. Ser.* **738**, 12063 (2016).

179. Gartner, T. E. & Jayaraman, A. Modeling and Simulations of Polymers: A Roadmap. *Macromolecules* **52**, 755–786 (2019).

180. Kruse, T. M., Woo, O. S., Wong, H.-W., Khan, S. S. & Broadbelt, L. J. Mechanistic Modeling of Polymer Degradation: A Comprehensive Study of Polystyrene. *Macromolecules* **35**, 7830–7844 (2002).

181. Coile, M. W., Harmon, R. E., Wang, G., SriBala, G. & Broadbelt, L. J. Kinetic Monte Carlo Tool for Kinetic Modeling of Linear Step-Growth Polymerization: Insight into Recycling of Polyurethanes. *Macromol. Theory Simulations* **31**, 2100058 (2022).

182. Chylek, L. A. *et al.* Guidelines for visualizing and annotating rule-based models. *Mol. Biosyst.* **7**, 2779–2795 (2011).

183. Gao, H., Oakley, L. H., Konstantinov, I. A., Arturo, S. G. & Broadbelt, L. J. Acceleration of Kinetic Monte Carlo Method for the Simulation of Free Radical Copolymerization through Scaling. *Ind. Eng. Chem. Res.* **54**, 11975–11985 (2015).

184. Vinu, R., Levine, S. E., Wang, L. & Broadbelt, L. J. Detailed mechanistic modeling of poly(styrene peroxide) pyrolysis using kinetic Monte Carlo simulation. *Chem. Eng. Sci.* **69**, 456–471 (2012).

185. Snyder, M. A., Chatterjee, A. & Vlachos, D. G. Net-event kinetic Monte Carlo for overcoming stiffness in spatially homogeneous and distributed systems. *Comput. Chem. Eng.* **29**, 701–712 (2005).

186. De Keer, L. *et al.* Benchmarking Stochastic and Deterministic Kinetic Modeling of Bulk and Solution Radical Polymerization Processes by Including Six Types of Factors Two. *Macromol. Theory Simulations* **29**, 2000065 (2020).

187. de Oliveira, L. C. P. Développement d’une méthodologie de modélisation cinétique de procédés de raffinage traitant des charges lourdes. (École Doctorale de Chimie de Lyon, 2013).

188. Costa da Cruz, A. R., Verstraete, J. J., Charon, N. & Joly, J.-F. A Monte Carlo method for the simulating hydrotreating of bio-oil model compounds. *Chem. Eng. J.* **377**, 120144 (2019).

189. Rathinam, M., Petzold, L. R., Cao, Y. & Gillespie, D. T. Stiffness in stochastic chemically reacting systems: The implicit tau-leaping method. *J. Chem. Phys.* **119**, 12784–12794 (2003).

190. Cao, Y., Gillespie, D. T. & Petzold, L. R. Avoiding negative populations in explicit Poisson tau-leaping. *J. Chem. Phys.* **123**, 54104 (2005).

191. Hermans, J. J. *et al.* 2D-IR spectroscopy for oil paint conservation: Elucidating the water-sensitive structure of zinc carboxylate clusters in ionomers. *Sci. Adv.* **5**, eaaw3592 (2019).

192. Pickett, J. E. & Coyle, D. J. Hydrolysis kinetics of condensation polymers under humidity aging conditions. *Polym. Degrad. Stab.* **98**, 1311–1320 (2013).

193. Morsch, S., van Driel, B. A., van den Berg, K. J. & Dik, J. Investigating the Photocatalytic Degradation of Oil Paint using ATR-IR and AFM-IR. *ACS Appl. Mater. Interfaces* **9**, 10169–10179 (2017).

194. Boyatzis, S., Ioakimoglou, E. & Argitis, P. UV exposure and temperature effects on curing mechanisms in thin linseed oil films: Spectroscopic and chromatographic studies. *J. Appl. Polym. Sci.* **84**, 936–949 (2002).

195. Frankel, E. N. Chemistry of free radical and singlet oxidation of lipids. *Prog. Lipid Res.* **23**, 197–221 (1984).

196. Lu, T. & Law, C. K. On the applicability of directed relation graphs to the reduction of reaction mechanisms. *Combust. Flame* **146**, 472–483 (2006).

197. Bhattacharjee, B., Schwer, D. A., Barton, P. I. & Green, W. H. Optimally-reduced kinetic models: reaction elimination in large-scale kinetic mechanisms. *Combust. Flame* **135**, 191–208 (2003).

Appendix A. Appendix for Chapter 4

A.1 Functional Group Patterns

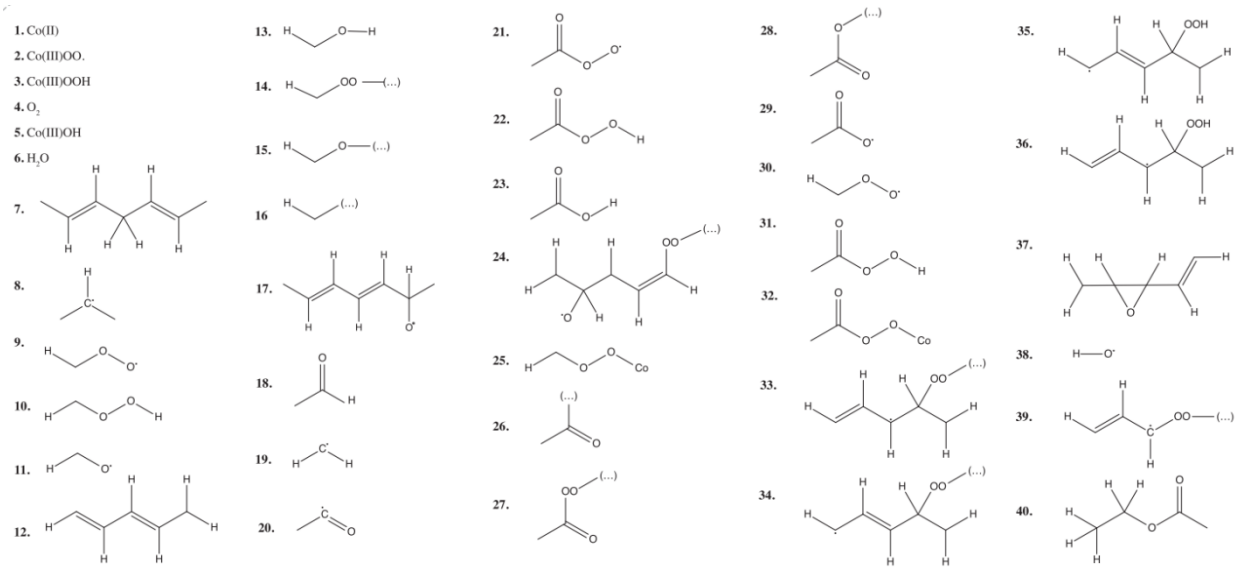

Figure A.1. Reactive patterns used to identify functional groups on monomer chemical graphs. Adapted from Orlova et al.[17]

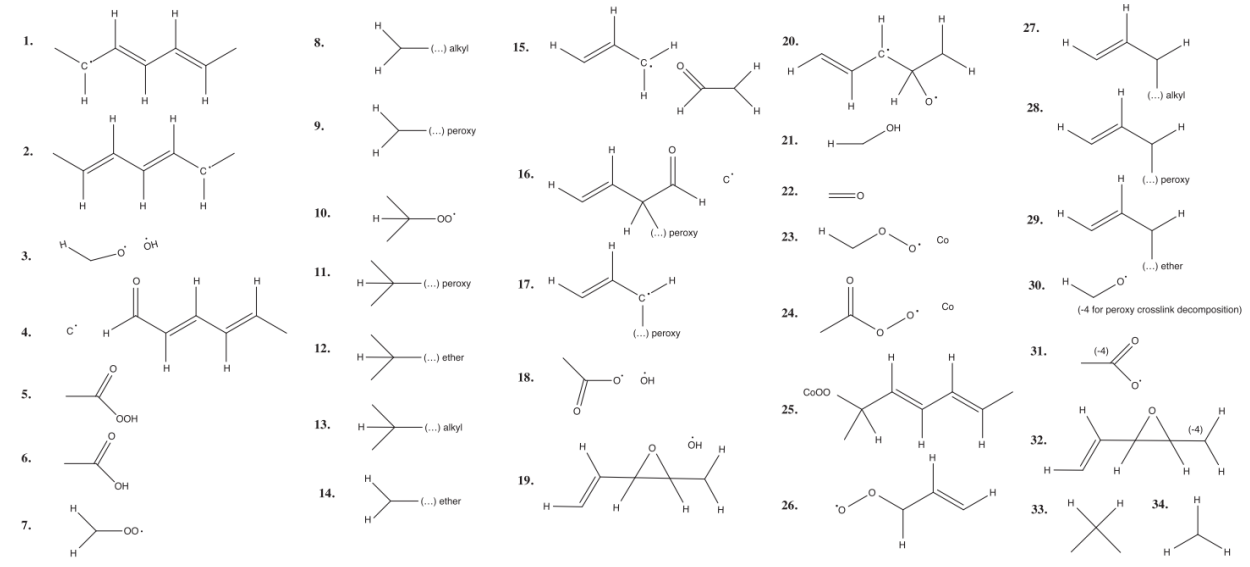

Figure A.2. Complex, non-reactive patterns used mainly in product species graph manipulation. Adapted from Orlova et al.[17]

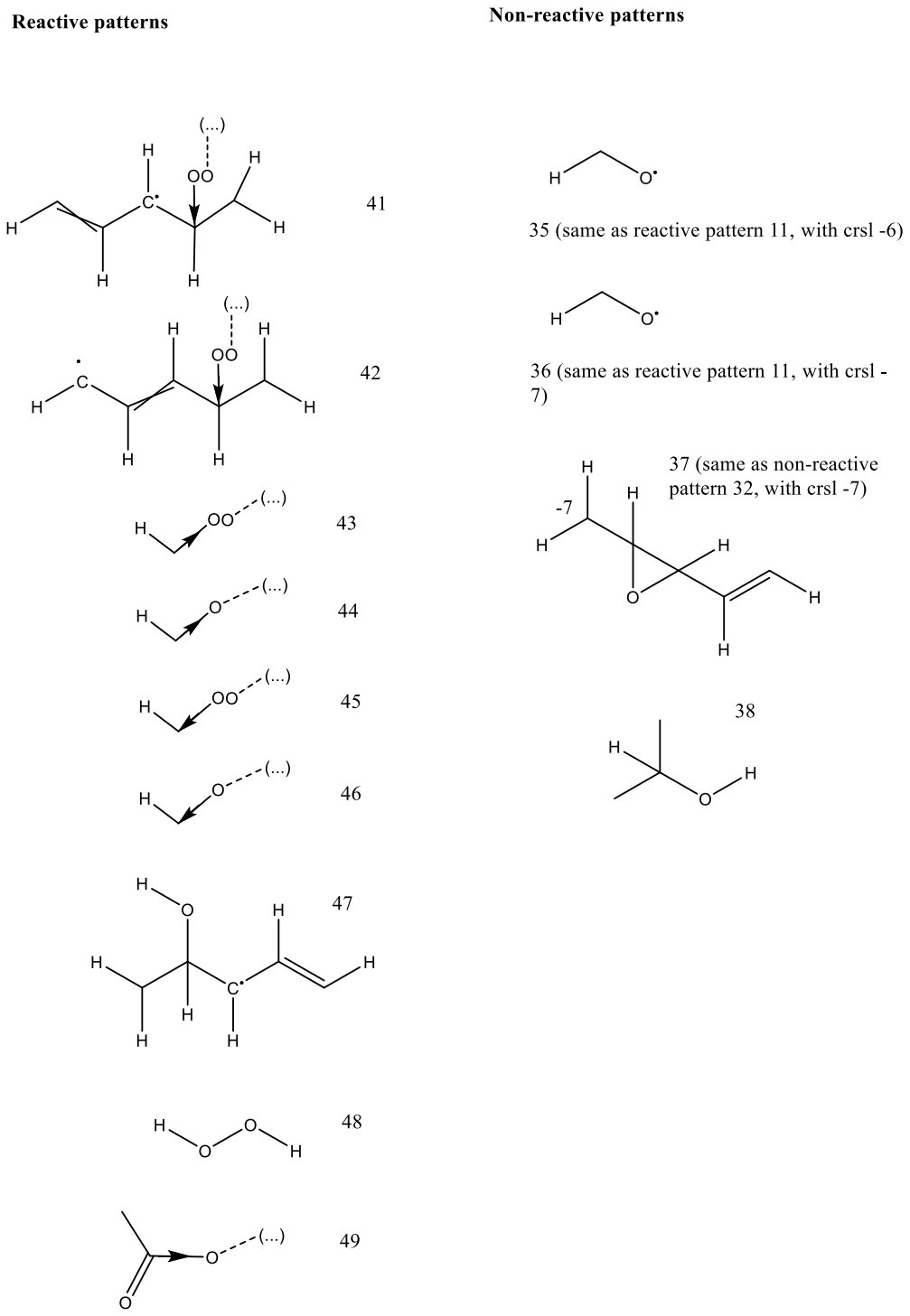

Figure A.3. New reactive and non-reactive patterns beyond those used in Orlova et al.[17] Note this includes directed crosslink edges.

A.2 Sensitivity Analyses Plots

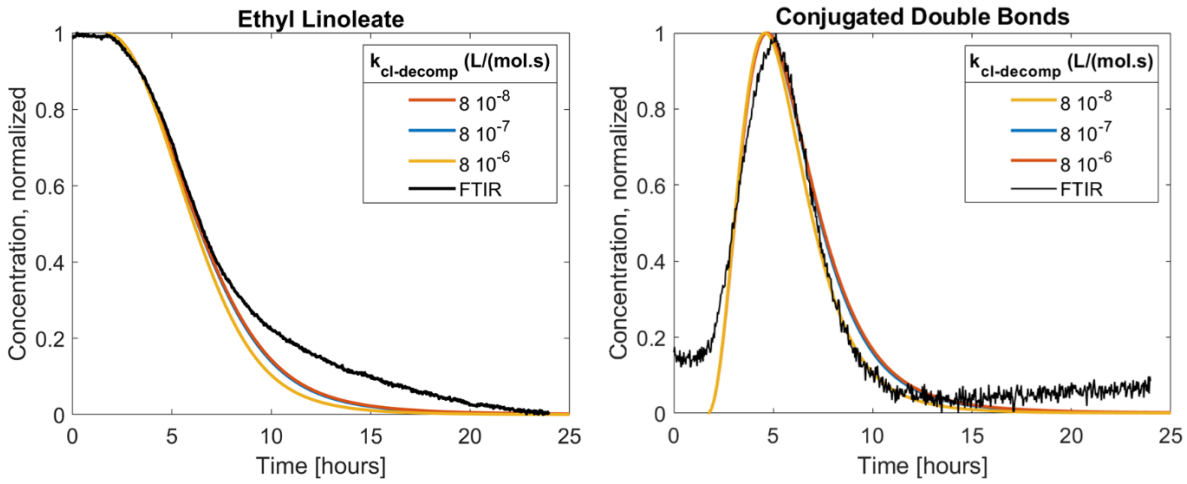

Figure A.4. Sensitivity of ethyl linoleate conversion and b) conjugated double bonds to the peroxy crosslink decomposition rate overlayed on normalized FTIR absorbance intensity for cis-alkenes at 3010 cm^{-1} and conjugated alkenes at 987 cm^{-1}, respectively.

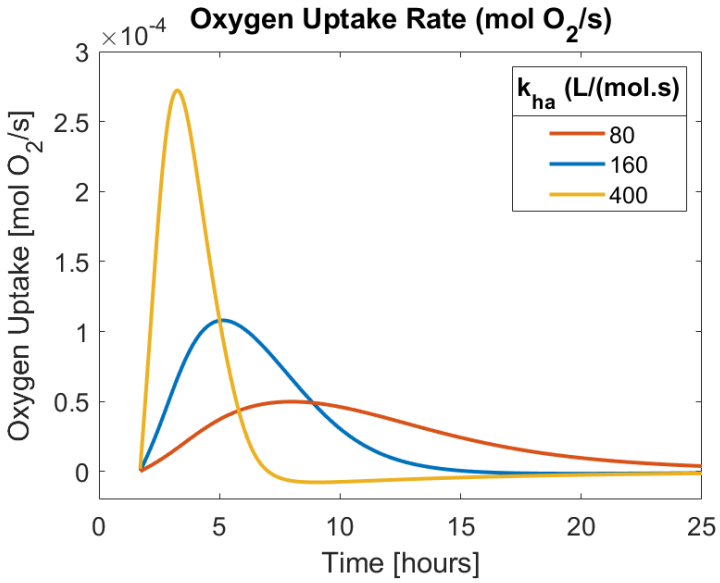

Figure A.5. Sensitivity of the rate of oxygen uptake to bi-allylic hydrogen abstraction over 25 hours.

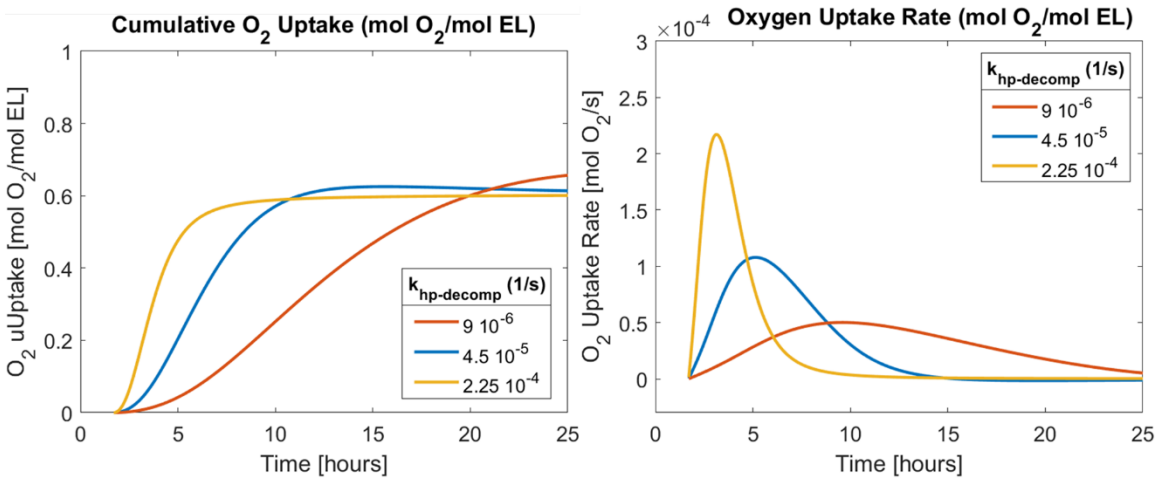

Figure A.6. Sensitivity of the a) cumulative oxygen uptake and b) rate of oxygen uptake to hydroperoxide decomposition over 25 hours.

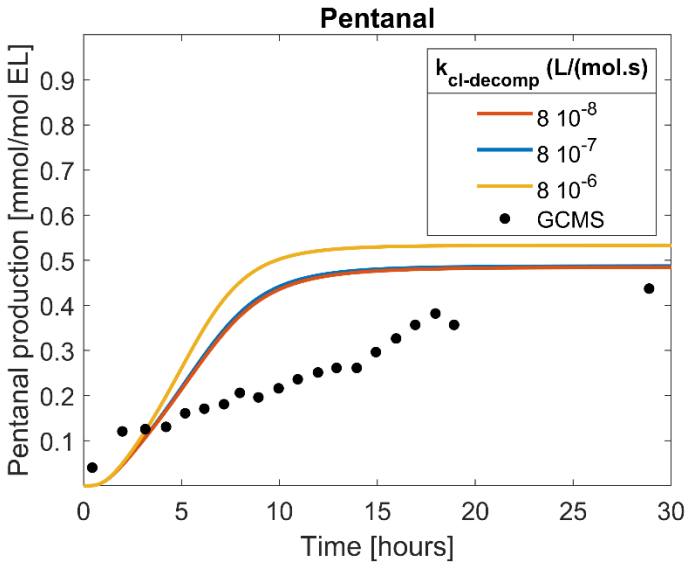

Figure A.7. Sensitivity of the production of pentanal to peroxy crosslink decomposition over 30 hours compared to GC-MS data published by Oakley et al.[19]

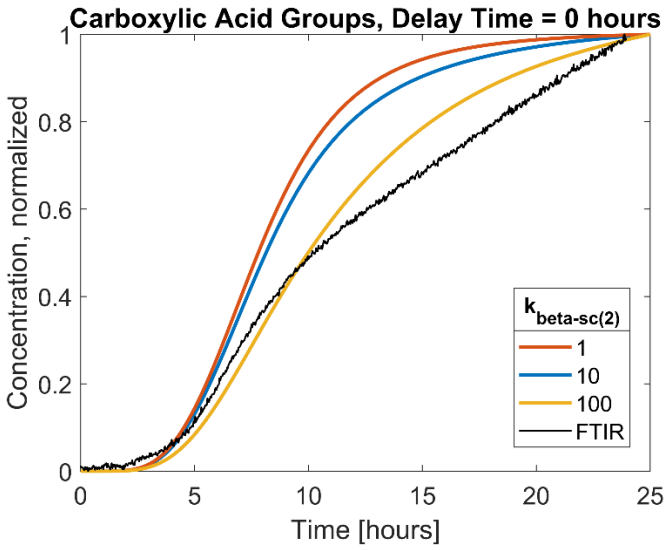

Figure A.8. Sensitivity of carboxylic acids to β-scission from dimer species (Type 2, Table 4.1) over 25 hours.

A.3 ESI-MS Peak Identification

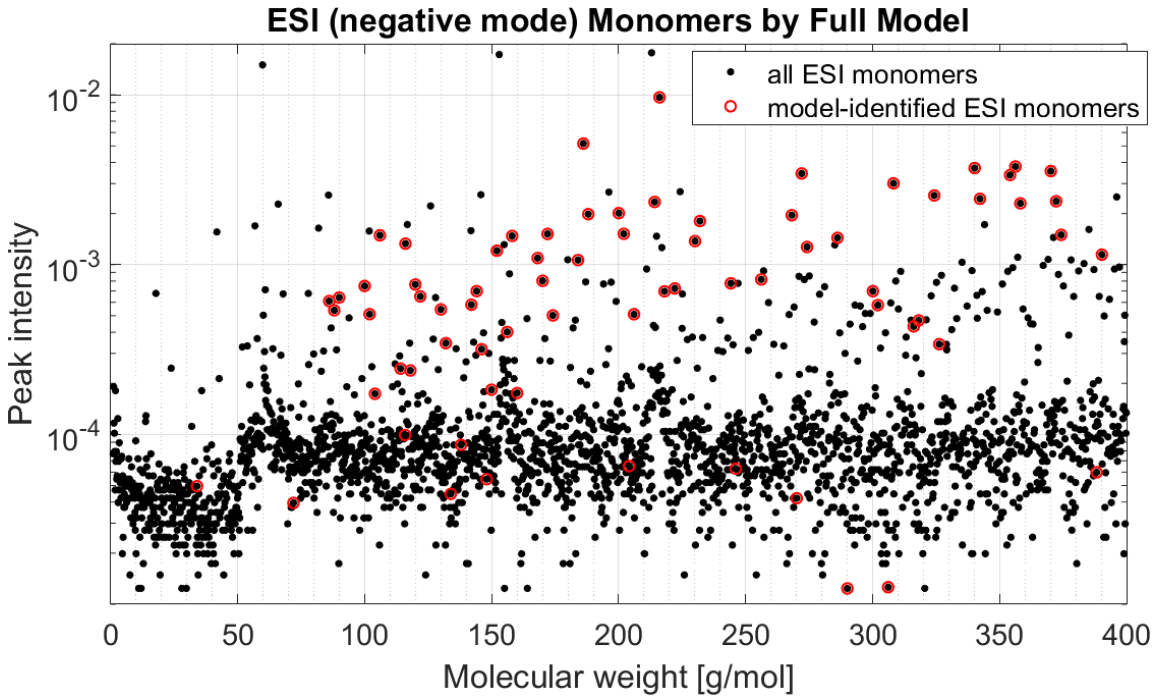

Figure A.9. ESI molecular weight spectrum in the negative mode showing measured peak intensity vs molecular weight (rather than *m/z*) of monomers after 146 hours of heating. Red circles are peaks that could be matched to model-predicted molecular weight products and corrected for calculated concentrations.

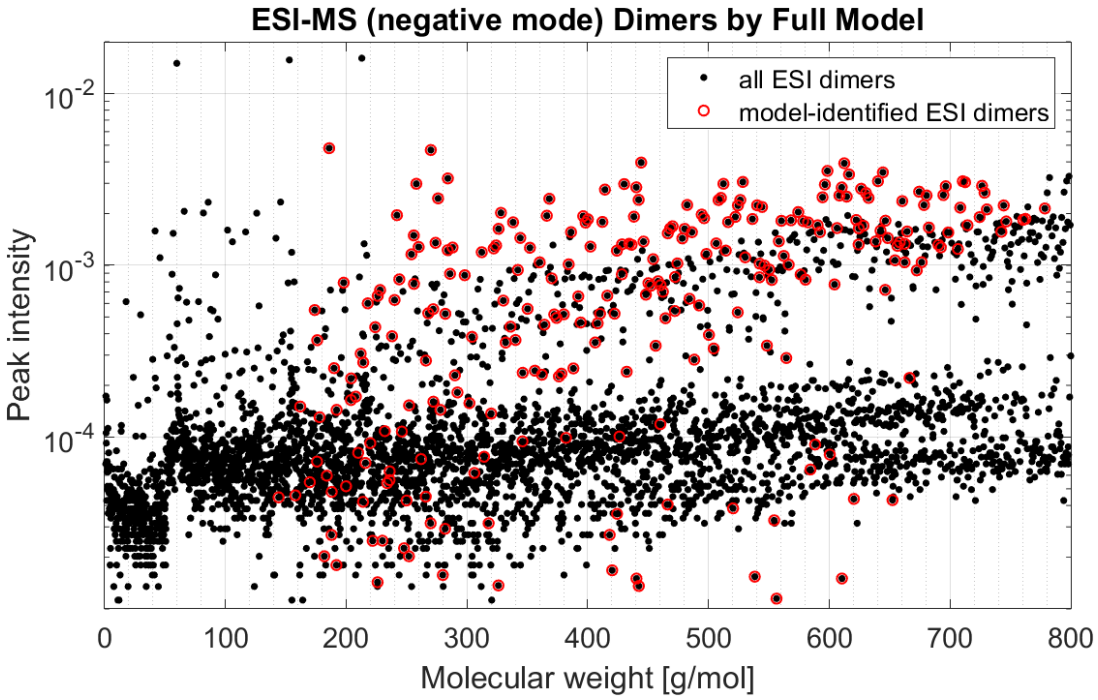

Figure A.10. ESI molecular weight spectrum in the negative mode showing measured peak intensity vs molecular weight (rather than *m/z*) for dimers after 146 hours of heating. Red circles are peaks that could be matched to model-predicted products and corrected for calculated concentrations.

The ESI mass peaks that could be matched to monomers and dimers predicted by the ARNG-model (red circles in ESI MW spectrums above) are used to calculate the concentrations of eight functional groups (patterns). Thus, ESI peak counts are used to find the functional group concentrations. The model is used to identify the monomers matching with the peaks according to the procedure explained in Chapter 4. Note that also concentrations predicted by the model are used to resolve multiplicity and overlapping issues. The plot in Figure A.11 shows the 8 main functional groups' concentrations at the times that correspond to the ESI sample times. In most cases, a clear upward or downward trend is observed. This result is compared to model-predicted time profile for the 8 functional groups. For EL (non-conj. db.), conj. db., aldehyde, peroxy acids:

fair agreement. Hydroperoxides remain the same in ESI, but model predicts strong increase. Carboxylic acid decrease in ESI, but only increase in model as they are assumed to not further react.

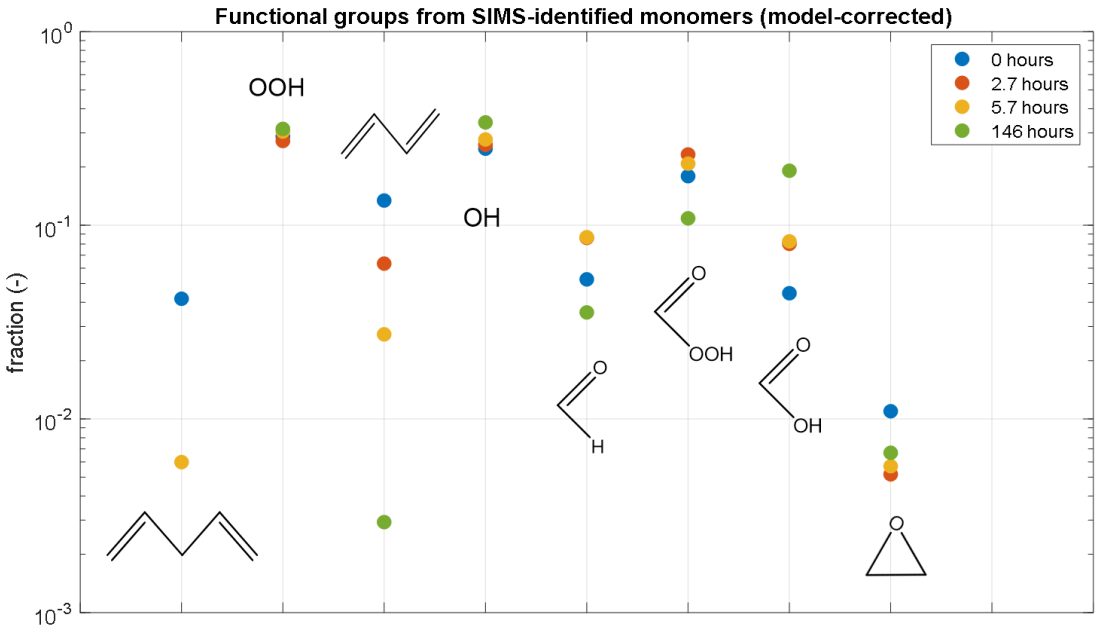

Figure A.11. Mole fraction of lumped functional groups identified in monomers identified in the ESI-spectra over time, based on concentrations predicted by the ARNG model.

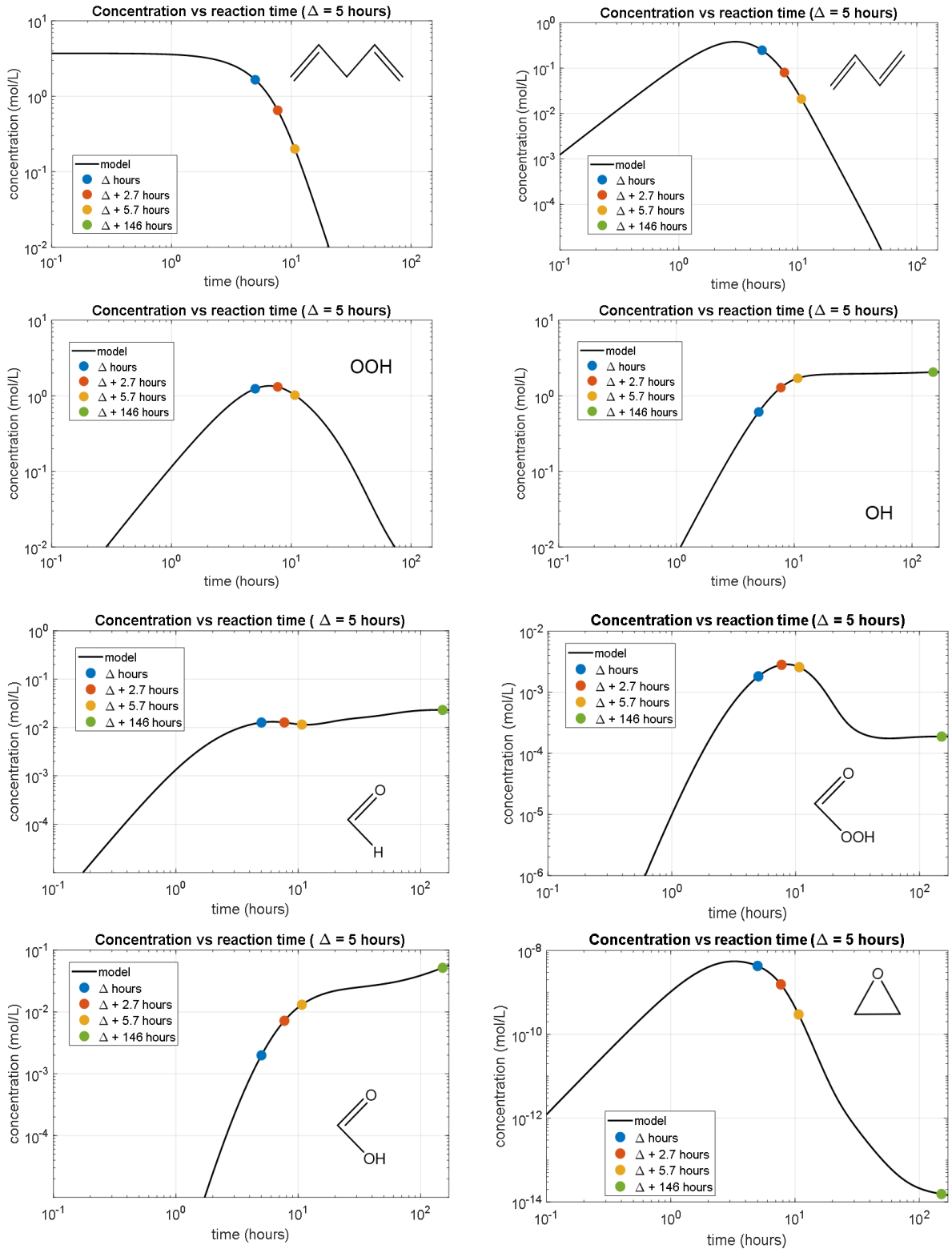

Figure A.12. Model predicted concentrations of functional groups identified in the ESI spectra.

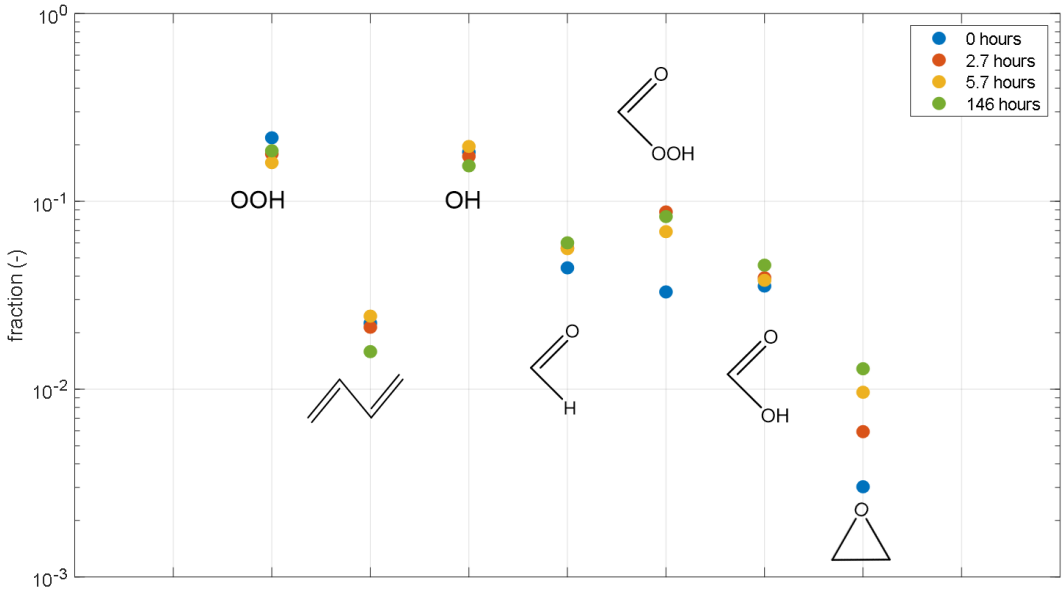

Figure A.13. Time evolution of the mole fraction of lumped functional groups identified in in the ESI-MS spectra using an ARNG model prediction of concentration of dimers.

There is a consistent disagreement: according to model, OH-group monomers increase; however, ESI-identified alcohol monomers decrease (Figure A.14). This is in contrast with identified dimers: especially at higher MW, dimers with only alcohol functional groups increase. Some possible explanations for this observation are that alcohol-containing groups are volatile and disappear during heating, thus evading measurement or an incorrect assumption that the carbon atom adjacent to the alcohol group does not undergo H-abstraction.

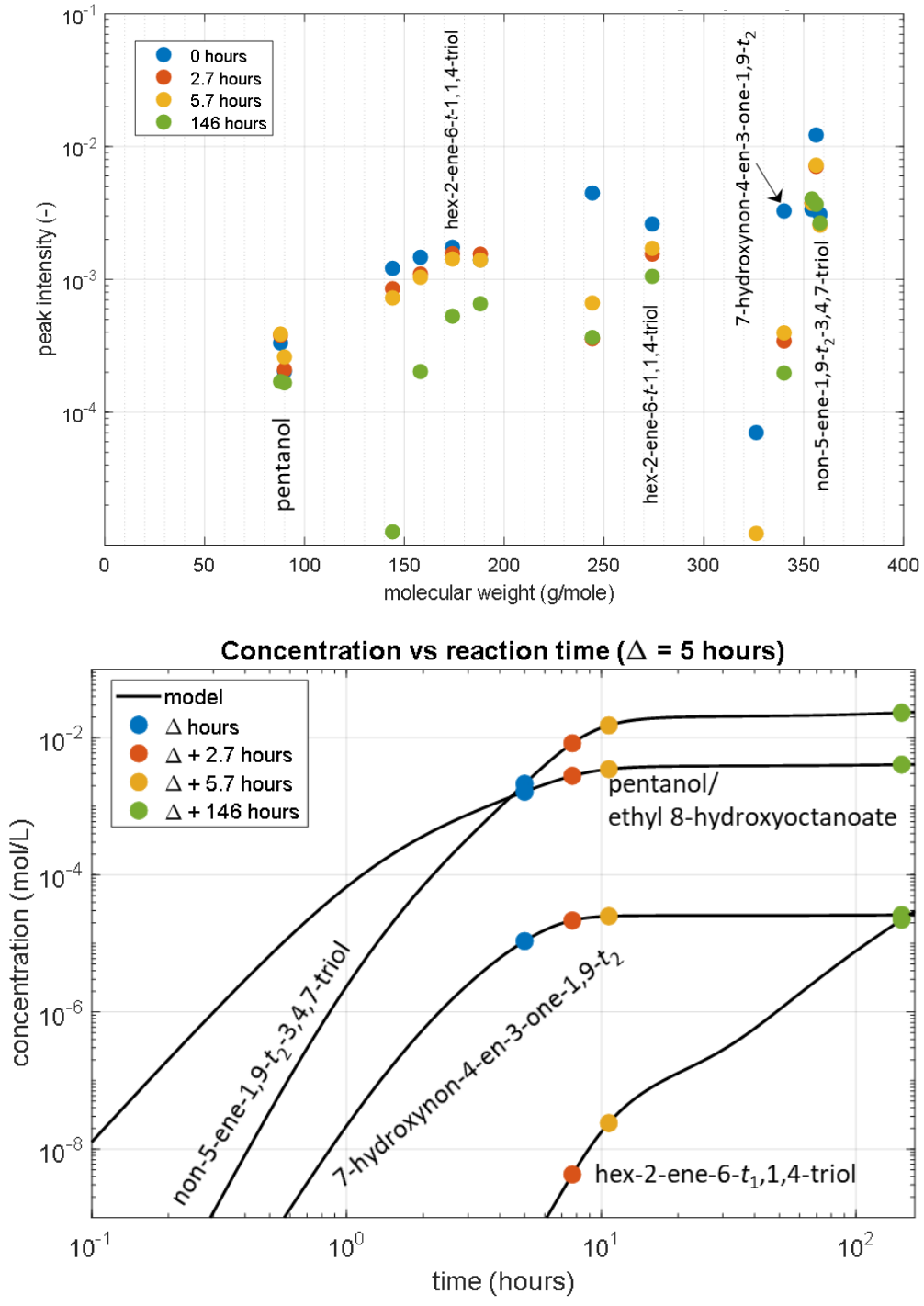

Figure A.14. (Top) Alcohols identified in the ESI spectrum. (Bottom) model-predicted concentrations.

In comparing the ESI-MS peak intensities and model predictions for pentanal, hexanal, and heptanal, experimentally the aldehydes decrease in intensity rather than accumulate as predicted (Figure A.15). This difference may be readily explained by the known volatility of these aldehydes. Additionally, β-scission producing hexanal and heptanal may be overestimated by the model, where there are not enough additional pathways for alkoxy radicals included. However, for pentanal, the model is in agreement on the decreasing trend in concentration, which may also be attributed to the mechanism and relevance of Russell termination.

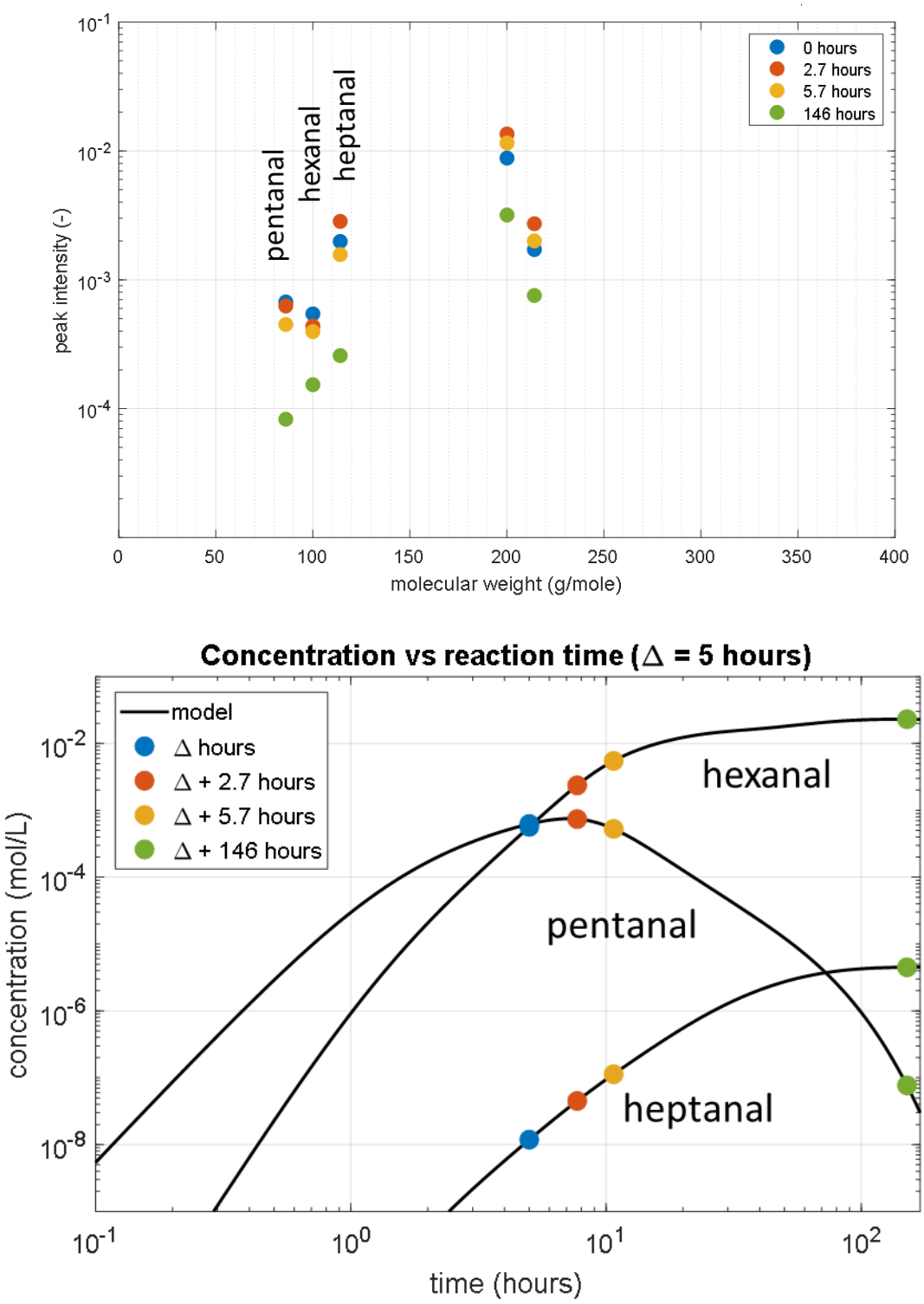

Figure A.15. (Top) Monomeric aldehydes identified in the ESI mass spectra. (Bottom) Model-predicted concentration of pentanal, hexanal, and heptanal.